Chapter 2

Climate change and variability overview

Yongqiang Liu, Scott Goodrick, Marcus Williams and Aoxing Zhang
Center for Forest Disturbance Science, USDA Forest Service, Southern Research Station, Athens, GA, United States

Background

Atmospheric conditions and their variations are classified into weather and climate, depending on spatial and temporal scales. Weather is commonly defined as the day-to-day state of the atmosphere and short-term (up to weeks) variations in a region. Climate is the average of the atmospheric state over a long period (usually 30 years). Sunlight, temperature, water, and carbon conditions are important environmental factors for tree growth. These conditions could experience dramatic and adverse changes in response to climate change, primarily due to the greenhouse effect, imposing a significant threat to the health and sustainability of forest ecosystems.

Climate change is the variation of the average atmospheric state over long periods, which appears either as a shift of the average state over decades, such as the worldwide warm spell in the early 20th century (Hegerl, Brönnimann, Schurer, & Cowan, 2018) and the dry spell in the western United States since the 1990s (Williams et al., 2020), or more often as a trend over centuries, millennia, or longer. For example, the global warming trend since the preindustrial period is due mainly to the increasing concentrations of greenhouse gases in the atmosphere (Intergovernmental Panel on Climate Change [IPCC], 2021). Global warming is part of a much larger issue of natural and human-caused climate change that also includes other changes like melting glaciers, heavier rainstorms, or more frequent drought (USGS, 2021). Atmospheric conditions also vary over short terms (e.g., months, seasons, and years) around the average state without causing the average state itself to change. Such variations are called climate variability. Examples of climate variability include extreme weather events such as droughts and floods, El Niño/La Niña, and multiyear and multidecade changes in temperature and precipitation patterns.

Climate change and variability could impact forests both positively and negatively. Sunlight, temperature, and water conditions are important environmental factors for the structure and function of forest ecosystems. However, these conditions could be modified adversely under climate change and altered climate variability, such as increasing extremes, imposing significant threats to forest health (Brack, 2019; Connecticut Department of Energy and Environmental Protection, 2021). Droughts cause plant water deficit and contribute to wildfires and insect and disease outbreaks (Halofsky, Peterson, & Harvey, 2020). Floods cause soil erosion and nutrient deposition (Natarajan, Hegde, Naidu, & Raizada, 2010). Windstorms lead to fallen and dead trees (Tanner, Rodriguez-Sanchez, & John, 2014). Climate change can lead to forest species migration and biomass reduction (Wang, He, Thompson, Fraser, & Dijak, 2017).

Catastrophic climate anomalies have grown dramatically in recent decades, including extremely severe droughts and heat waves in the western United States, massive wildfires in western North America, South Europe, and Siberia, and deadly floods in Central Europe, East and South Asia, and Africa in 2021 with the anthropogenic greenhouse effect very likely to be one contributor (IPCC, 2021). One of the key developments with the IPCC Sixth Assessment Report (AR6) (IPCC, 2021) is the strengthening of the links between human-caused warming and increasingly severe extreme weather (Singer, 2021). The projected climate change with increasing extreme weather imposes risks to forest health and human-derived forest ecosystem services.

The purpose of this chapter is to provide information on climate change and variability for evaluating the individual threats to forest ecosystems. The objectives are to describe the fundamentals and projections of climate change and variability, summarize and analyze the temporal and spatial patterns of climate change and variability in the past (until the late 19th century), at present (the late 19th century to the early 21st century), and in the future (the early 21st century to the end of this century), and illustrate applications to assessing the forest impacts of climate change and variability and manage the uncertainties.

Future Forests. DOI: https://doi.org/10.1016/B978-0-323-90430-8.00010-1

Fundamentals of climate change and variability

Atmospheric conditions are described by air temperature, precipitation, humidity, wind, and pressure. Climate change and variability are variations of the atmospheric conditions at various temporal scales due to the internal dynamics, interactions with the underlying Earth's components, and external forcing. The variations could occur at all spatial scales, from local to global, but those due to the greenhouse effect occur mainly at a global scale. The future climate change and variability due to external forcing can be projected using global climate models (GCMs) and Earth system models (ESMs). An external forcing is a type of climate-forcing agent that impacts the climate system while being outside of the climate system itself. External forcings are drivers for atmospheric variations, including solar and Earth orbital variations and gas and particle emissions into the atmosphere from natural (e.g., wildfires, dust storms, and volcanos) and human resources (such as industry and vehicle). For example, the anthropogenic emissions contributing to recent global warming are mainly CO_2 and other greenhouse gases from industrial activity. Climate change and variability, their drivers, and projections are illustrated in Fig. 2.1 and Photo 2.1 and described in detail in this section.

Processes and factors for climate change and variability

Atmospheric conditions' spatial distributions and temporal variations are controlled by atmospheric radiation, convections, circulation, and planetary-layer boundary (PBL) processes. Short-wave solar radiation is the ultimate energy source of atmospheric movement. The atmosphere and the ground surface absorb or reflect incoming solar radiation. Heat energy is then obtained by the atmosphere through direct absorption and from the sensible heat and long-wave thermal radiation from the ground surface. Atmospheric convection leads to clouds and precipitation, which affect the radiation and the water cycle. Atmospheric circulations transfer heat, water, and momentum between different geographic regions. The PBL processes include turbulence, eddies, and convection that exchange heat, water, momentum, trace gases, and particles between the atmosphere and the underlying surfaces.

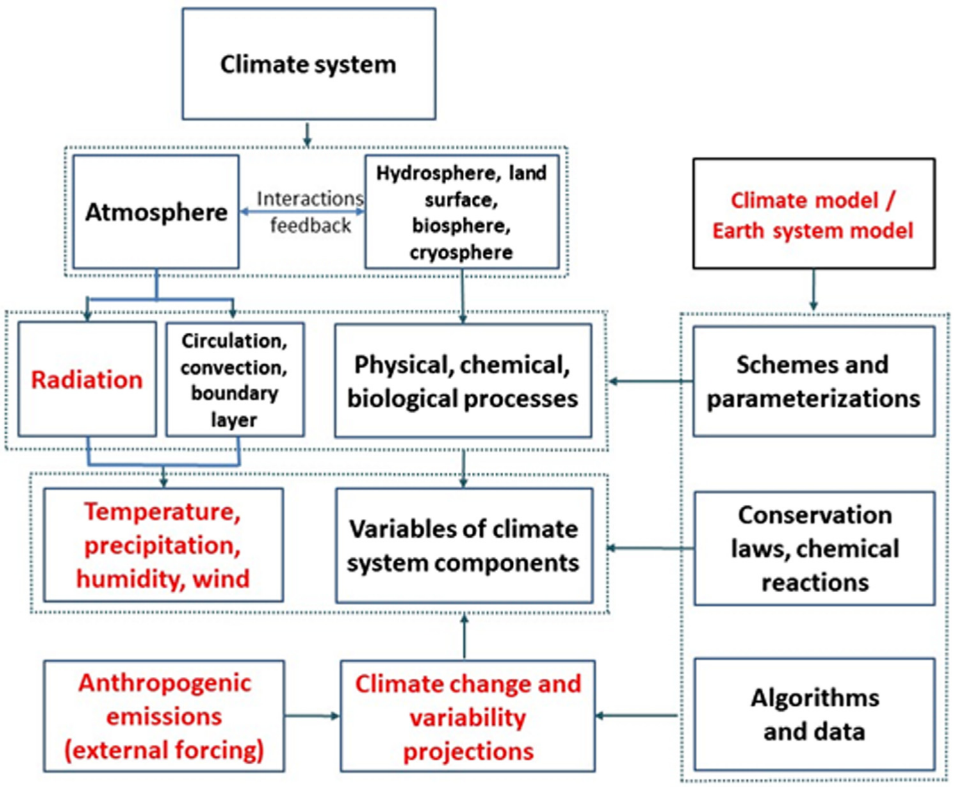

FIGURE 2.1 A diagram of the climate system, processes, and projection. The boxes closely related to climate change and variability due to the greenhouse effect are shown in red. The boxes within dotted lines are climate system components, atmospheric processes, atmospheric conditions (from top to bottom, left column), and model components (right column). The box (es) pointed by arrows are either components or consequences.

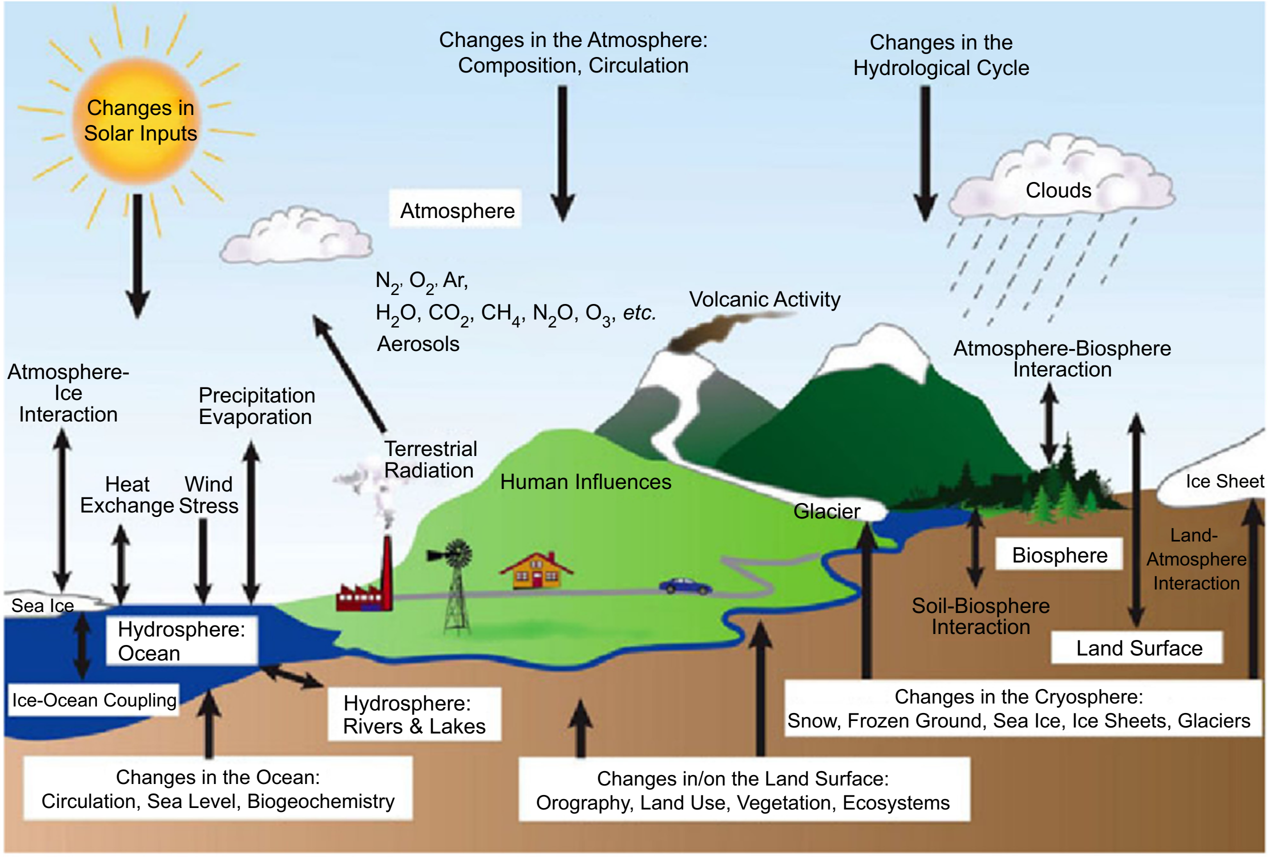

PHOTO 2.1 Climate system. *Intergovernmental Panel on Climate Change. (2007). Climate change 2007: The scientific basis. In S. S. D. Qin, M. Manning, Z. Chen, M. Marquis, K. B. Averyt, M. Tignor, & H. L. Miller (Eds.), Report of the Intergovernmental Panel on Climate Change. Cambridge and New York: Cambridge University Press.*

It was found about half a century ago that some extreme events, such as the prolonged droughts in Africa during the early 1970s, could not be explained by only looking at atmospheric processes themselves. Charney, Stone, and Quirk (1975) proposed a geo-biophysical feedback mechanism to link the drought to the reduced grasses due to overgrazing in the Sahel region: reduced vegetation increases albedo, which reduces net solar radiation absorbed by the ground surface; heat loss results in stronger descending motions of warm and dry air; increased warm, dry air results in more severe and extended drought; and grasses are further reduced. The recognition of the roles of the processes outside the atmosphere contributed to the development of the concept called *climate system*, which, besides the atmosphere, also consists of the hydrosphere, the land surface, the biosphere, and the cryosphere (IPCC, 2001). The terrestrial biosphere includes more than two dozen key processes that can affect the atmosphere, including biophysical and biogeochemical cycling across carbon, water, and nutrient stocks, fluxes, and transformations, as well as dynamic and ecological processes (Fisher, Huntzinger, Schwalm, & Sitch, 2014). Forests are one of the significant components of the biosphere on the land surface, which is the lower boundary of the atmosphere. Forests can affect atmospheric temperature, humidity, and wind by modifying the heat, water, and momentum fluxes at the air-land interface (Fig. 2.2).

Climate variability is attributed mainly to natural factors. El Nino-Southern Oscillation (ENSO), the North Pacific Oscillation (NPO), North Atlantic Oscillation (NAO), and Interdecadal Pacific Oscillation (IPO) (Norel, Kałczynski, Pinskwar, Krawiec, & Kundzewicz, 2021) affect interannual and decadal fluctuations. ENSO is the predominant mode of natural climate variability in the 2- to 7-year range. ENSO is a recurring climate pattern involving water temperature changes in the central and eastern tropical Pacific Ocean and appearing in three phases: El Niño, La Niña, and Neutral. ENSO influenced global temperatures from 0.39°C to 0.64°C during 1979–2010, which is greater than the influence of solar variation and volcanoes during the same period (Foster & Rahmstorf, 2011). The NAO is an alternation of pressure between the area near the Azores and subpolar low pressure near southeast Greenland in the negative and positive phases and acts to modulate precipitation. For example, when the NAO is positive, drier than average conditions exist

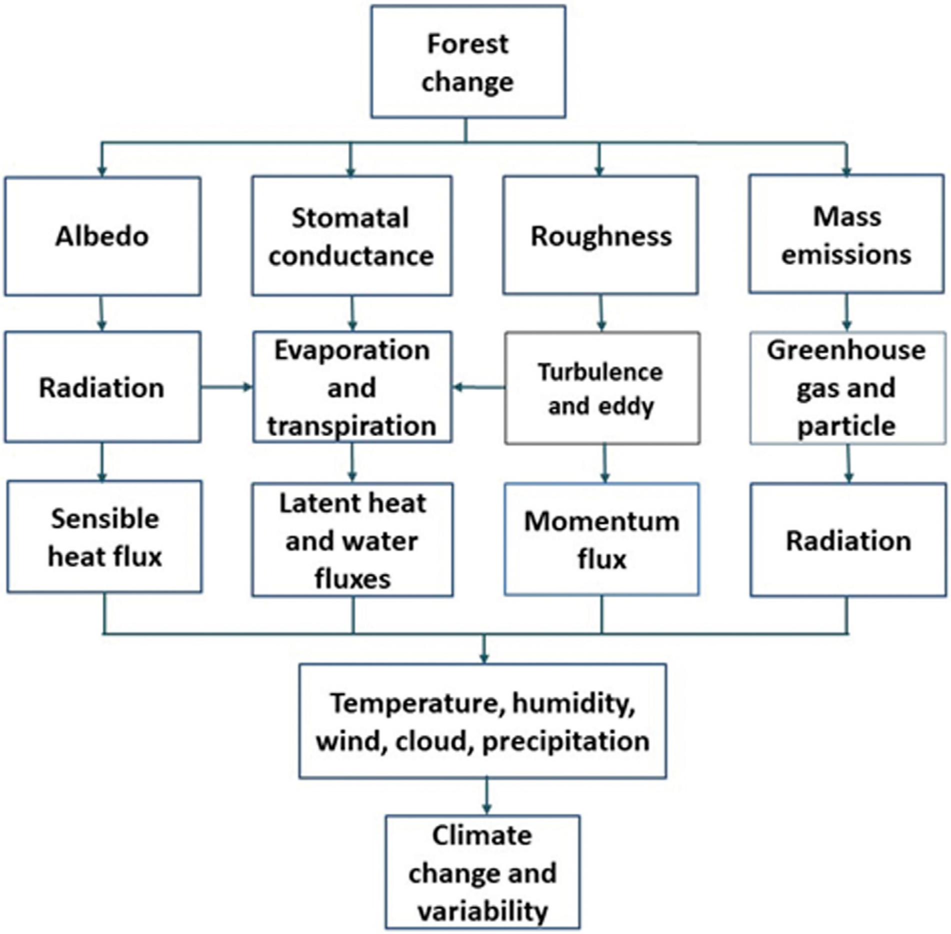

FIGURE 2.2 Climatic effects of forest conditions. Arrow indicates the direction of impacts between two boxes.

over southern Europe and the Mediterranean. During most of the Holocene, variations in predominantly three natural drivers (orbital, solar, and volcanic) were the primary influences on global climate (Beer & Wanner, 2012). Climate variability in the late 19th century was primarily driven at decadal time scales by IPO and at interannual time scales by ENSO and NAO. The global influence of the NAO on precipitation can be seen in Fig. 2.3. The IPO is an ENSO-like feature in the positive and negative phases that are believed to cyclically shift the climate at the rate of one to three decades. During the positive phase of the IPO, multiple-model averages suggested that the IPO accounted for 71%−75% of the rapid warming between the epochs of 1910−1941 and 1971−1995. The negative phase of the IPO accounts for 27% of the cooling trend seen in the late 1990s (Meehl, Hu, Santer, & Xie, 2016).

Snow and soil moisture anomalies affect monsoon intensity and progress. Land cover changes due to dust storms, wildfires, and other natural disturbances affect monthly and seasonal land-atmosphere fluxes. Natural factors also include emissions of gases and particles from wildfires and volcanoes that affect atmospheric radiation and convections. Note that although wildfires (and emissions from wildfires) can often be considered "natural," anthropogenic climate change has increased fire frequency, area, and/or severity enough to alter (increase) emissions due to wildfires in some regions. Thus it could be described as only partly natural and partly human-caused. In addition, a combination of the variations of Earth's orbit (i.e., Milankovitch Orbital Cycles) (Campisano, 2012) and sunspot activity (Hathaway, 2015) influenced incoming solar radiation and caused the Little Ice Age.

Global climate models

Climate models have been developed based on general circulation models, which have the same acronym (GCM) as global climate models, to simulate and predict climate change and variability. GCMs, in this context, refer to the very early stages of the GCM when it only describes air motions at short time scales (subseasonal) driven by internal

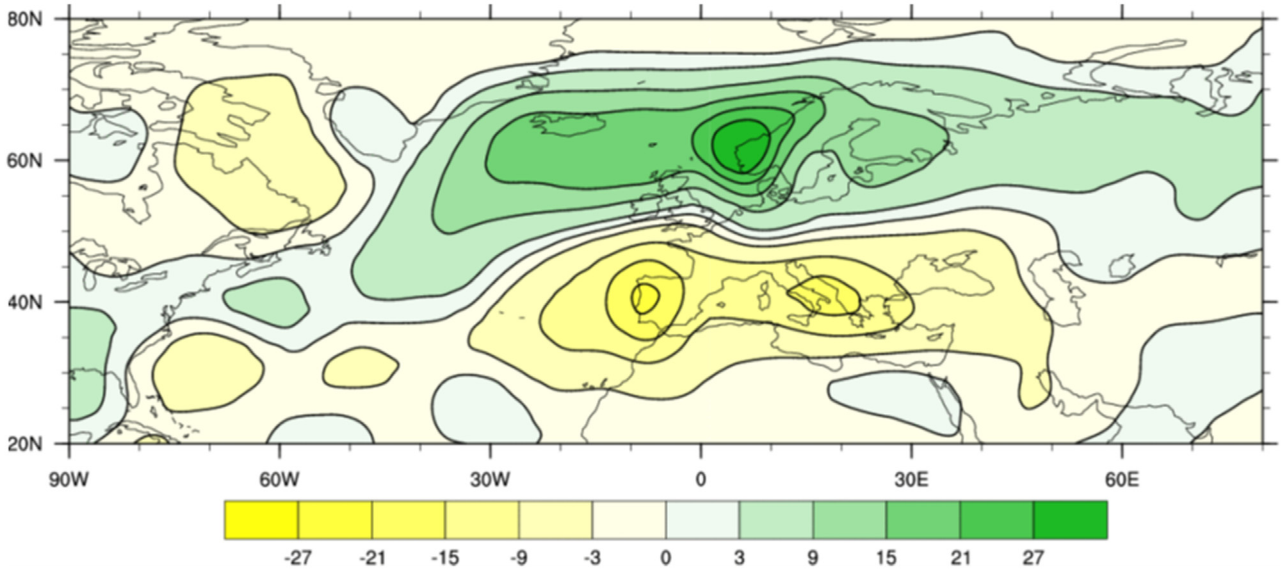

FIGURE 2.3 Change in winter (December−March) precipitation corresponding to a unit deviation of the NAO index over 1979−2003. The contour increment is 0.3 mm day^{-1} (Hurrell, Kushnir, Ottersen, & Visbeck, 2003). *Hurrell, J. W., Kushnir, Y., Ottersen, G., & Visbeck, M. (2003). An overview of the North Atlantic Oscillation. In: J. W. Hurrell, Y. Kushnir, G. Ottersen, & M. Visbeck (Eds.),* The North Atlantic Oscillation: Climatic significance and environmental impact *(Vol. 134, pp. 1−35). Geophysical Monograph Series. https://doi.org/10.1029/134gm01.*

atmospheric dynamics. For a climate model, processes of atmospheric variations at longer scales, such as radiation and air-land heat and water exchanges, become important. Also, other components of the climate system, especially the ocean, become part of a climate model. The traditional GCM becomes a part (subclass) of a climate model and is often called AGCM (atmospheric GCM) in distinction to OGCM (Oceanic GCM).

A climate model consists of three primary components: (1) A set of mathematical equations for predicting temporal variations and spatial distributions of atmospheric conditions, including (a) the atmospheric momentum conservation (Newton's second law of motion) for three-dimensional winds, (b) the heat energy conservation (the first law of thermodynamics) for temperature, (c) the conservation law of water mass for air humidity, (d) the conservation law of air mass (continuous equation), and (e) the equation of state. (2) Schemes (approximations and assumptions, etc.) and parameterizations (expressing unknown parameters and processes using known atmospheric variables) to describe atmospheric physical processes. (3) Numerical algorithms to solve the equations, which are nonlinear by nature and include turbulence without analytical solutions. A climate model usually also includes some chemical processes.

Climate models have been expanded to ESMs, such as the NCAR Community Earth System Model (CESM) (Hurrell, Holland, & Gent, 2013). ESMs are a more sophisticated tool for simulating and predicting climate-ecosystem interactions (Liu, 2018). Besides variations in the atmosphere, ocean, land surface, and ice that provide the environmental conditions for ecosystem processes, many ESMs describe variations in the biosphere, including changes in the carbon, water, and nitrogen cycles in the terrestrial ecosystems, disturbances in forests such as fires, and changes in forest structure, types, and distributions using dynamic global vegetation models (DGVMs) (Bachelet, Neilson, Lenihan, & Drapek, 2001; Fisher et al., 2014).

Greenhouse effect

Human activities have influenced climate change since the preindustrial time of 1750 (IPCC, 2021). Fossil fuel burning from industrial and other activities emits greenhouse gases and particles into the atmosphere that modify radiation, clouds, and other atmospheric processes. Greenhouse gases (GHGs) include carbon dioxide (CO_2), methane (CH_4), nitrous oxide (NOx), and fluorinated gases. They are transparent to solar radiation but can absorb long-wave thermal radiation from the ground, acting like a greenhouse of the Earth. The CO_2 concentrations in the atmosphere have increased by 47.5% from about 278 parts per million (ppm) during the preindustrial period to 405 ppm in 2019 (Lan, Hall, Dutton, Mühle, & Elkins, 2020). The IPCC AR5 (IPCC, 2013) indicated that average global temperatures increased about 0.85°C from 1880 to 2012 and concluded that more than half of the observed increase in global average temperatures was caused by elevated emissions of CO_2 and other greenhouse gases.

As shown later in Section 3.3, glacial and interglacial epochs alternated over the last one million years during the Quaternary. The temperature was about −4°C during glacial and 2°C during interglacial periods. The most recent glacial period (i.e., "Ice Age") peaked 18k years ago and was followed by the interglacial Holocene epoch (IPCC, 2013). As a result, the temperature increased by about 1°C from 1600 to 1900. The warming trends have continued since then, with a temperature increase of approximately 1.5°C. This warming rate, caused mainly by anthropogenic forcing, accelerated faster than the previous rates caused by natural factors.

Emission scenarios/pathways

Weather and climate variability predictions are made mainly based on the conditions of the atmosphere and other climate system components at the time of predictions (initial conditions) and external forcing, such as gases and particles emitted into the atmosphere. Climate scientists usually do not know what will happen exactly with the emissions over a long period in the future. Therefore they must assume possible situations called scenarios. A climate prediction using scenarios rather than a specifically known forcing is often called climate projection.

The increasing trend of atmospheric CO_2 concentrations since the industrial revolution is likely to continue during the rest of this century and beyond, to 2300 and 2400 in some scenarios. The increasing rate depends on many factors, such as industrial activity and the development of new environmental technology. The IPCC has produced three sets of emission scenarios/pathways (plausible trajectories of development in specific fields that can be combined with other assumptions or conditions to create scenarios) with various ranges of future forcing for projections of future climate change by GCMs (Table 2.1) following the early scenarios of SA90 and IS92 developed in 1990 and 1992. Note that this only provides an analog of these scenarios/pathways rather than strictly scientific comparisons. The Special Report on Emissions Scenarios (SRES) (IPCC 2001, 2007; Nakicenovic et al., 2000) have four scenarios from different combinations of global and regional economic growth and environmental sustainability determined by future greenhouse emissions, population (social), and economic growth. There are two problems with the SRES scenarios. First, the SRES emission scenarios used in climate models must be converted into greenhouse gas concentrations using global biogeochemical cycle models and further to radiative forcing using climate models. With different representations of physics and chemistry and different bias levels, the ultimate radiative forcing varies from one climate model to another, even with the same emission scenarios. This conversion makes it difficult to compare projections of climate change among models. Secondly, there are discrepancies between the assumed social and economic development and the actual changes over the most recent two decades.

The representative concentration pathways (RCPs) and shared socioeconomic pathways (SSPs) (IPCC, 2013, 2021; Moss et al., 2010; O'Neill et al., 2014; Van Vuuren et al., 2011) were developed as solutions for these problems. RCPs are forcing-based scenarios that specify mean different levels of radiative forcing of future greenhouse gases, mainly at 2.6, 4.5, 6.0, and 8.5 W m^{-2} by 2100. The corresponding CO_2 equivalent concentrations are about 400, 560, 710, and 1250 ppm (IPCC, 2013). SSPs are socioeconomic-based scenarios that specify pathways to qualify and quantify factors of future population, economic growth, education, urbanization, and the rate of technological development and combine

TABLE 2.1 IPCC emission scenarios and pathways.

Set	SRES	RCP	SSP
Year released	2000	2007	2017
IPCC AR version	3, 4	5	6
CMIP phase	3	5	6
Scenario/pathway case			
Low end	B1	(1.9)	1
Sub-medium end	B2	2.6	2
Medium end	A1B	4.5	3
Sub-high end	A2	6.0	4
High end	A1F1	8.5	5

the mitigation targets of RCPs. The five primary scenarios (SSP1−SSP5) assume a world of sustainability-focused growth and equality, a "middle of the road" world where trends broadly follow their historical patterns, a fragmented world of "resurgent nationalism," a world of ever-increasing inequality, and a world of rapid and unconstrained growth in economic output and energy use. GHG concentrations peak mid-century for several SSPs and 2100 for others. CO_2 concentrations by 2100 range from 393 to 1135 ppm (Meinshausen et al., 2020).

Atmospheric aerosols are another source of emissions that affect radiation. Unlike greenhouse gases, aerosols are emitted mainly by natural processes (e.g., volcanos and wildfires) over a shorter lifetime, often localized, and most importantly, mainly reducing solar radiation (except black and brown carbons). Over the 1750−2011 period, the radiative forcing from the major anthropogenic sources was about 1.8 $W\ m^{-2}$ from CO_2, 1 $W\ m^{-2}$ from other greenhouse gases, 0.4 $W\ m^{-2}$ from ozone, and −0.8 $W\ m^{-2}$ from aerosols (IPCC, 2013). The net-radiative forcing was about 2.3 $W\ m^{-2}$. The forcing from the natural process of solar irradiance was minimal, at less than 0.1 $W\ m^{-2}$. Measurements of historical aerosols emissions from wildfires are expected to change significantly in the future under a warming and drying climate in most of the major fire regions such as the western United States (Liu, Goodrick, & Stanturf, 2021). Future aerosol emission projection is an important uncertainty source.

Global climate change projections

Climate models and ESMs have been used to project future climate change in response to the increasing greenhouse gases and other forcings under different emission scenarios. Among many efforts is implementing the Coupled Model Intercomparison Project (CMIP), a collaborative framework with the participation of several dozen climate models and ESMs from multiple countries. CMIP is aimed to improve climate modeling and knowledge of climate change and support national and international assessments of climate change, including IPCC's assessment reports (AR). The assessments are essential to understanding the scientific basis of climate change, its potential impacts, and adaptation and mitigation options. CMIP3 (Meehl et al., 2007), CMIP5 (Taylor, Stouffer, & Meehl, 2012), and CMIP6 (Eyring et al., 2016) used SRES for the IPCC AR3 and AR4 (IPCC, 2001, 2007), the RCPs for the IPCC AR5 (IPCC, 2013), and SSPs for the IPCC AR6 (IPCC, 2021), respectively. The projected warming from various CMIP phases is compared in Fig. 2.4.

CMIP6 provides four experiments (Eyring et al., 2016): (1) Atmospheric Model Intercomparison Project (AMIP) to evaluate atmospheric models and analyze atmospheric variability. SST, sea ice cover (SIC), and CO_2 concentrations are prescribed using observations. The simulation period is 1979−2014. (2) Preindustrial control simulation to evaluate climate models and ESM models and analyze variability without CO_2 forcing. SST and SIC are predicted using coupled models. CO_2 concentrations are prescribed or calculated. The simulation period is at least 500 years. (3) Abrupt CO_2 increase simulation to test climate sensitivity, feedback, and fast responses. CO_2 concentrations are prescribed in the way that they are abruptly quadrupled and then held constant. The simulation period is at least 150 years. (4) Gradual CO_2 increase simulation to obtain climate sensitivity, feedback, and idealized benchmark. CO_2 concentrations are prescribed at a rate of 1% per year. The simulation period is at least 150 years. In addition, CMIP6 also provides historical simulations to evaluate model performance. CO_2 concentrations are prescribed or calculated. The simulation period is from 1850 to the present.

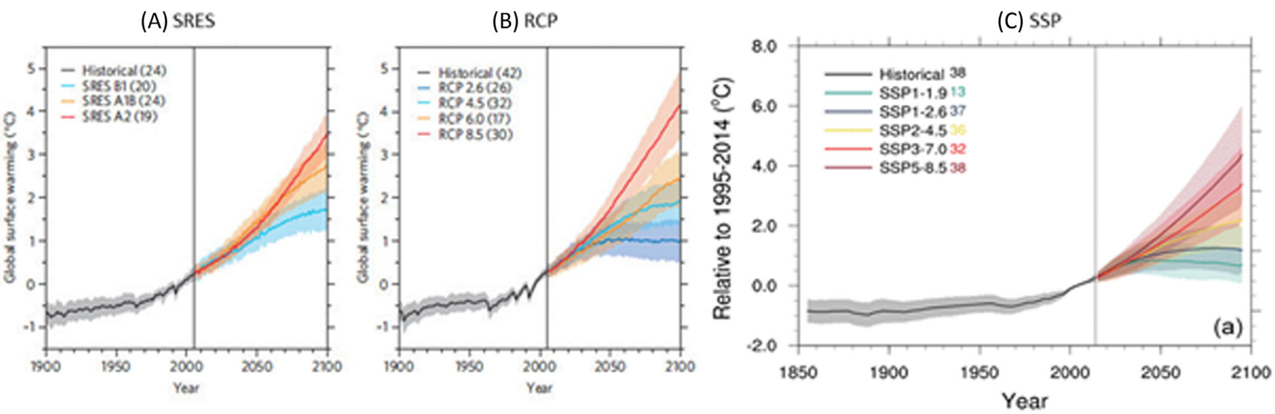

FIGURE 2.4 Comparisons of warming under different emissions scenarios/pathways of SRES (A), RCP (B), and SSP (C).

Besides averages, CMIP models also project changes in variability, extremes of meteorological conditions, and the time when a threshold warming level will be reached. Traditionally, the intensity of Earth's temperature response to increasing CO_2 or the related radiative forcing is indicated by a certain warming level (i.e., degrees in temperature increase) by a specific time (e.g., the end of this century). A new indicator is how soon a certain warming level (increase by 1°C, 2°C, or 3°C, averaged over 5 or 10 years to smooth out interannual variability) will be reached. For example, an increase of 3°C in temperature is projected to occur by 2075 under SSP4 and 2050 under SSP6, but that increase is not seen during the rest of this century under SSP1 and SSP2.

The primary mechanism for the anthropogenic greenhouse effect is the increased absorption of atmospheric long-wave radiations and the related changes in temperature, precipitation, and other atmospheric conditions. Climate models have a good handle on the physics of these mechanisms. A primary issue is how much warming is expected under specified greenhouse gas concentrations. The absorption of greenhouse gases only contributes to a small portion of the simulated warming, while a large portion is attributed to climate models' feedback. With increasing greenhouse gases, the atmosphere retains more long-wave radiation that causes air temperature to increase. Various feedbacks follow this increase. One is called radiation-temperature-cloud positive feedback: increasing temperature reduces relative humidity and clouds. The ground surface receives more solar radiation that turns into sensible heat flux, and air temperature increases, which further reduces clouds. Another is called the radiation-ice-albedo positive feedback: increasing temperature reduces snow and ice coverage and ground albedo. More solar radiation is absorbed, and therefore the temperature is increased. This change further reduces snow and ice coverage. These feedbacks are very complex, with the intensity and even directions affected by the parameterizations and parameter specifications in climate models. This model interaction is an important source for the uncertainty of climate change projections and differences among models.

The capacity to project future climate variability, especially extreme climate events such as droughts, floods, hurricanes, and tornadoes, is much lower than projections of future climate trends and varies significantly with climate models. This difference is due to the internal or natural processes that largely determine climate variability in the climate system, such as ENSO and PDO, rather than external forcing. For example, ENSO and PDO play an essential role in the winter and spring precipitation extremes (and consequently floods) over the US Southwest and West (Gershunov et al., 2013). A critical uncertainty for the US Southwest, therefore, is the relevant modes of natural variability in ENSO and PDO and their combined influences on climate. Such processes are difficult to predict even at present and more localized in nature.

Validation of climate models

Validation of climate models is to evaluate the capacity of climate models to represent the observed behavior of past climate. Validation is a prerequisite to applying the models confidently to projecting future climate change and variability in response to natural and anthropogenic forcing (Contzen, Dickhaus, & Lohmann, 2022; Flato, Marotzke, Abiodun, & Zhan, 2013). The capacity is validated by comparing simulation with and without forcing and examining if and how much the differences could explain the observed climate change, such as warming since the preindustrial era. The differences in the past and future are often used as the signals of anthropogenic forcing in the evaluation study of climate change impacts.

Comparisons are made to statistics, temporal (e.g., average, seasonal and interannual variability, low-frequency fluctuations, and extreme events), and spatial distributions of either individual meteorological variables, atmospheric circulation systems (e.g., subtropical highs, intertropical convergence zone, westerly stream, polar vortex), and coupled processes such as ENSO, or metrics. Average statistical properties are obtained over time and space and over categories of physically distinct regimes such as circulation, cloud, and thermodynamic states. The criteria include popular error measures, indices, and empirical cumulative distribution functions (Sillmann, Kharin, Zhang, Zwiers, & Bronaugh, 2013; Zhang et al., 2011).

Besides independent validation of individual models, an important and influential effort in model validation is the implementation of the CMIP project, which compares the performance of many models under preset protocols. The ensemble technique is often used to evaluate CMIP models. Comparisons are also made between different CMIP phases. Many atmospheric variations over time, including increasing extreme weather frequency and intensity, are not caused but are affected by climate change. A technique called attribution analysis is used to evaluate how much climate change is contributed to the observed trends in extreme weather and the projected trends in the future (Diffenbaugh, 2020).

The confidence in projecting climate change and variability in response to both natural and anthropogenic forcing has increased with many positive findings from model validation studies, together with increasing model resolution, improved parameterization, expanded capabilities (e.g., from climate models to ESMs), and more data such as satellite and reanalysis (Fasullo, 2020). Analysis indicates that climate models published over the past five decades were skillful in predicting global mean surface temperature changes, with most models showing warming consistent with observations. However, there are still uncertainties in the simulated magnitude and pace, depending on variables, region, and season (Miao et al., 2014; Sheffield, Barrett, Colle, & Yin, 2013). For example, Carvalho et al. (2022) found that the global warming projected by 15 CMIP3, 27 CMIP5, and 30 CMIP6 models project global warming slightly lower than the observed one.

Downscaling of global climate change and variability projections

GCMs usually have horizontal resolutions of hundreds of kilometers. Global processes such as ENSO and synoptic systems such as cyclones and fronts can be identified at these resolutions. However, regional climate and mesoscale processes such as convective storms are largely missed. In addition, the effects of local and regional forcing, such as terrain, land cover variability, and aerosols emitted from local or regional natural and anthropogenic sources, are often not well represented. Therefore downscaling is required to provide high-resolution climate information for regional and local applications of climate change impacts (Photo 2.2).

Various dynamical and statistical downscaling techniques have been developed (Liu, Liu, et al., 2021). Dynamical downscaling utilizes regional climate models (RCMs) with boundary conditions provided by GCMs or ESMs. RCMs have similar components of dynamics and physics to the global models but with resolutions of tens of kilometers or higher to identify storms and local circulations. Dynamical downscaling provides a wide range of variables in the atmosphere and other climate system components. The frequency of the downloaded data can be as high as daily or even hourly. Among the efforts of dynamical downscaling is CORDEX (Giorgi & Gutowski, 2015), which currently encompasses 14 domains covering essentially all land areas of the globe at a resolution of about 50 km. Dynamical downscaling has been conducted using many RCMs under the forcing of CMIP models. Both GCMs and RCMs have been improved from CMIPs, especially in simulating extreme weather (Chen, Hsu, & Liang, 2021; Kusunoki & Arakawa, 2015). Other efforts include downscaling for East Africa using a GCM of EC-EARTH and four RCMs (20 years, 25 km) (Nikulin, Asharaf, Eugenia, & Wysera, 2018), eastern Australia using CMIP3 and CMIP5 and two RCMs (20 years each for present and future climate, 60 km) (Grose, Bhend, Argueso, & Timbal, 2015), China using CMIP5 and WRF (10 years each for present and future climate, 30 km) (Chen et al., 2018), Europe using EC-EARTH global model and three RCMs (22 years, 30 km) (Manzanas et al., 2018), western South

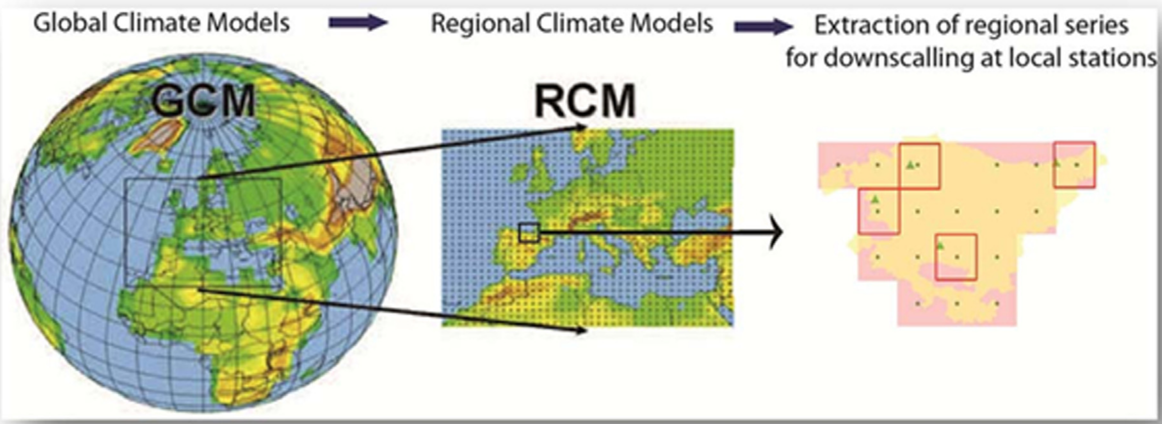

PHOTO 2.2 Climate downscaling. *Iratxe Gonzalez-Aparicio, "Air quality and meteorological modelling of urban areas in the context of climate change," Universidad del Paiś Vasco, 2012.*

America using a GCM and reanalysis data and two RCMs (25−35 years, 10−50 km) (Bozkurt et al., 2019), and the United States using the National Center for Environmental Prediction Climate Forecast System and the UCLA-ETA regional model (22 years, 40 km) (De Sales & Xue, 2013).

Dynamical downscaling provides many energy and water fluxes and soil temperature and moisture conditions needed for forest conditions and change modeling. In addition, RCMs include many physical interactions and feedback important for projections of climate change, which are largely missed in GCMs due to coarse grid spacing. The snow-radiation-warming feedback is an example. The summits of mountains in middle latitudes are often covered by snow; due to global warming, decreases in the snowpack are possible. This reduction in the snowpack leads to reduced albedo, more solar radiation absorption, and a positive feedback loop with warming.

A significant limitation of dynamical downscaling is the need for considerable computation resources. As a result, dynamical downscaling usually has much lower spatial resolutions, uses fewer GCM projections, and considers fewer emission scenarios than statistical downscaling. As a result, it is challenging to update dynamical downscaling products using combinations of multiple GCMs and RCMs for multiple emission scenarios and to obtain ensemble results. For example, the North American Regional Climate Change Assessment Program (NARCCAP) (Mearns, Arritt, Biner, & Snyder, 2012), a CORDEX project component covering North America, conducted such downscaling of climate change projected from CMIP3 but did not conduct similar downscaling for CMIP5 and CMIP6.

Statistical downscaling utilizes statistical tools to obtain relationships between historical meteorological conditions at local sites and GCM grids for high-resolution (meters to tens of kilometers) climate information. Statistical downscaling methods include (1) transfer functions that relate large-area climate to local weather or from upper air to the ground. This method can be further classified as scaling methods and regression-based approaches (Schoof, 2013), (2) weather typing that relates large-scale circulation systems or patterns to local weather, and (3) weather generator that relates parameters from large- to local-scale. There are several tools and products for statistical downscaling. The tools include Climate Wizard (Girvetz, Zganjar, Raber, Maurer, & Kareiva, 2009), ENSEMBLES Regional Scenario Web Portal (Cofino, San-Martın, & Gutiérrez, 2007), and LOCA (Pierce & Cayan, 2014). The products include WorldClim (Fick & Hijmans, 2017), NASA Earth Exchange Global Daily Downscaled Projections (NEX-GDDP-CMIP6) (Thrasher et al., 2022), National Climate Change Viewer (NCCV) (Alder & Hostetler, 2015), MACA CONUS Daily Downscaled Climate Projections (Abatzoglou & Brown, 2012), ClimateNA (Wang, Hamann, Spittlehouse, & Carroll, 2016).

Fewer computational resources are needed in comparison with dynamical downscaling. Because of this, statistical downscaling for a specific region can be conducted using multiple GCMs, emission scenarios, and statistical methods, allowing for ensemble results. An ensemble is an approach to obtain more representative or robust results from multiple runs rather than a single run. The runs can be conducted using multiple climate models, model versions, emission scenarios or forcings, input data, initial conditions, and/or simulation setups.

Statistical downscaling needs a large amount of observational data to build empirical relationships with the present climate simulated by a GCM. Such relationships may not exist for a particular variable at a specific location. Also, developing such relationships in complex terrain such as mountains where data are spatially sparse and may lack representativeness is especially difficult. Another major limitation of statistical downscaling is that the relationships developed using the current data are assumed to be applicable in the future, which is referred to as the assumption of statistical stationarity (Dixon, Lanzante, Nath, & Gaitán, 2016). This assumption may not be valid. For example, more extreme conditions are projected for the future.

Downscaling climate variability, especially extreme events, presents a challenge for both approaches. Because RCMs include all physical processes needed to simulate mesoscale weather systems and better represent topography and other local forcings for convective precipitation, dynamical downscaling can directly simulate weather and climate extremes. However, many studies have indicated limited capacity of RCM simulations of weather and climate extremes. For example, Yang, Franzke, and Fu (2020) examined four RCMs. They found that they performed poorer in representing the spatial dependency and intensity characteristics of extreme precipitation in eastern Germany than in a statistical model.

Nevertheless, many of the statistically downscaled datasets have daily temporal resolution and do produce extremes. More evaluation studies are needed, especially regarding their performance with RCMs. In addition, the development and application of the extreme value theory (EVT) may increase the capacity for statistical downscaling of extremes. Unlike traditional statistical techniques focused on events with large probability, EVT deals with the event with small probability and prediction of statistics such as average instead of specific events.

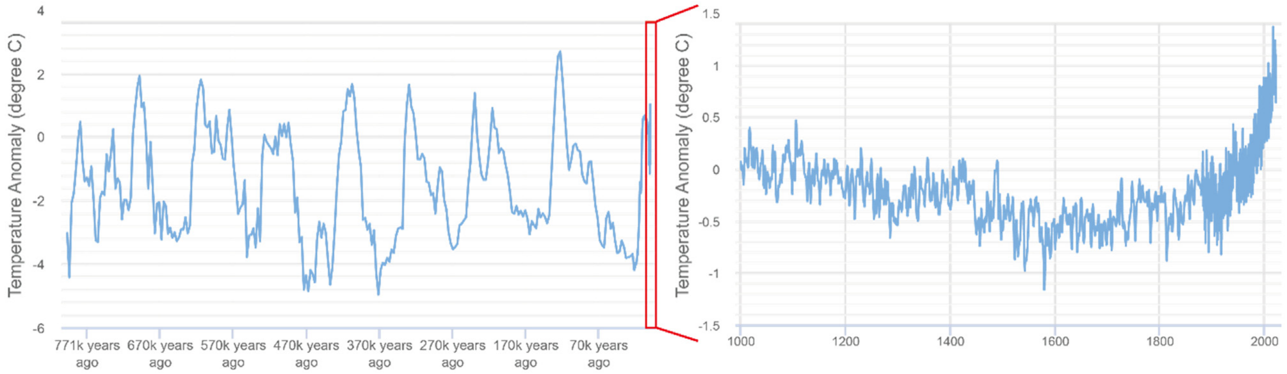

FIGURE 2.5 Variation in temperature anomaly over the past 1 million years (left) and since 1000 AD. *https://www.temperaturerecord.org/*.

Temporal changes

Past climate change and variability

During Earth's history and biological evolution, the climate experiences large fluctuations at long time scales (Fig. 2.5). Scientists have identified five major ice ages throughout Earth's history. The most recent glaciation period commonly referred to as the "Ice Age," peaked 18,000 years ago before giving way to the interglacial Holocene epoch 11,700 years ago. Since then, the Earth's climate has been relatively stable.

At high latitudes during the ice age, glacier cover expanded, and polar high pressure increased, forcing the polar belt to move south to mid-latitudes (as far as 57°N during the recent ice age). In the mid-latitudes, polar front belt cyclone activity was frequent, rainfall was abundant, and inland lake water rose. Conversely, when high latitudes were in the interglacial epoch, continental ice sheets and high polar pressures shrank to the polar regions, the climate belt moved north, and dry climates occurred in some parts of the mid-latitudes.

The most recent widespread cold event occurred from about the beginning of the 15th century to the beginning of the 20th century. The average winter temperature in central England between 1500 and 1650 was about 1.5°C lower than it is today. This period was named the "Little Ice Age" (Matthes, 1939). The impact of the Little Ice Age on global agriculture was disastrous. Famines around the world led to wars and plagues. In addition, the extension of the northern glaciers led to natural disasters such as floods and landslides. As a result, cold-resistant crops (e.g., potatoes, corn) began to be planted more widely.

For the paleoclimate research in the million-year-long time scale, scientists can infer climate changes in ancient times through information such as geological strata, fossils, and isotopes in ice cores (Jouzel, Hoffmann, Koster, & Masson, 2000; McElwain, Beerling, & Woodward, 1999). In addition, the development of human civilization before the industrial revolution left a lot of historical records that could be used to infer climate conditions around the world. For example, the temperature in Europe since the 18th century can be constructed using the lengthy record of the current alpine glaciers (Nussbaumer et al., 2011). Through historical data of temperature and pressure, historical documents, observations of tree rings, and the use of an atmospheric circulation model, the annual variability of the global temperature has been reconstructed for the past 2000 years (Moberg, Sonechkin, Holmgren, Datsenko, & Karlén, 2005). Additionally, a monthly reanalysis database (a dataset built by combining observed with simulated data) of global atmospheric historical conditions since 1600 has also been constructed (Franke, Brönnimann, Bhend, & Brugnara, 2017) (Fig. 2.6).

Preindustrial climate changes, including the formation of the Little Ice Age, were closely related to natural factors such as volcanic eruptions. Scientists found that the drop in the direct radiative effect due to volcano eruptions in the early 19th century can last 2−3 years, and the cooling effect can last decades (Robock, 2000). In addition, the increase in albedo caused by the formation of glaciers introduced feedbacks to the preindustrial climate change. The glacier formation and the consequent vegetation change have not only contributed to the development of the Little Ice Age but also played a critical role in the present-day climate change, which will be discussed in the following section.

Current climate change and variability

Recent studies have shown that the cooling of the Little Ice Age occurred sequentially in various parts of the world (Neukom, Steiger, Gómez-Navarro, Wang, & Werner, 2019), and there were regular secondary fluctuations within the

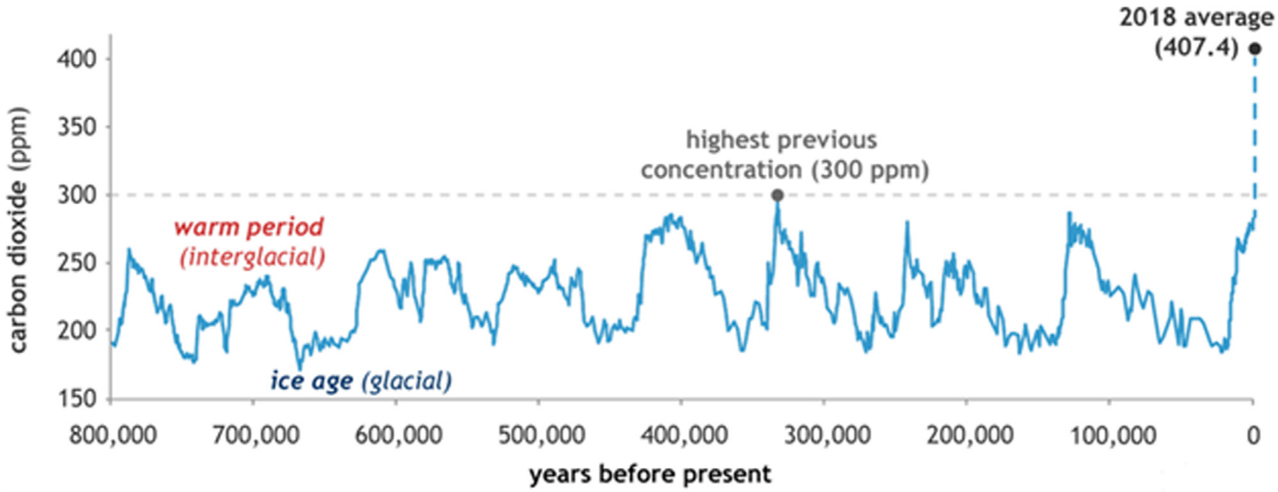

FIGURE 2.6 The abnormal increase of carbon dioxide after the Industrial Revolution (Keramidas, Vazquez, Weitzel, & Whn, 2020). *Keramidas, K., Diaz Vazquez, A., Weitzel, M., Vandyck, T., Tamba, M., Tchung-Ming, S., . . . Whn, X. (2020). Global energy and climate outlook 2019: Electrification for the low-carbon transition: The role of electrification in low-carbon pathways, with a global and regional focus on EU and China. https://doi.org/10.13140/RG.2.2.23781.35043.*

Little Ice Age. Unlike all climate fluctuations in the past 2000 years, the warming after the industrial revolution was almost synchronized globally. These findings indicate that the explosive growth of human activities has significantly contributed to global warming since 1850 (Royal Society & US National Academy of Science, 2020).

According to NASA (https://climate.nasa.gov/), evidence of climate change has been reported from multiple metrics. The CO_2 concentration after 1950 has been higher than the maximum during the past 800,000 years. The minimum Arctic Sea ice area has decreased by 13.1% per decade since 1979. Antarctica ice sheets lost 151 billion metric tons annually, and Greenland ice sheets lost 277 billion metric tons per year after 2002. The global sea level has risen more than 180 mm since 1850, and more than 0.33°C of ocean warming has been observed since 1969.

Reconstructed temperature records show cooling periods around 1450 and 1880 AD. The most recent cooling period can be seen around the end of the 19th century. Temperature observations and temperatures reconstructed from paleoclimate data have indicated a warming trend in the Northern Hemisphere since the late 19th century, as seen in Fig. 2.7 (Salinger, 2005).

Evidence shows that the observed present-day significant warming and climate variability are primarily attributed to human activities. Greenland, Antarctica, and tropical mountain glaciers have all provided ice cores that illustrate how the Earth's climate responded to fluctuations in greenhouse gas levels (Raynaud et al., 1993). In addition, tree rings, ocean sediments, coral reefs, and layers of sedimentary rocks all contain ancient data. According to paleoclimate evidence, the current rate of warming is nearly ten times greater than the usual rate of ice-age recovery. Also, the Vostok ice core data and NOAA Mauna Loa CO_2 record (Gaffney & Steffen, 2017) show that, after the last Ice Age, CO_2 from human activities increased more than 250 times faster than it did from natural sources (Fig. 2.6). Although temperature increased in the lower troposphere after 1850, it decreased in the upper troposphere (Randel et al., 2017), contributed by the heat-trapping effect of greenhouse gases.

Warming has been continuous over the last four decades. Human activities have led to well-mixed greenhouse gas concentrations since 1750 that increased global surface temperatures by approximately 1.1°C (IPCC, 2021). Looking at an observation-based regional breakdown of warming, Asia, Europe, and North America have seen nearly a 2°C increase in mean temperatures since 1961 (Fig. 2.8). The warming in Africa is slightly less, as mean average temperatures have increased close to 1°C since 1961 (not shown).

The contribution of human activities to climate change comes in many ways. The fossil fuel combustion required for industrial activities emits a large amount of greenhouse gases, which substantially affects the earth's radiation balance, leading to the melting of sea ice. The rapid population and economic development increase has brought about an increase in industrial and agricultural land. This land conversion has dramatically reduced the forest area, which not only weakens the ability of the forest ecosystem to absorb CO_2 but also affects aerosol content in the air (Roldin et al., 2019). Forest loss also leads to rapid changes in the surface albedo, which have a more complicated impact on climate change (Liu, 2011). Reduced forest cover increases albedo, which reduces solar radiation absorbed by the ground

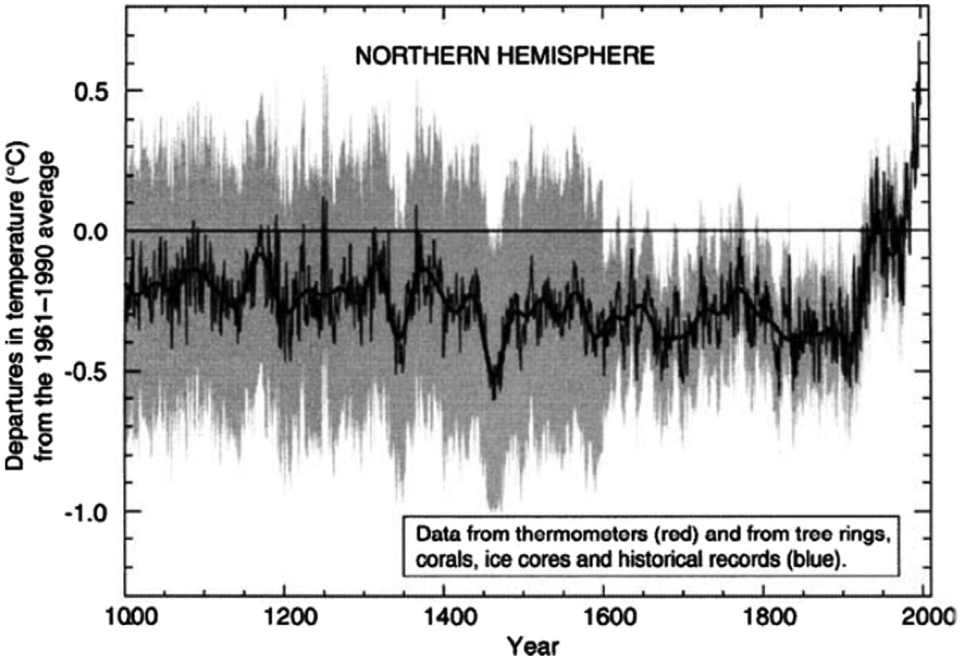

FIGURE 2.7 Northern Hemisphere average annual temperature variations over the last millennium from the proxy, historical, and instrumental observations. *Salinger, J. (2005). Climate variability and change: Past, present and future — an overview.* Climatic Change*, 9—29.*

surface and therefore reduces surface temperature. However, reduced evapotranspiration due to less absorption of solar radiation reduces latent heat loss, which increases the temperature. The net impacts of the two changes depend on many factors, such as the size of the forest coverage change and latitudes.

Projections under future climate scenarios

IPCC predicted a temperature rise of 1.5°C—5.5°C over the next century (IPCC, 2013). RCP 2.6, the lowest emissions route illustrated, anticipates fast and rapid emission reductions, resulting in around 1.5°C of warming this century. RCP 8.5, which is regarded as a high warming scenario, is expected to result in warming of more than 4.5°C by 2100, with a high-end probability of more than 6.0°C.

As a follow-up direct impact of the warming in the future, the sea level will rise 0.35—2.5 m by 2100 under RCP8.5, and the Arctic is likely to become ice-free (IPCC, 2013). Also, the frost-free season (and growing season) will lengthen. The complex effects of climate change have further affected the atmospheric ocean circulation, leading to more frequent forest fires and extreme drought events and an increase in the number and intensity of tropical storms. Precipitation patterns are expected to change in different ways depending on the region. Droughts may expand over the temperate zones and severely affect agriculture. See the next section for detailed spatial patterns of climate change.

Spatial scale

Current climate change and variability in different forests

Global temperatures are increasing, with the most significant temperature increases from climate change found in the Northern Hemisphere upper latitudes, where boreal forest resides (Fig. 2.9). Annual precipitation has also increased in boreal forest areas (Soja et al., 2007). There is high confidence in human-caused warming, according to the latest IPCC report (IPCC, 2021). The Climatic Research Unit gridded Time Series (CRU TS) dataset provides a high-resolution, monthly dataset that extends back to 1901 (Harris, Osborn, Jones, & Lister, 2020). The dataset is on a 0.5-degree by 0.5-degree grid derived from extensive weather observation station networks. Using 1961—2015 as a baseline, trends from the CRU TS data show that boreal forest regions have seen temperature increases near 1°C per decade, depending on the season (Gutiérrez et al., 2021; Iturbide et al., 2021). Winter season has seen the highest increases, with Table 2.2 showing the trends for N.W. North America, N.E. North America, N. Europe, and the Russian-Arctic regions for all seasons.

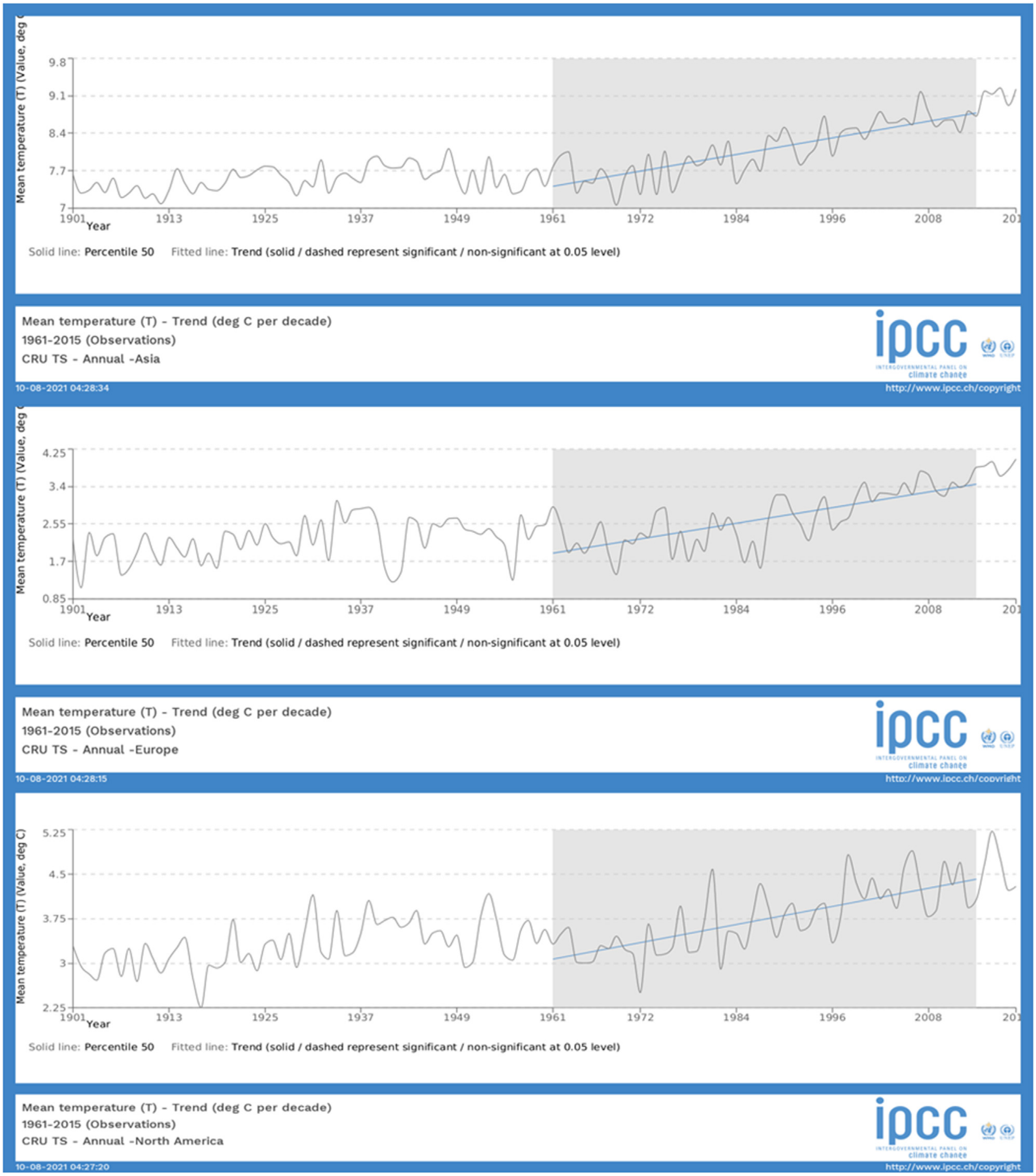

FIGURE 2.8 Observation-based regional breakdown of temperature trends derived from IPCC (2021) WGI Atlas. *Gutiérrez, J. M., Jones, R. G., Narisma, G. T., Alves, L. M., Amjad, M., Gorodetskaya, I.V., . . .Yoon, J.-H. (2021). Atlas. In V. Masson-Delmotte, P. Zhai, A. Pirani, S. L. Connors, C. Péan, S. Berger, . . . P. Zhou (Eds.), Climate change 2021: The physical science basis. Contribution of working group I to the 6th assessment report of the Intergovernmental Panel on Climate Change. Cambridge University Press. Interactive Atlas available from http://interactive-atlas.ipcc.ch/; Iturbide, M., Fernandez, M., Gutiérrez, J., Bedia, J. M., Cimadevilla, J., Diez-Sierra, E., & Yelekci, O. (2021). IPCC-WG1/Atlas: Repository supporting the implementation of FAIR principles in the IPCC-WGI Atlas. Retrieved from https://github.com/IPCC-WG1/Atlas.*

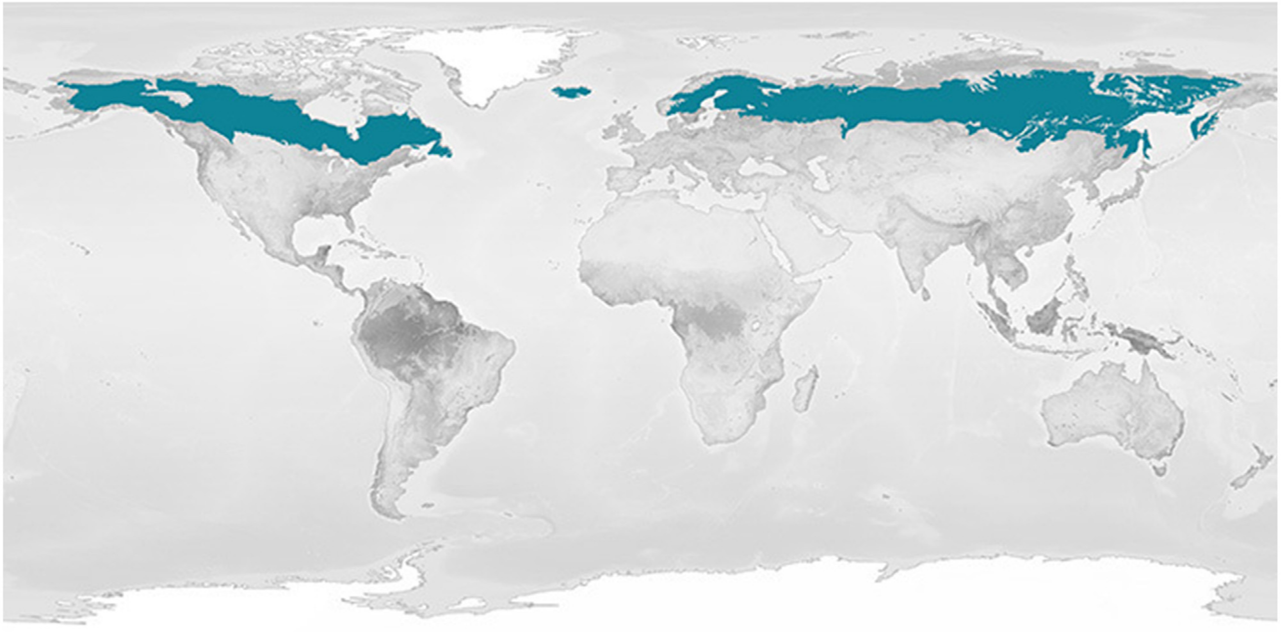

FIGURE 2.9 Location of Boreal Forest across the world (green shading). *https://earthobservatory.nasa.gov/biome/bioconiferous.php*.

TABLE 2.2 Change in mean temperature per decade in degrees Celsius from 1961 to 2015 for boreal forests.

	N.W. North America	N.E. North America	Northern Europe	Russian-Arctic
DJF	0.291	0.402	0.507	0.086
MAM	−0.127	0.23	0.344	0.829
JJA	0.212	0.331	0.399	0.388
SON	0.44	0.49	0.487	0.716

Based on CRU TS observations (Gutiérrez et al., 2021; Iturbide et al., 2021). *DJF*, December, January, and February; *MAM*, March, April, and May; *JJA*, June, July, and August; *SON*, September, October, and November.

Further breaking down the above regions into subregions, with their Koppen-Geiger climate classifications denoted in parenthesis (Kottek, Grieser, Beck, Rudolf, & Rubel, 2006). The data shows that Russian Arctic winters have warmed the most, followed by winters in Alaska and Western Canada (Fig. 2.10). Based on the same period as temperature, total annual precipitation has increased 0.010 mm day^{-1} per decade for the composite of areas with the boreal forest. This slight increase was primarily driven by increases in springtime precipitation, with N. Europe having the most significant increase at 0.089 mm day^{-1} per decade (Table 2.3). The middle latitudes are home to most temperate forests across the globe. Temperate forest experiences the widest range of variability in temperature and precipitation of all forest types. Temperate forests are located in North America, Europe, Central Asia, East Asia, Southwest and Southern South America, and Eastern Australia (Fig. 2.11; Gilliam, 2016). Composite mean temperatures (mean temperatures that consider inputs from multiple temperature detection sources) for regions with temperate forests have increased by 0.206°C $decade^{-1}$ (Iturbide et al., 2021). Most of the warming trend is driven by warming during the winter season, especially in Europe, where winters have warmed almost half a degree celcius per decade from 1961 to 2015 (Table 2.4). Total annual precipitation has slightly increased by 0.003 mm day^{-1} (~1.1 mm $year^{-1}$) per decade for temperate forest areas (Iturbide et al., 2021). The increase is driven by increased precipitation in June, July, and August (Table 2.5).

Tropical rainforests are known for their abundance of rain, receiving an average of 2000−10,000 mm $year^{-1}$ and remaining frost-free year-round (Rainforest, n.d.; earthobservatory.nasa.gov). Central America, the Caribbean, West & Central Africa, Madagascar, and South & Southeast Asia all have tropical rainforests (Fig. 2.12). On average, biomes with tropical rainforests have seen precipitation increase by 0.027 mm day^{-1} per decade based on observations from

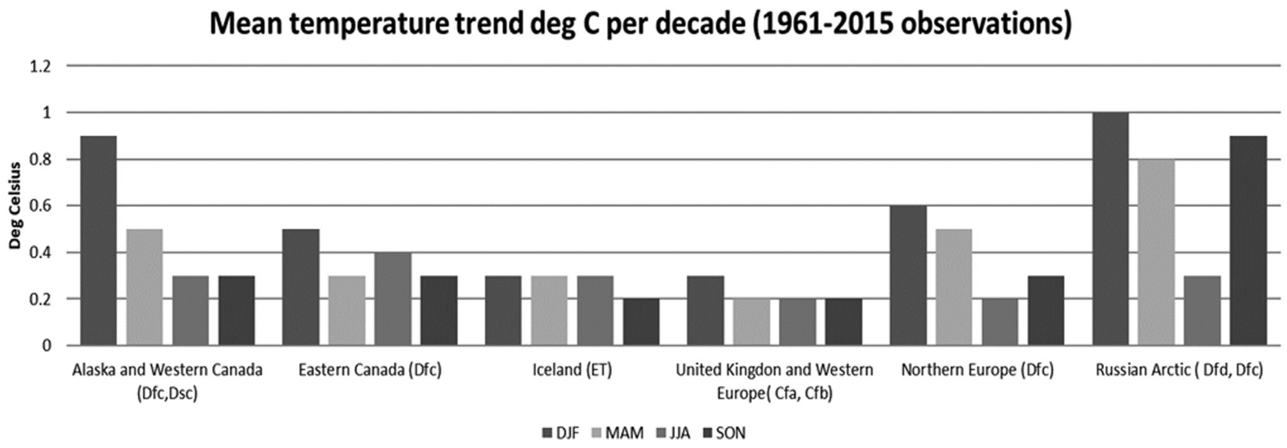

FIGURE 2.10 Mean temperature trend in degrees Celsius per decade based on observations from 1961 to 2015. The graph shows ecoregions that have boreal forests with their associated Koppen-Geiger climate classification (Kottek et al., 2006) in parentheses. A tabular breakdown of the Koppen-Geiger climate classification definitions can be found in Table 3.4. The trend for each season is shown on the *x*-axis, and the *y*-axis represents degrees Celsius per decade. *DJF*, December, January, and February; *MAM*, March, April, and May; *JJA*, June, July, and August; *SON*, September, October, and November IPCC (2021). *Derived from IPCC (2021) WGI Atlas (Gutiérrez, J. M., Jones, R. G., Narisma, G. T., Alves, L. M., Amjad, M., Gorodetskaya, I.V., . . .Yoon, J.-H. (2021). Atlas. In V. Masson-Delmotte, P. Zhai, A. Pirani, S. L. Connors, C. Péan, S. Berger, . . .P. Zhou (Eds.), Climate change 2021: The physical science basis. Contribution of working group I to the 6th assessment report of the Intergovernmental Panel on Climate Change. Cambridge University Press. Interactive Atlas available from http://interactive-atlas.ipcc.ch/; Iturbide, M., Fernandez, M., Gutiérrez, J., Bedia, J. M., Cimadevilla, J., Diez-Sierra, E., & Yelekci, O. (2021). IPCC-WG1/Atlas: Repository supporting the implementation of FAIR principles in the IPCC-WGI Atlas. Retrieved from https://github.com/IPCC-WG1/Atlas).*

TABLE 2.3 Percent change in total precipitation shown in mm day^{-1} per decade for boreal forests.

	N.W. North America	N.E. North America	Northern Europe	Russian-Arctic
DJF	−0.025	−0.008	0.089	−0.01
MAM	0.003	0.008	0.023	0.003
JJA	0.028	0.011	0.063	0.001
SON	0.005	0.009	0.009	−0.002

Based on CRU TS observations using a baseline of 1961−2015. *DJF*, December, January, and February; *MAM*, March, April, and May; *JJA*, June, July, and August; *SON*, September, October, and November (Gutiérrez et al., 2021; Iturbide et al., 2021).

1961 to 2015 (Iturbide et al., 2021). During this period, precipitation has increased in all regions, apart from the African region (Table 2.6; Gutiérrez et al., 2021; Iturbide et al., 2021). The Caribbean region has experienced the most significant increase in precipitation. As with boreal and temperate forests, regions with tropical forests have warmed from 1961 to 2015 (Table 2.7).

Future climate change and variability

The periods assessed by the IPCC AR6 working groups for possible future climates are near-term (2015−2040), mid-term (2041−2060), and long-term (2081−2100) (IPCC, 2021). The predicted changes for each time are relative to a baseline from 1850 to 1900. A suite of anthropogenic drivers, including greenhouse gas emissions and land cover scenarios drive the CMIP6 models. The scenarios have an assumed starting year of 2015, and one example, SSP3-7.0, assumes high greenhouse gas emissions and CO_2 emissions that will double from current levels by 2100 (IPCC, 2021). The SSP3-7.0 represents the medium to high end of the range of future forcing and lies between RCP6.0 and RCP8.5 from the previous IPCC assessment (Abram, Gattuso, Prakash, & Pandey, 2019). Research conducted by Brown, Li, Cordero, and Mauget (2015) compared the model-simulated global warming signal to observations using empirical estimates of unforced noise (EUN) and found that recently observed global mean temperatures and trends were close to a

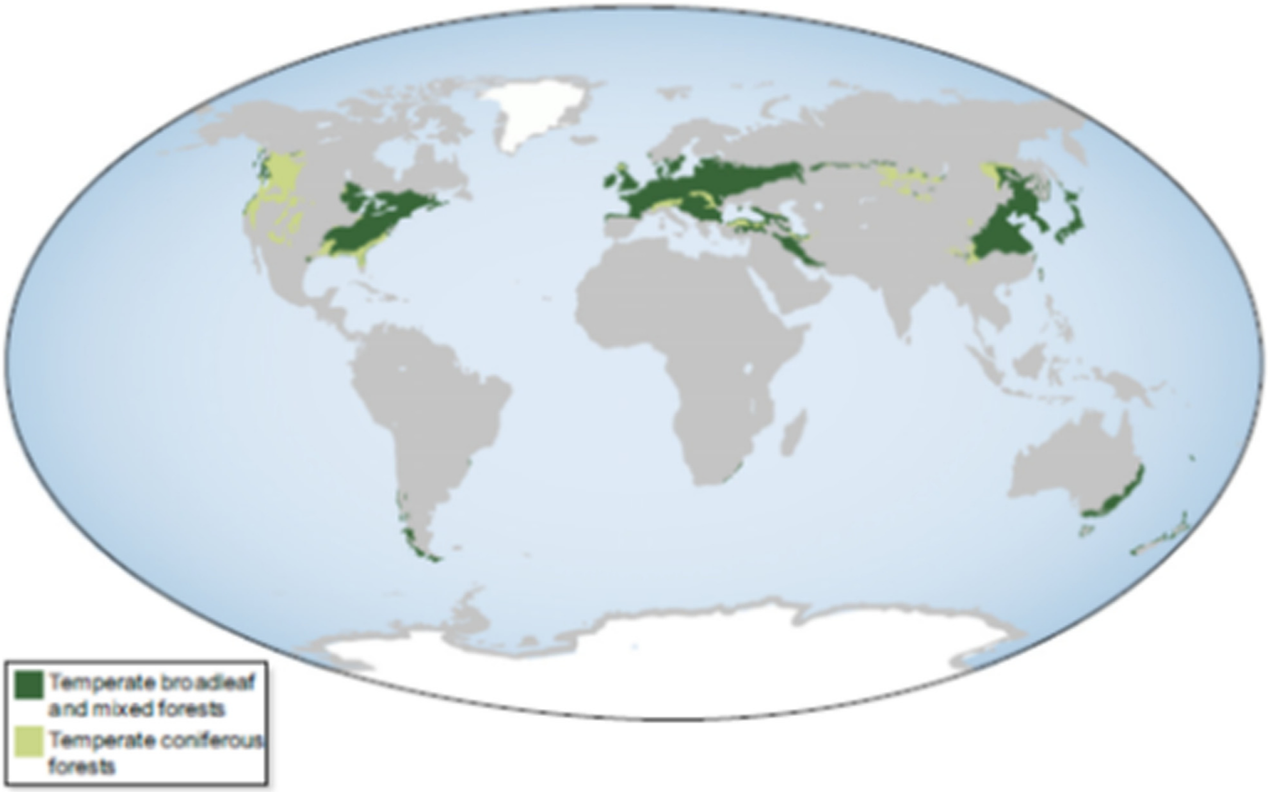

FIGURE 2.11 Global distribution of temperate forests. *Adapted from Gilliam, F.S. (2016). Forest ecosystems of temperate climatic regions: From ancient use to climate change.* New Phytologist, *212(4), 871–887. https://doi.org/10.1111/nph.14255*.

TABLE 2.4 Change in mean temperature per decade in degree Celsius from 1961 to 2015 for temperate forests.

	W. North America	E. North America	Europe	Central Asia	East Asia	S.W and S. South America	E. Australia
DJF	0.221	0.284	0.436	0.270	0.263	0.127	0.146
MAM	0.235	0.184	0.333	0.299	0.209	0.045	0.087
JJA	0.178	0.023	0.334	0.282	0.121	0.072	0.153
SON	0.135	0.112	0.194	0.257	0.197	0.071	0.2

Based on CRU TS observations (Gutiérrez et al., 2021; Iturbide et al., 2021). *DJF*, December, January, and February; *MAM*, March, April, and May; *JJA*, June, July, and August; *SON*, September, October, and November.

TABLE 2.5 Percent change in total precipitation shown in mm day^{-1} per decade for temperate forests.

	W. North America	E. North America	Europe	Central Asia	East Asia	S.W and S. South America	E. Australia
DJF	−0.021	−0.001	0.015	0.001	0.018	0.007	0.015
MAM	0.027	0.028	0.005	−0.023	−0.011	−0.008	−0.18
JJA	−0.031	0.055	0.012	0.007	0.02	0.005	0.016
SON	−0.021	0.066	0.019	0.013	−0.045	−0.034	−0.04

Based on CRU TS observations using a baseline of 1961–2015. *DJF*, December, January, and February; *MAM*, March, April, and May; *JJA*, June, July, and August; *SON*, September, October, and November (Gutiérrez et al., 2021; Iturbide et al., 2021).

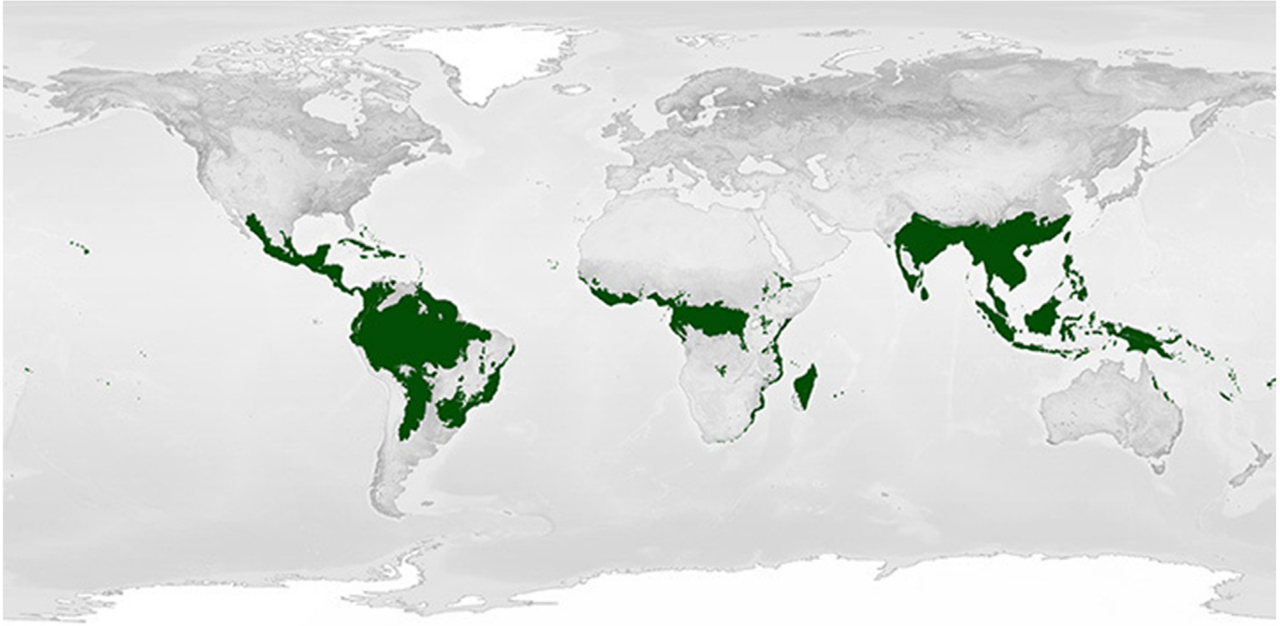

FIGURE 2.12 Global distribution of tropical forest. *Adapted from NASA Earth Observatory.*

TABLE 2.6 Percent change in total precipitation shown in mm day^{-1} per decade for temperate forests.

	Central America	Caribbean	West Africa, Central Africa, and Madagascar	South Asia and S.E. Asia
DJF	−0.03	0.026	−0.005	0.072
MAM	0.038	0.086	−0.059	0.068
JJA	−0.013	0.087	−0.059	0.025
SON	0.047	0.106	−0.007	0.069

Based on CRU TS observations using a baseline of 1961−2015. *DJF*, December, January, and February; *MAM* March, April, and May; *JJA*, June, July, and August; *SON*, September, October, and November (Gutiérrez et al., 2021; Iturbide et al., 2021).

TABLE 2.7 Change in mean temperature per decade in degree Celsius from 1961 to 2015 for tropical forests.

	Central America	Caribbean	West Africa, Central Africa, and Madagascar	South Asia and S.E. Asia
DJF	0.21	0.196	0.143	0.16
MAM	0.219	0.144	0.172	0.128
JJA	0.209	0.178	0.146	0.125
SON	0.169	0.171	0.149	0.138

Based on CRU TS observations (Gutiérrez et al., 2021; Iturbide et al., 2021). *DJF*, December, January, and February; *MAM*, March, April, and May; *JJA*, June, July, and August; *SON*, September, October, and November.

signal corresponding to the RCP8.5 emission scenario. Additionally, observations were not inconsistent with a forced signal corresponding to the RCP6.0 emission scenario. With this information, the authors felt that SSP3-7.0 would be a "best practice" choice to represent current and future forcing trends.

Based on SSP3-7.0, tropical forests in Central America and the Caribbean will experience a decrease in precipitation in the near, mid, and long term. Long-term projections show a 14.2% and 15.3% decrease in Central America and the Caribbean, respectively (Table 2.8) relative to 1850−1900. The opposite is expected for tropical forests in Africa and Asia, as precipitation is expected to increase during the 21st century. Examining the percent change in total precipitation for tropical forests, increases in fall and winter precipitation are the dominant trends in the expected increases in precipitation (Fig. 2.13). All areas with tropical forests are expected to warm in the near, mid, and long term. Warming is expected to be above 1°C in the near-term and approaching 3°C or greater in the long term (Table 2.9).

Using SSP3-7.0 as a guideline, all regions with temperate forests are expected to warm from 2015−2100 (Table 2.10). In the near term, Central Asia will warm the least, at half a degree Celsius relative to 1850−1900. The end-of-century warming will be most significant for Central Asia, as it is expected to warm by 6.2°C. Europe is projected to warm the most, increasing 2.3°C in the near-term and 3.4°C in the mid-term. Near, mid, and long-term precipitation is projected to decrease in East Asia, South America, and Australia relative to the 1850−1900 baseline (Table 2.11). South America is projected to have the largest percent decrease in precipitation. In contrast, near, mid, and long-term precipitation is expected to increase in North America, Europe, and Central Asia. As a result, long-term annual total precipitation is expected to rise by 13.8% relative to 1850−1900.

TABLE 2.8 **CMIP6 projected percent changes in total precipitations for tropical forest near-term, middle-term, and long-term trends.**

	Near-term (2021−2040)	Mid-term (2041−2060)	Long-term (2081−2100)
Central America	−4.7	−7.5	−14.2
Caribbean	−3.3	−6.3	−15.3
Africa	5.2	6.9	8.9
Asia	0.5	2.2	6.2

Based on the IPCC (2021) SSP3-7.0 scenario and relative to the 1850−1900 baseline (Gutiérrez et al., 2021; Iturbide et al., 2021).

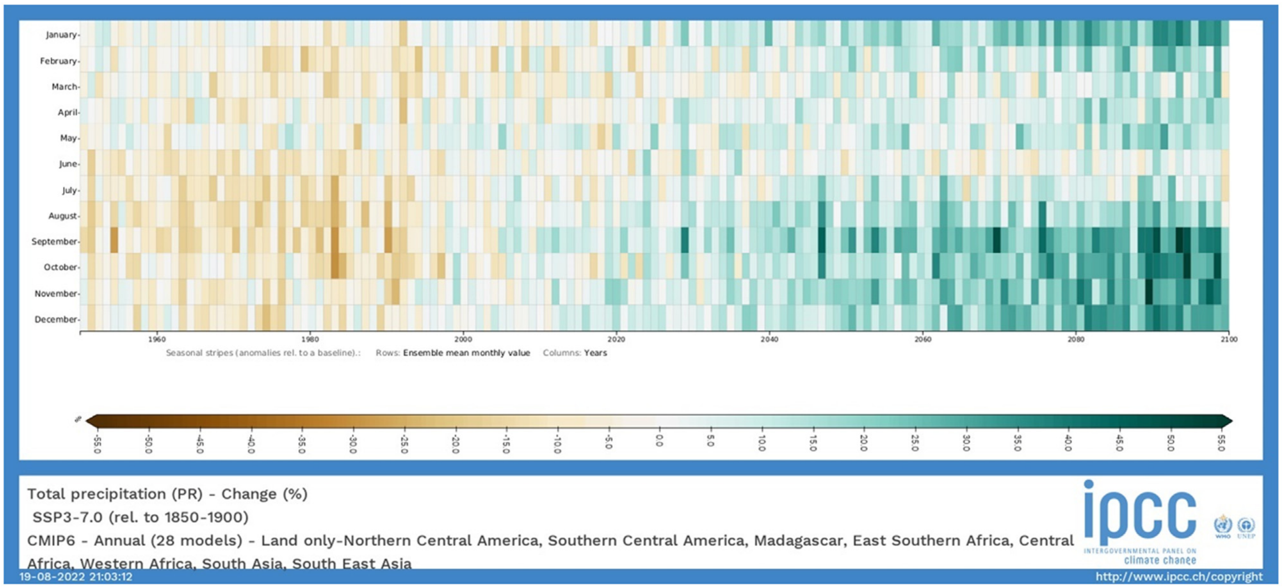

FIGURE 2.13 Percent change in total precipitation over land for tropical forests. *Adapted from IPCC (2021) WGI Atlas (Iturbide, M., Fernandez, M., Gutiérrez, J., Bedia, J. M., Cimadevilla, J., Diez-Sierra, E., & Yelekci, O. (2021). IPCC-WG1/Atlas: Repository supporting the implementation of FAIR principles in the IPCC-WGI Atlas. Retrieved from https://github.com/IPCC-WG1/Atlas).*

TABLE 2.9 CMIP6 projected percent changes in mean temperature for tropical forest near-term, middle-term, and long-term trends.

	Near-term (2021–2040)	Mid-term (2041–2060)	Long-term (2081–2100)
Central America	1.7	2.5	4.4
Caribbean	1.4	2.1	3.6
Africa	1.5	2.3	4.2
Asia	1.3	2	3.7

Based on the IPCC (2021) SSP3-7.0 scenario and relative to the 1850–1900 baseline (Gutiérrez et al., 2021; Iturbide et al., 2021).

TABLE 2.10 CMIP6 projected percent changes in mean temperature for the temperate forest for near-term, middle-term, and long-term trends.

	Near-term (2021–2040)	Mid-term (2041–2060)	Long-term (2081–2100)
W. North America	2	2.9	5.1
E. North America	2.1	3	5.3
Europe	2.3	3.4	5.6
W. Central Asia	0.5	2.2	6.2
East Asia	1.4	2.2	4.3
South America	1.5	2.2	3.7
Australia	1.6	2.4	4.2

Based on the IPCC (2021) SSP3-7.0 scenario and relative to the 1850–1900 baseline (Gutiérrez et al., 2021; Iturbide et al., 2021).

TABLE 2.11 CMIP6 projected percent changes in total precipitations for temperate forest near-term, middle-term, and long-term trends.

	Near-term (2021–2040)	Mid-term (2041–2060)	Long-term (2081–2100)
W. North America	2	3.8	7
E. North America	3.9	5.7	10.4
Europe	4.9	5.8	7.8
Central Asia	5.4	4	13.8
East Asia	−3.8	−2	4.4
South America	−5.1	−7.2	−11.4
Australia	−1.4	−1.5	−1.3

Based on the IPCC (2021) SSP3-7.0 scenario and relative to the 1850–1900 baseline (Gutiérrez et al., 2021; Iturbide et al., 2021).

Projected changes in mean temperature indicate that regions with boreal forests will experience more significant warming compared to temperate and tropical forests (Table 2.12). Boreal forests are also projected to experience the highest percentage increase in annual precipitation (Table 2.13). Projected changes for boreal forests are again based on the SSP3-7.0 scenario and are relative to the 1850–1900 baseline. Near-term increases in temperature for N.W. North America, N.E. North America, Northern Europe, and the Russian-Arctic are all projected to eclipse 2°C, with the Russian-Arctic region increasing by 3.5°C. Long-term mean temperatures are projected to increase by at least 5°C for all regions with boreal forests. Boreal forest regions are also expected to see substantial increases in annual precipitation. Near-term precipitation is expected to increase by 6%–13%, mid-term increases from 8% to 19%, and long-term

TABLE 2.12 CMIP6 projected percent changes in mean temperature for boreal forest near-term, middle-term, and long-term trends.

Temperature	Near-term (2021–2040)	Mid-term (2041–2060)	Long-term (2081–2100)
N.W. North America	2.7	3.9	6.8
N.E. North America	3.2	4.6	8
Northern Europe	2.3	3.3	5.3
Russian-Arctic	3.5	5	8.5

Based on the IPCC (2021) SSP3-7.0 scenario and relative to the 1850–1900 baseline (Gutiérrez et al., 2021; Iturbide et al., 2021).

TABLE 2.13 CMIP6 projected percent changes in total precipitations for boreal forest near-term, middle-term, and long-term trends.

	Near-term (2021–2040)	Mid-term (2041–2060)	Long-term (2081–2100)
N.W. North America	7.5	11.3	21.7
N.E. North America	9.5	13.8	24.6
Northern Europe	6.2	8.3	14
Russian-Arctic	13.1	19.1	35

Based on the IPCC (2021) SSP3-7.0 scenario and relative to the 1850–1900 baseline (Gutiérrez et al., 2021; Iturbide et al., 2021).

increases in total annual precipitation are expected to increase from 14% to 35%. The Russian-Arctic region is projected to experience the most significant warming and increases in precipitation.

Note that focus on the three general types of forest ecosystems (boreal, temperate, and tropical) at continental and subcontinental scales. Researchers working on other chapters used the information on these scales to evaluate the forest impacts of climate change. For brevity, subregional tables and figures are not shown here but are shown in the appendix. This section's CMIP6 climate change information has resolutions high enough for regional and subregional forest ecosystems but not for local forests. In the latter case, downscaled information is needed, which is not used in this section.

Evaluating climate change and variability projections for forest impact assessments

Selection of appropriate climate information

There is no shortage of climate information on which to base forest impact assessments. The climate community produces a prodigious amount of information on future climatic conditions ranging from peer-reviewed journal articles to the complex datasets generated by climate models. However, as described by Barsugli et al. (2013), the "practitioner's dilemma" has transformed from a lack of information at appropriate scales to the problem of having to wade through a vast amount of data options and choose an appropriate dataset, assess its credibility, and use it wisely. Ideally, this decision would involve assessing a given model's suitability for a particular geographic region or decision-making application. However, datasets are more often selected based on availability, the convenience of format, familiarity with the provider, availability of variables of interest, and suitable spatial resolution than any systematic comparison.

Assessing a dataset's applicability to a specific problem requires expert knowledge of the strengths and weaknesses of different models, and such information is often not readily available to end users (Briley et al., 2020). To begin reducing this "practitioner's dilemma," some boundary organizations (i.e., the organizations that operate in multiple fields on different scales and with different stakeholders) have emerged which serve as knowledge brokers to bridge the gap between the producers and consumers of climate information (Briley, Ashley, Rood, & Krmenec, 2017). While these boundary organizations are often of limited geographic scope and all regions of the globe are not covered, some of the general practices these organizations follow to best inform consumers of climate information can provide useful guidance to those curating climate products for their own assessment.

Briley et al. (2020) describe a suite of consumer report-style tools to guide the selection of appropriate climate information. While their specific products are targeted at a particular geographic region, we examine the general qualities that their reports attempt to highlight to aid users in identifying appropriate climate information. One report is a climate model checklist for choosing GCMs for a particular location and application. Criteria in the checklist focus on geographic coverage, temporal coverage, both historical observations and projections, time steps of the model output (e.g., daily or monthly), and the available variables. While Briley et al. (2020) focus their discussion on global models, the elements of their checklist are equally valid for evaluating the suitability of downscaled climate information. It is also essential to consider specific factors for some applications. In the example checklist supplied by Briley et al. (2020), the geographic region of interest is the Great Lakes region of the United States. A critical aspect of the climate of this region is tied to ice formation on the lakes. The checklist requires recommended models to possess at least a one-dimensional lake submodel capable of forming ice cover and specifies that the model should reproduce current trends in ice cover. While every region may not have a need as specific as the inclusion of an ice submodel, regions will have defining aspects of their local climate, which the model should reproduce well for it to be considered for use in an assessment.

Strategies for selecting climate information

Future global, regional, and local climate change and variability in response to the greenhouse effect are projected based on the assumed emission scenarios, description of physical processes in climate models and ESMs, and applications of downscaling techniques, which are determined by many complex factors (Fig. 2.14). As described in

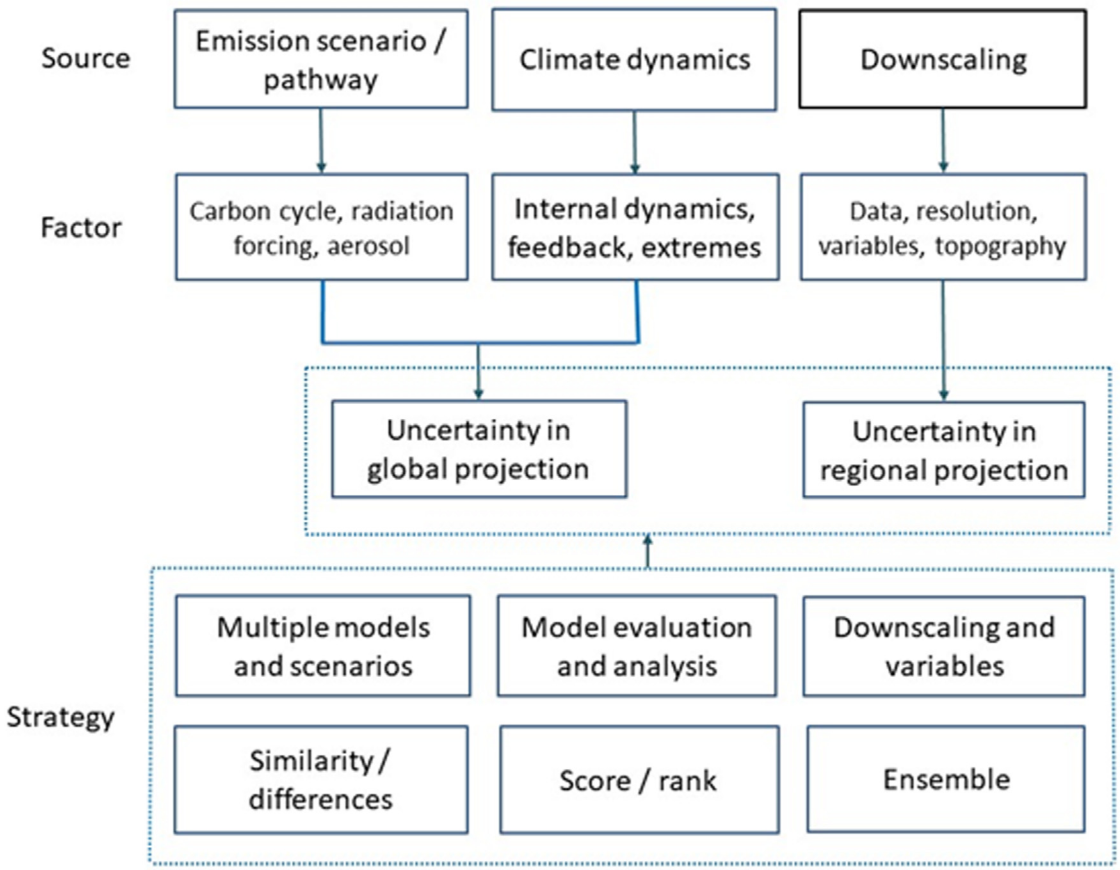

FIGURE 2.14 Uncertainties with climate change projections and impacts on fire evaluations.

Section 3.2, many limitations exist with these factors, leading to uncertainties in the magnitudes, seasonal patterns, temporal pace, and spatial distributions of future climate projections (Giorgi, 2010; Hawkins, 2013). For example, Li et al. (2021) showed significant historical and future precipitation uncertainties and extremes from 8 CMIP5 and CMIP6 GCMs over 21 global regions.

The uncertainties are a great challenge, and reducing the impact of uncertainty is key to evaluation studies of the climate impacts on forests (Fajardo, Corcoran, Roehrdanz, Hannah, & Marquet, 2020; Vano, Kim, Rupp, & Mote, 2015). Many strategies can be used to help select models and manage uncertainties, some of which are listed in Fig. 2.14 and described below.

1. Multiple models and scenarios. Using multiple climate models can help understand how the results of an impact evaluation study vary with internal model dynamics and physics. For example, NARCAP dynamical downscaling can test up to four GCMs and six RCMs. There is no assumption of the possibility of the occurrence of a specific scenario, though there is a scenario that represents a more moderate case in contrast to extreme cases. Using multiple emission scenarios/pathways can examine the ecosystem response to external model forcing under various intensities.
2. Validation and analysis of projections. Projections by a specific GCM/ESM are usually only analyzed across some (not all) regions. This analysis is especially true for regional and local projections downscaled from global projections using RCMs or local data. Thus, it is common to select the projections made by the models developed for the region for an impact evaluation study. Also, it would help improve the study by conducting bias correlation by a user based on local meteorological and/or ecosystem data.
   Depending on the application, understanding basic summary statistics of model performance can be insufficient for evaluating model suitability (Thorarinsdottir, Sillmann, Haugen, Gissibl, & Sandstad, 2020). Alternatively, evaluations should focus on comparing probability distributions of model output to that of observed data (Guttorp, 2011; Rupp, Abatzoglou, Hegewisch, & Mote, 2013; Sheffield et al., 2013; Thorarinsdottir, Gneiting, & Gissibl, 2013), particularly when climate extremes are of interest. Simple summary statistics may not provide sufficient information to properly evaluate the underlying processes, as extremes are, by definition, rare events (Maraun et al., 2017). Thorarinsdottir et al. (2020) evaluate CMIP5 and CMIP6 simulations of monthly maximum and minimum near-surface air temperature over Europe and North America against both observation-based data and reanalysis products. Overall, their findings indicate climate models show better skill when compared against gridded reanalysis products than when compared against extremes based on observational data.
3. Availability of downscaling and variables. Some tools and datasets provide worldwide regional and local downscaling of global projections. Others provide downscaling for specific geographic regions. There are also differences in spatial and temporal resolutions. Another important consideration while selecting a tool/product is the available variables. The restriction in variable availability is one of the significant differences between dynamical and statistical downscaling. Also, some downscaling tools/products are developed for specific applications of, for example, hydrology (Alder & Hostetler, 2019) and wildfires (Abatzoglou & Brown, 2012).
   The choice of downscaling approach and the spatial resolution of the observations used to train the downscaling model can have unintended impacts. For example, Pourmokhtarian, Driscoll, Campbell, Hayhoe, and Stoner (2016) examined the effects of three statistical climate downscaling techniques on projections from a forest biogeochemical watershed model (PnET-BGC) for a watershed in the White Mountains of New Hampshire, USA. Although the choice of downscaling method slightly affected model results, all downscaling methods were highly sensitive to the observations used in developing the downscaled data, as projections differed drastically between station-based observations and grid-based. A closer examination of the impacts of using gridded versus station-based observations revealed little effect on temperatures. However, precipitation impacts were profound, substantially altering the daily distribution of precipitation events and their magnitude. These findings illustrate how choices in the development of a climate dataset can influence subsequent projections of ecosystem responses, particularly for precipitation in mountainous landscapes. For example, Jiang et al. (2018) found significant disagreement in precipitation in elevated areas of the US Pacific Northwest among five statistically downscaled datasets.
4. Similarity/differences. Some assessments focus on using a single model or synthesis report for a region; others are more interested in evaluating climate conditions based on a range of possible future climate scenarios derived from a suite of models. In selecting among the wide range of climate models available for building a collection of scenarios, it is essential to consider the genealogy of the different models (Knutti, Masson, & Gettelman, 2013). Several studies (e.g., Sabzevari, Martínez-Muñoz, & Suárez, 2022) have shown that selecting a large and heterogenous ensemble of GCMs produces the most reliable results, rather than picking a small number of GCMs. Even picking just the "best" GCMs is worse than picking a heterogenous set that includes poorly performing GCMs.

Climate models are continually evolving, with new versions inheriting many of the strengths and weaknesses of their predecessors but also benefiting from other models through the exchange of code and ideas between modeling groups. Using a similarity metric based on the Kullback-Leibler divergence, a distance metric that considers the spatial field of monthly values in a control simulation without external forcing, Knutti et al. (2013) constructed "family trees" of climate models through hierarchical clustering (Fig. 2.15). For a broader range of potential climate scenarios, models should be selected from different branches of the tree.

5. Score/rank. Many studies have compared models that participated in the CMIP project. Besides validation for projections of historical climate, results are available for differences of each model from the average of all models selected to compare. For example, Miao et al. (2014) compared 22 CMIP5 models in projecting

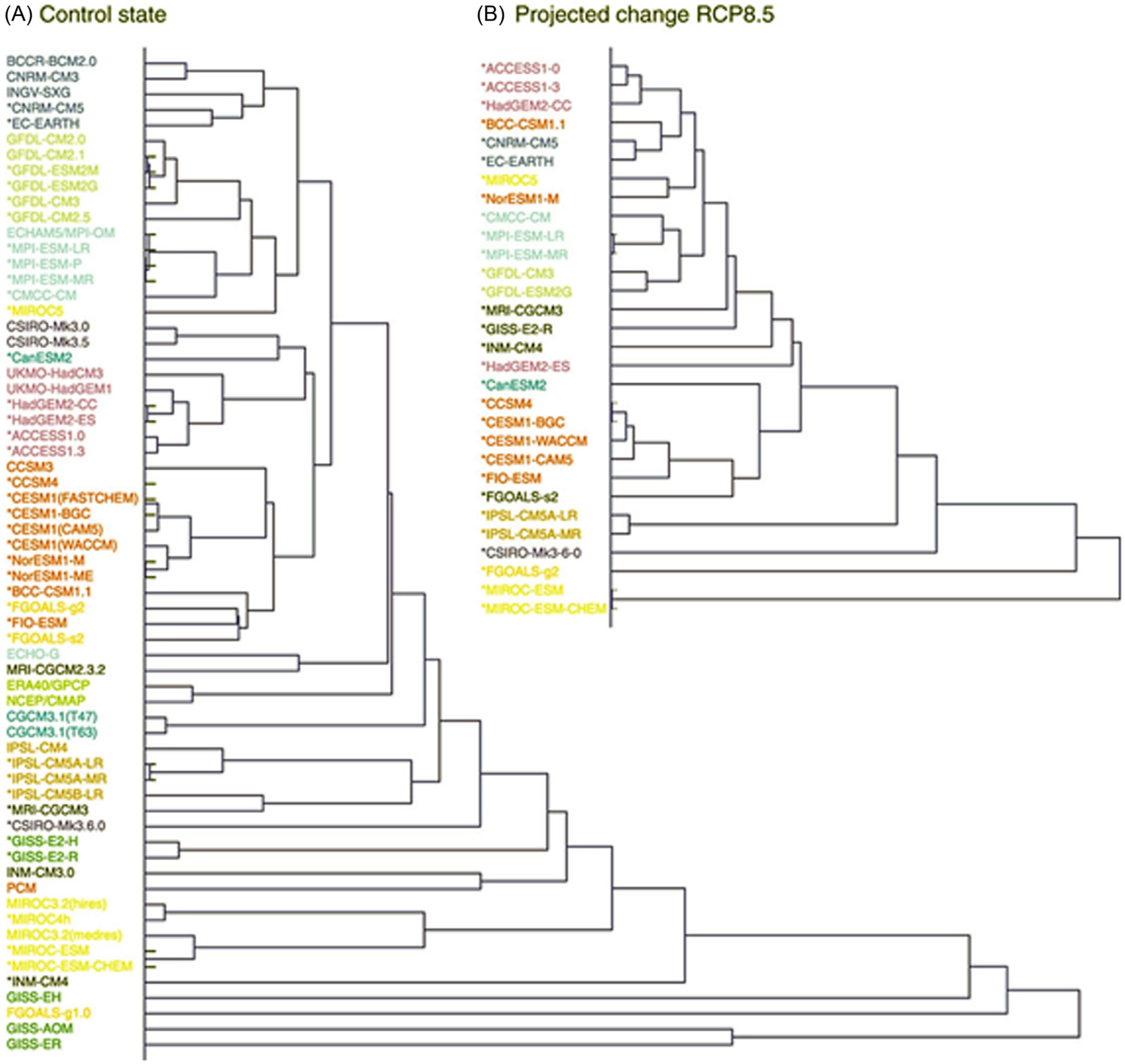

FIGURE 2.15 (A) The model "family tree" from CMIP3 and CMIP5 (marked with asterisks) control climate plus observations (ERA40/GPCP and NCEP/CMAP), shown as a dendrogram (a hierarchical clustering of the pairwise distance matrix for temperature and precipitation fields, see text). Some of the models with similarities in code or produced by the same institution are marked with the same color. Models appearing in the same branch are close, and similarity is more significant the more to the left the branches separate (for a detailed description of the method, see Masson and Knutti, 2011). (B) As with (A) but based on the projected change in temperature and precipitation fields for the end of the 21st century in the RCP8.5 scenario relative to the control. *From Knutti, R., Masson, D., & Gettelman, A. (2013). Climate model genealogy: Generation CMIP5 and how we got there.* Geophysical Research Letters, 40*, 1194–1199.*

historical and future surface temperatures over Northern Eurasia. The differences among the models in seasonal and annual mean values and trends over the past century under various RCPs are provided. An evaluation study could select one or more models with similar results to most other models. Some studies score climate models using different criteria. For example, Fasullo (2020) used an objective approach to score CMIP climate models through an evaluation against satellite and reanalysis datasets. The criteria included minimum sensitivity to internal variability, external forcings, and model tuning. Scores are between 0.46 and 0.78 for 24 CMIOP3 models, 0.67 and 0.81 for more than 70 CMIP5 models, and 0.74 and 0.86 for 22 CMP6 models. The scores could be used as one reference for GCM selection.

6. Ensemble. The ensemble is an approach to develop a climate change projection based on multiple projections. Multiple projections could be made by multiple emission scenarios/pathways, GCMs, downscaling products, and/or a specific GCM but with various initial conditions, parameters, and physical/chemical schemes/parameterizations. The same or different weighting factors could be used for all projections. Ensemble projection is an efficient way to reduce uncertainties from multiple sources.

Summary

This chapter on climate change and variability provides a basic understanding of climate fundamentals, the temporal variations and spatial patterns in the past, present, and future, and applications to assessing forest impacts. The information summarized below is expected to support the efforts to evaluate the impacts of climate change and variability on various forest processes described in succeeding chapters. The main take-home points of this chapter include:

1. Global climate and ESMs have been developed and validated to simulate atmospheric processes and interactions with other climate system components due to natural and anthropogenic forcing. They are potent tools for projecting atmospheric responses to the greenhouse effect.
2. IPCC has developed several climate change scenarios, including SRESs, RCPs, and SSPs. In addition, the CMIP has been conducted to project future global climate change, which is further used to obtain regional and local climate change scenarios using dynamical and statistical techniques.
3. The observed global temperature increased by about 0.85°C in the past 150 years, more than half of which was caused by elevated atmospheric CO_2 concentrations, which have increased nearly 50% since the industrial revolution era. The trends are expected to continue this century, warming from 1.5°C under RCP 2.6 to more than 4.5°C under RCP8.5 by the end of this century.
4. Boreal Forest is projected to experience higher temperature and annual precipitation percentage increases than temperate and tropical forests, with long-term temperature increases under SSP3-7.0 by at least 5°C for the boreal forest. Near-term temperature is projected to increase by 3.5°C the Russian-Arctic region and 2°C for N.W. North America, N.E. North America, and N. Europe. Precipitation will increase for tropical forests in Africa and Asia but decrease for tropical forests in Central America and the Caribbean.
5. Some organizations that operate in multiple fields on different scales and with different stakeholders have emerged to bridge the gap between the producers and users of climate information. This linkage helps select appropriate climate information to assess forest impacts of climate change for a particular geographic region or decision-making application. The impacts of the uncertainty in climate change and variability projections can be reduced by considering multiple models and scenarios, model validation and analysis, availability of downscaling and variables, model similarity, score/rank, and ensemble analysis.

Acknowledgments

The authors thank three anonymous reviewers for providing in-depth and constructive comments and suggestions and editing the draft manuscript, which has helped improve both the science and writing of our manuscript. This work was supported by an agreement on fire and smoke impacts of air quality and human health study between the USDA Forest Service and the Oak Ridge Institute for Science and Education (ORISE).

Appendix

A value of zero represents no discernable trend in the ecoregion.

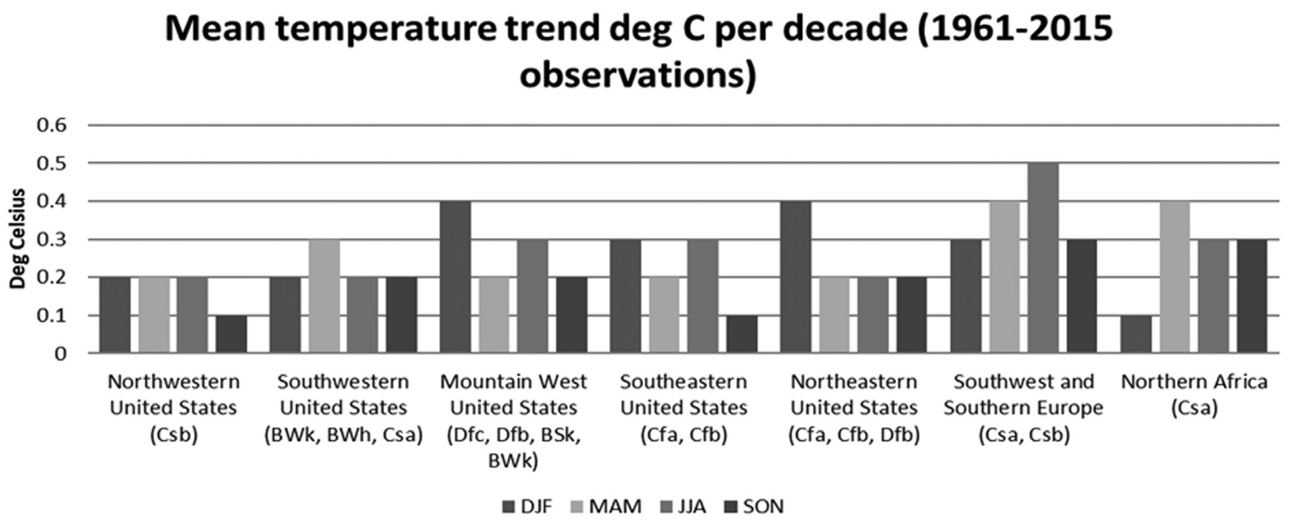

FIGURE A2.1 Mean temperature trend in degrees Celsius per decade based on observations from 1961 to 2015. Shown in the graph are ecoregions that have temperate forest with their associated Koppen-Geiger climate classification (Kottek et al., 2006) in parentheses. The trend for each season is shown on the *x*-axis and the *y*-axis represents degrees Celsius per decade.

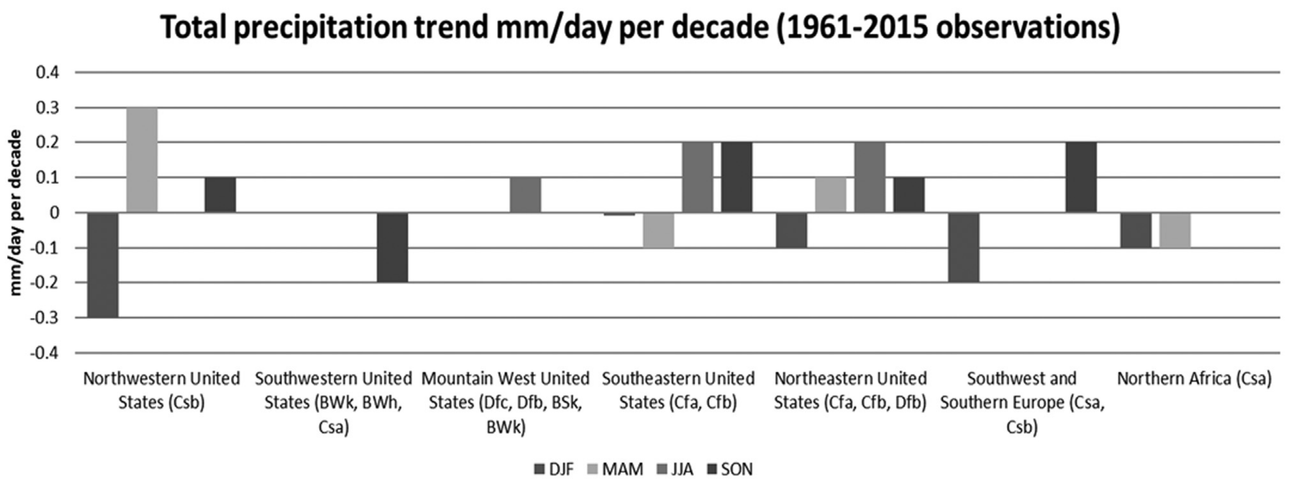

FIGURE A2.2 Total precipitation trend in mm day^{-1} per decade for ecoregions with temperate forest. A value of zero represents no discernable trend in the ecoregion.

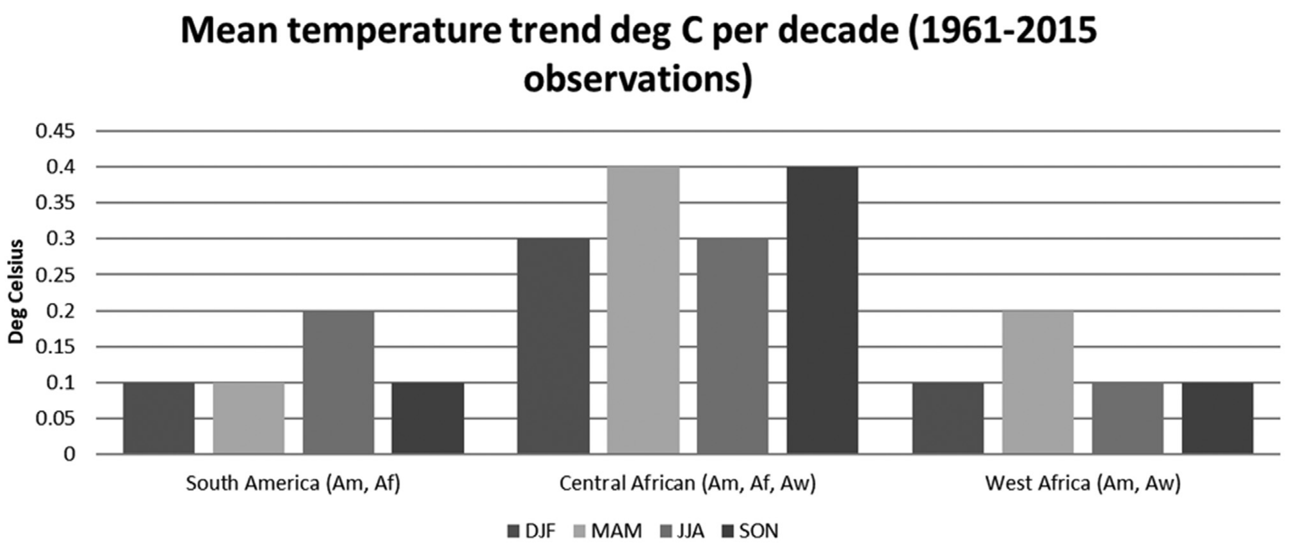

FIGURE A2.3 Mean temperature trend in degrees Celsius per decade based on observations from 1961 to 2015. Shown in the graph are ecoregions that have tropical forest with their associated Koppen-Geiger climate classification (Kottek et al., 2006) in parentheses. The trend for each season is shown on the *x*-axis and the *y*-axis represents degrees Celsius per decade.

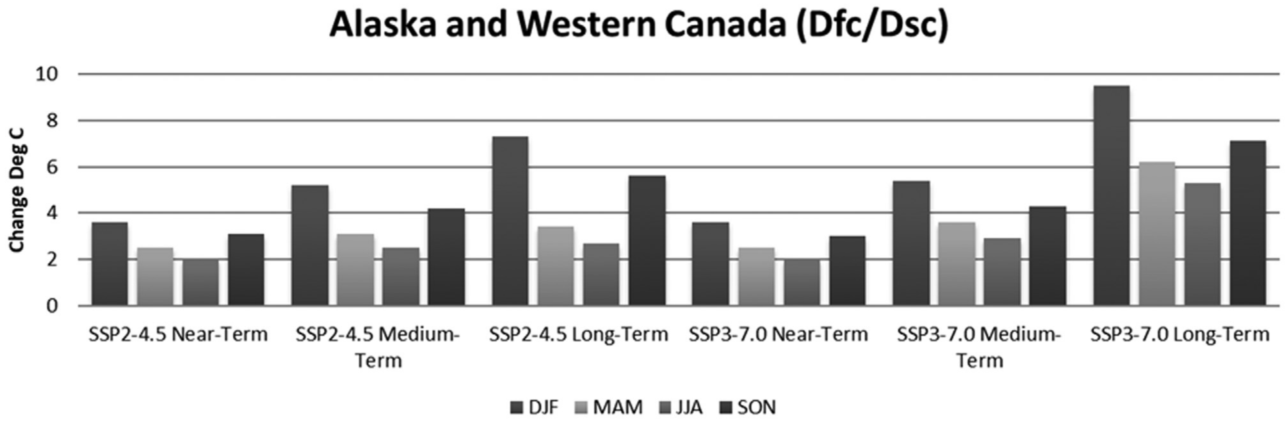

FIGURE A2.4 Near-term, medium-term, and long-term changes in temperature by season. Change reported in degrees Celsius from the 1850 to 1900 baseline for the Alaska and Western Canada boreal forest ecoregion. Projected changes are based on the IPCC SSP2-4.5 and SSP3-7.0 scenarios.

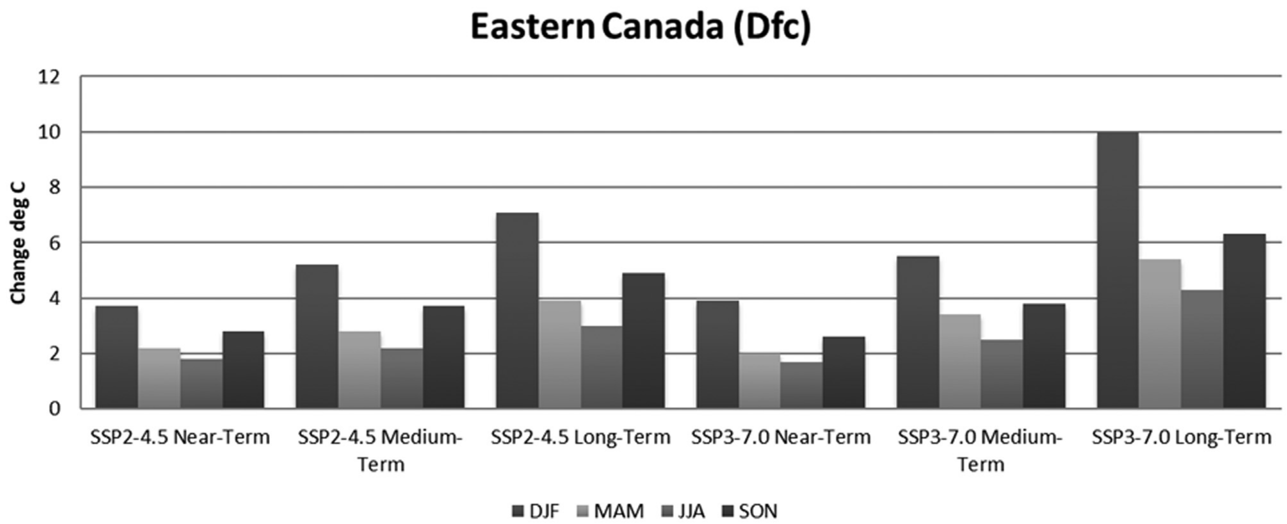

FIGURE A2.5 Same as figure A2.4 except for Eastern Canada ecoregion.

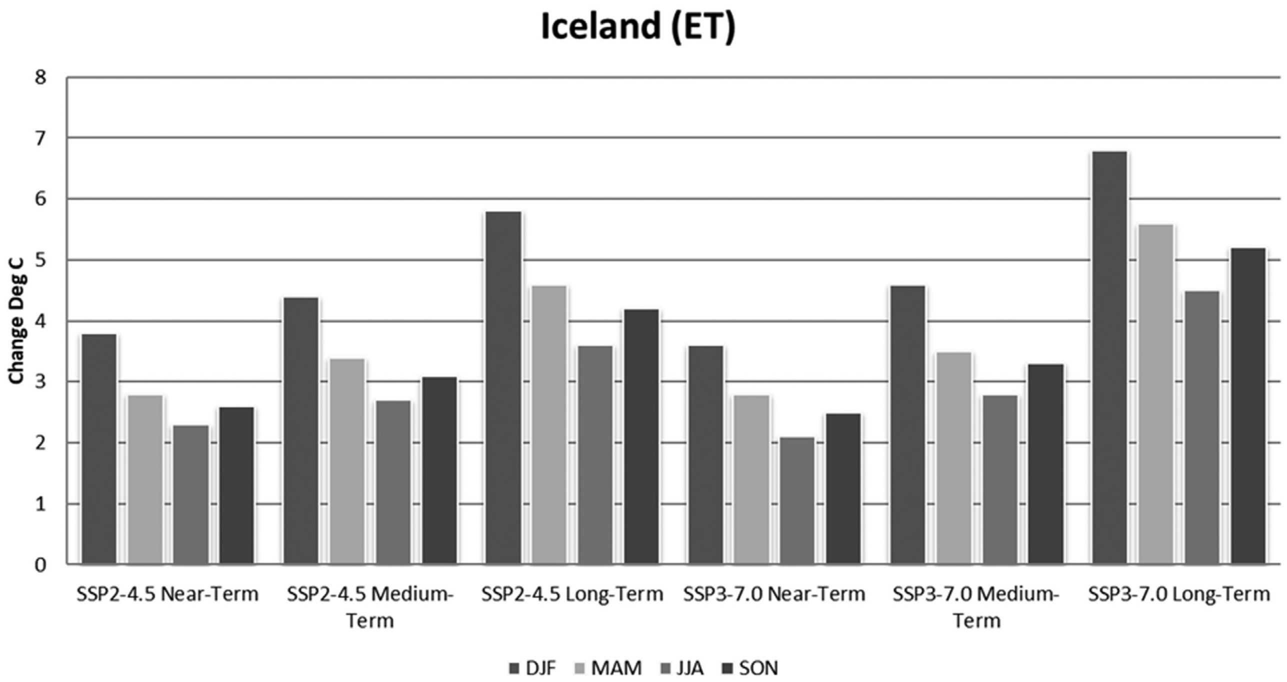

FIGURE A2.6 Same as A2.4 except Iceland ecoregion.

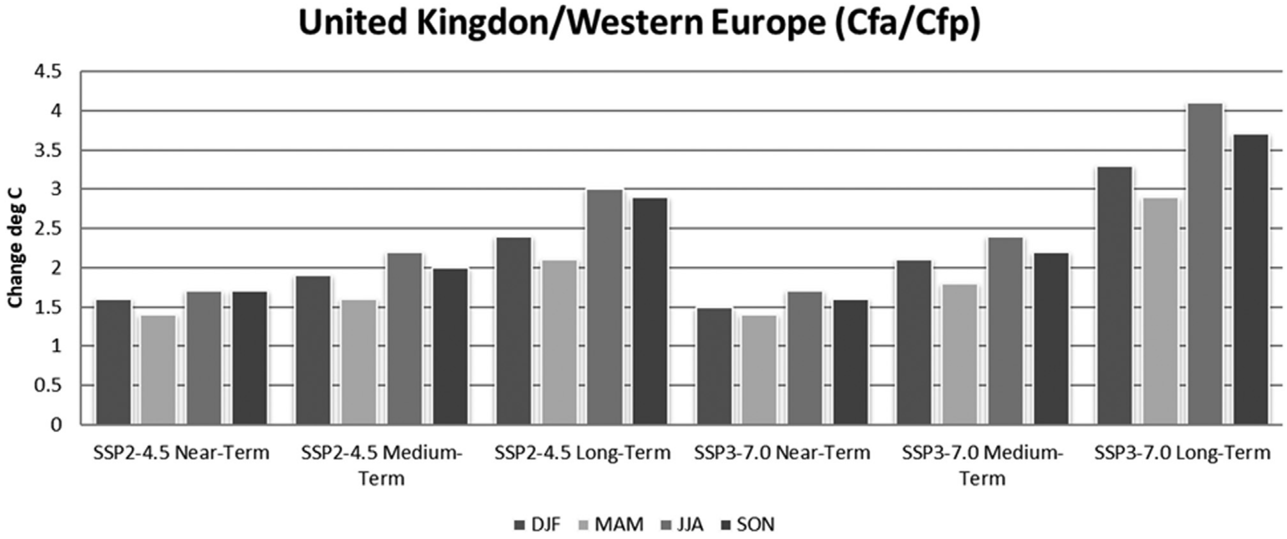

FIGURE A2.7 Same as A2.4 except for the United Kingdom/Western Europe ecoregion.

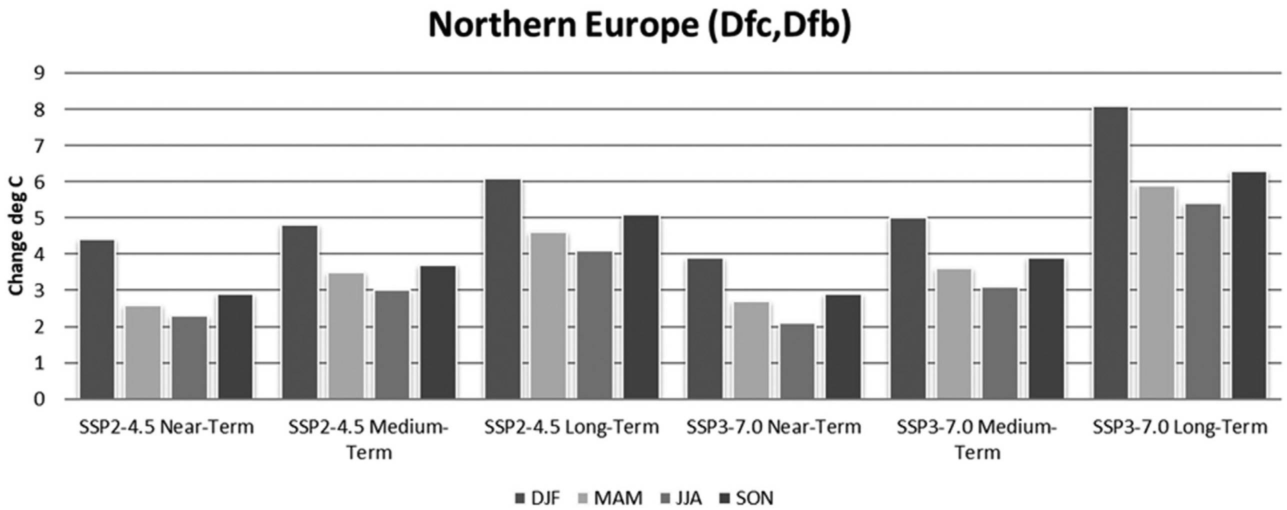

FIGURE A2.8 Same as A2.4 except for Northern Europe ecoregion.

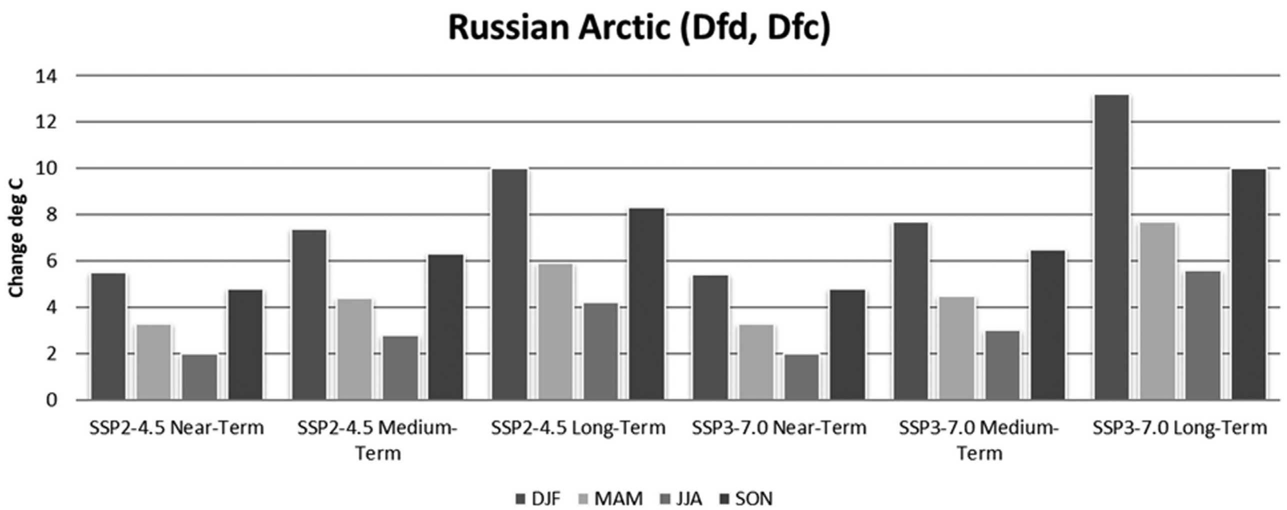

FIGURE A2.9 Same as A2.4 except for Russian Arctic ecoregion.

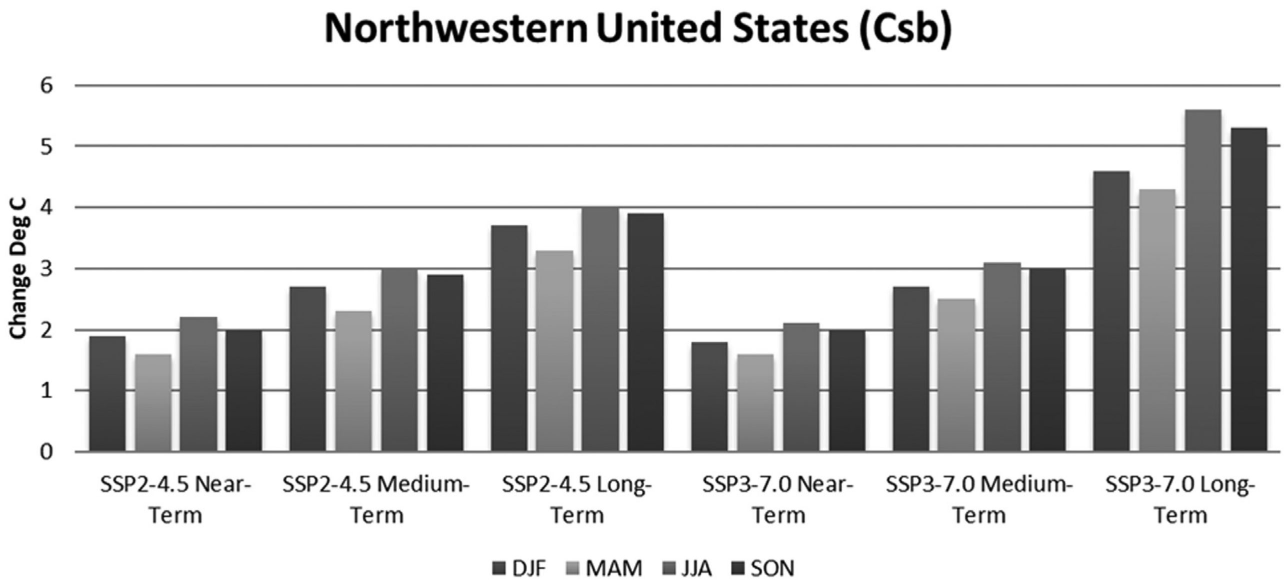

FIGURE A2.10 Same as A2.4 except for Northwestern United States ecoregion.

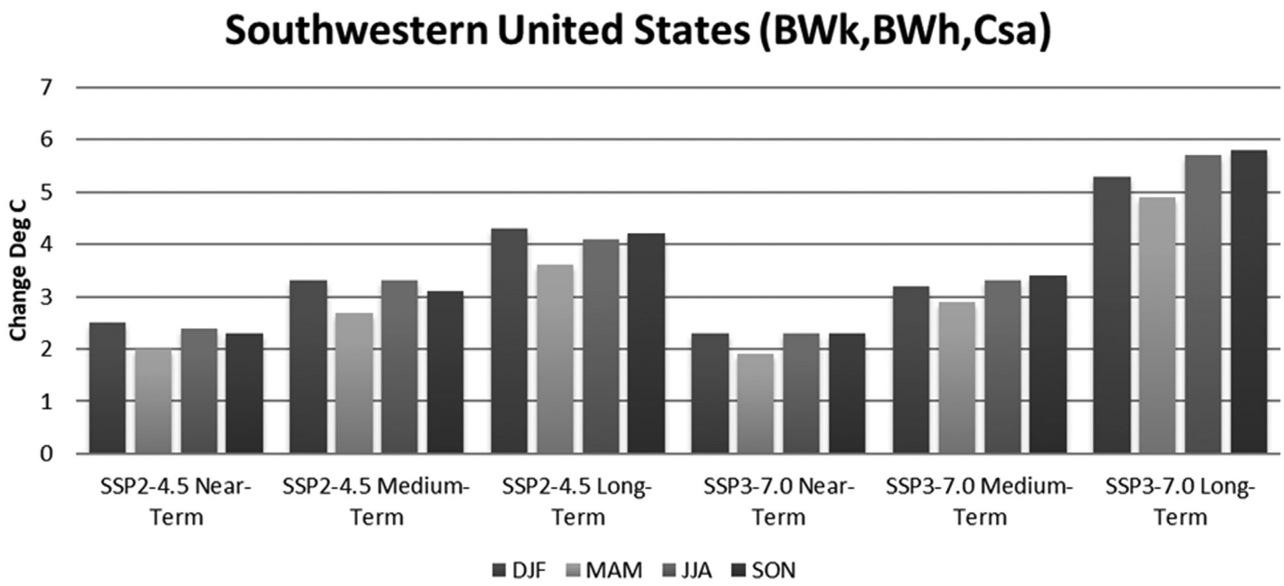

FIGURE A2.11 Same as A2.4 except for the Southwest United States ecoregion.

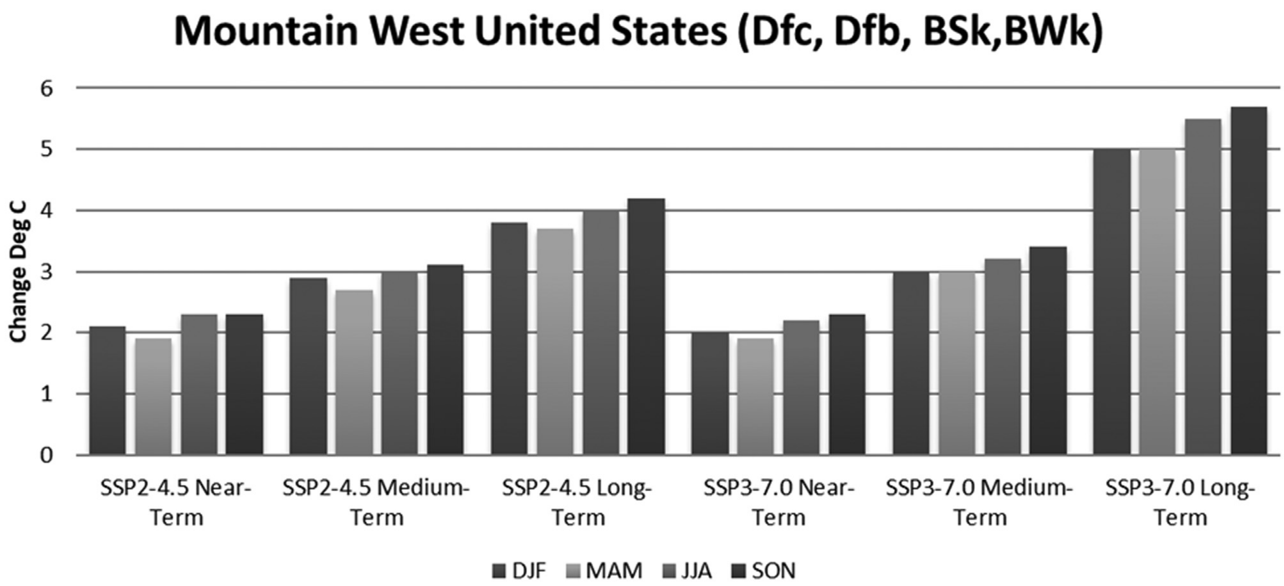

FIGURE A2.12 Same as A2.4 except for the Mountain West United States ecoregion.

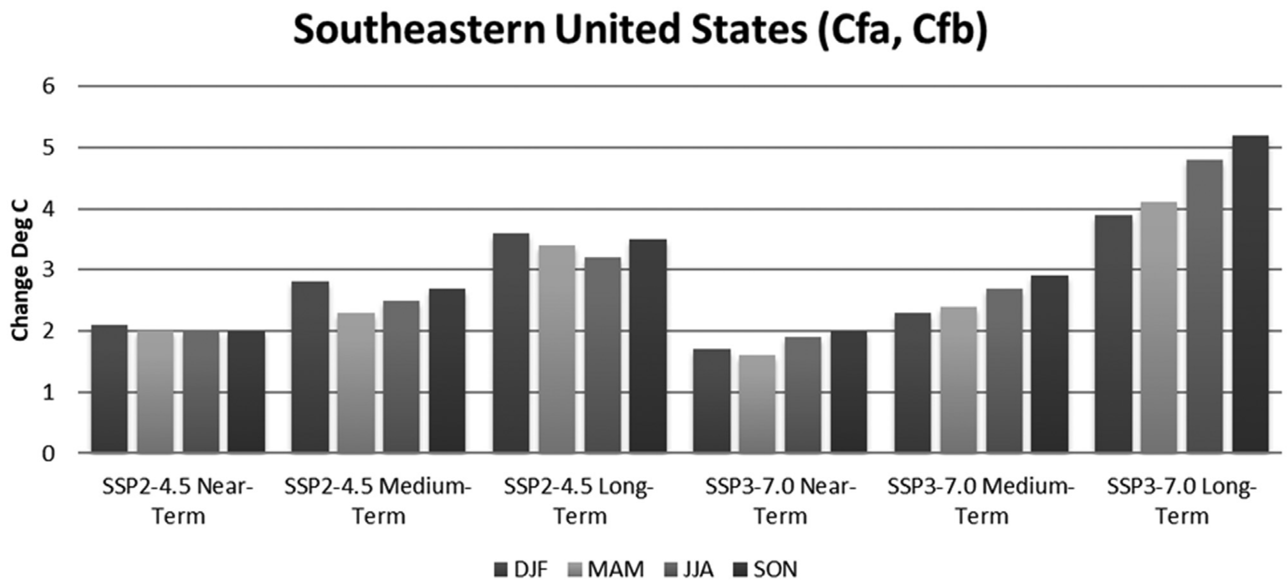

FIGURE A2.13 Same as A2.4 except for the Southeastern United States.

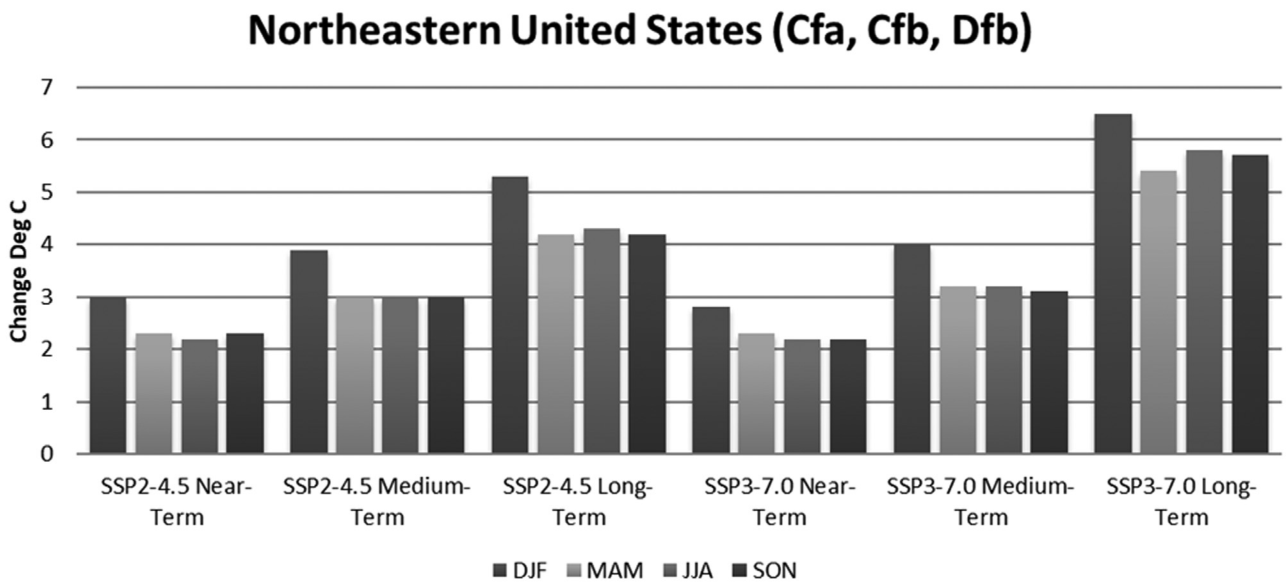

FIGURE A2.14 Same as A2.4 except for the Northeastern United States ecoregion.

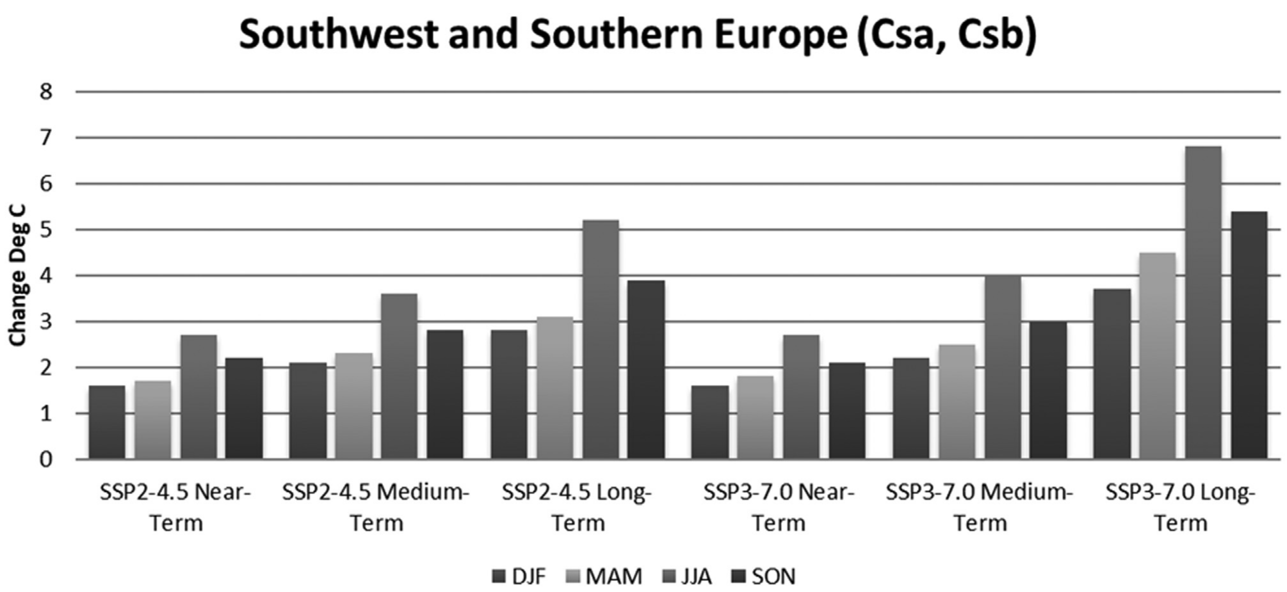

FIGURE A2.15 Same as A2.4 except for Southwest and Southern Europe ecoregions.

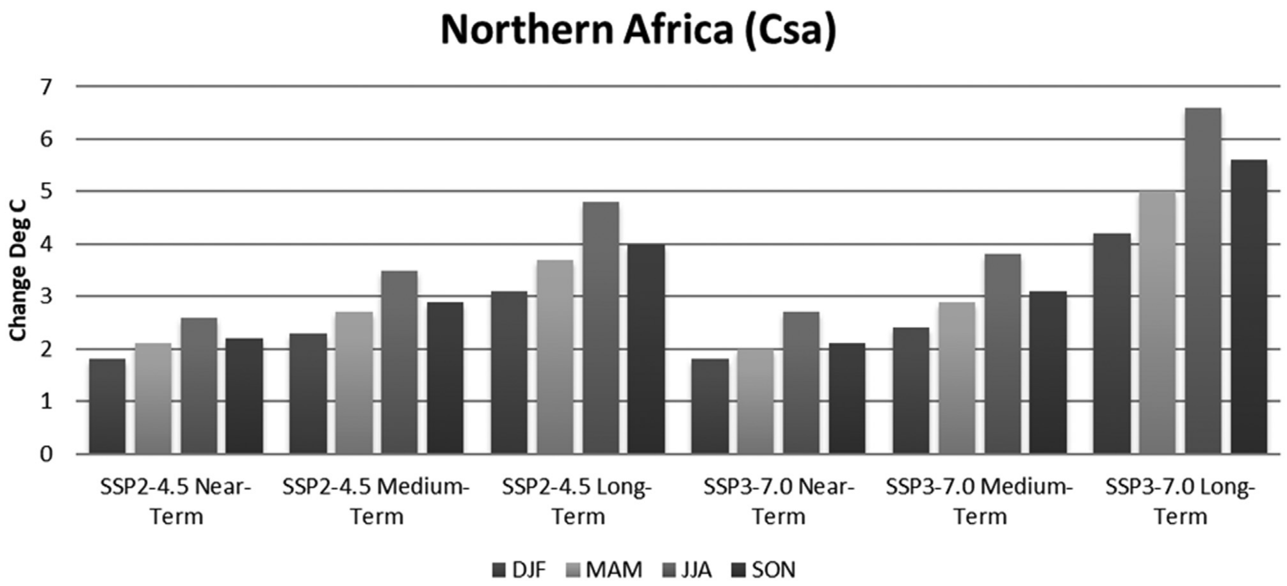

FIGURE A2.16 Same as A2.4 except for the Northern Africa ecoregion.

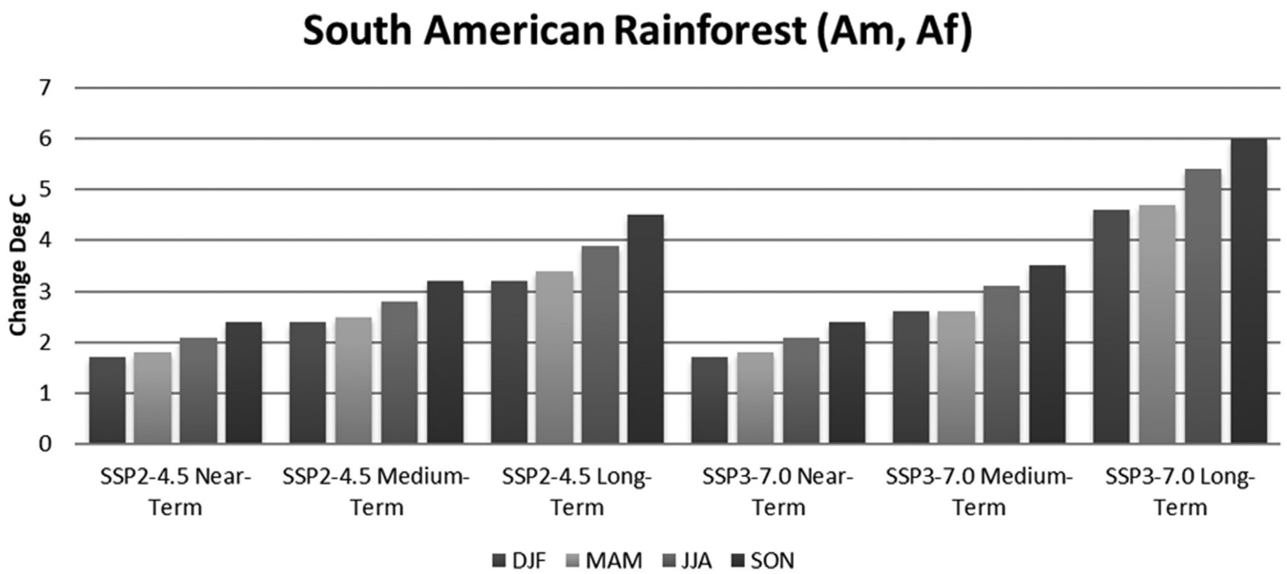

FIGURE A2.17 Same as A2.4 except for the South American Rainforest ecoregion.

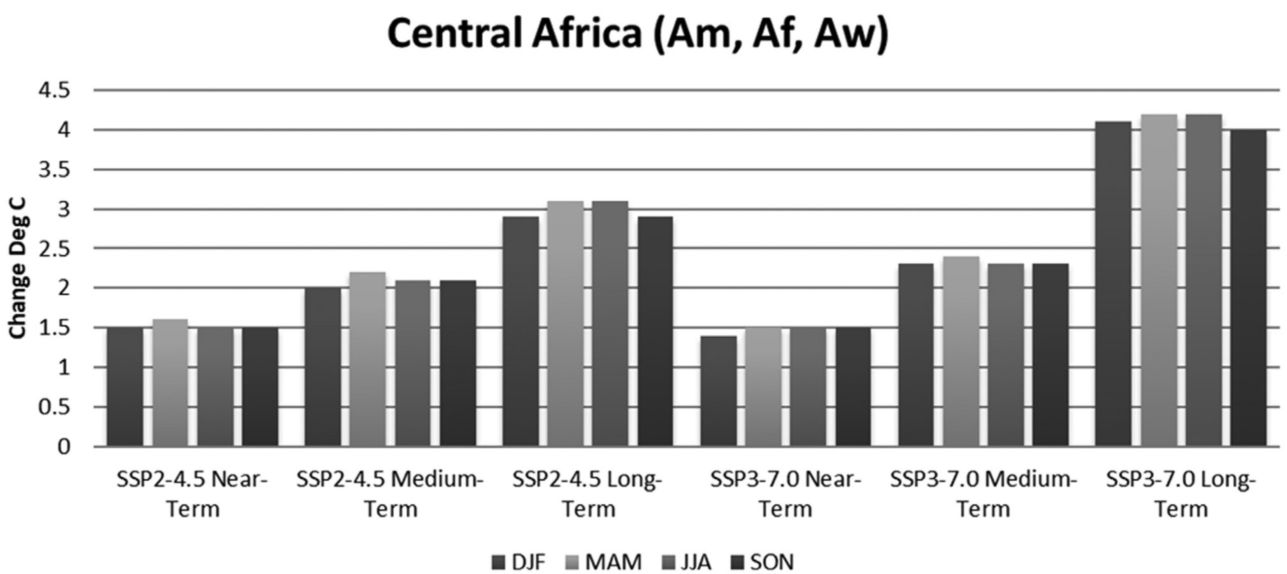

FIGURE A2.18 Same as A2.4 except for the Central Africa ecoregion.

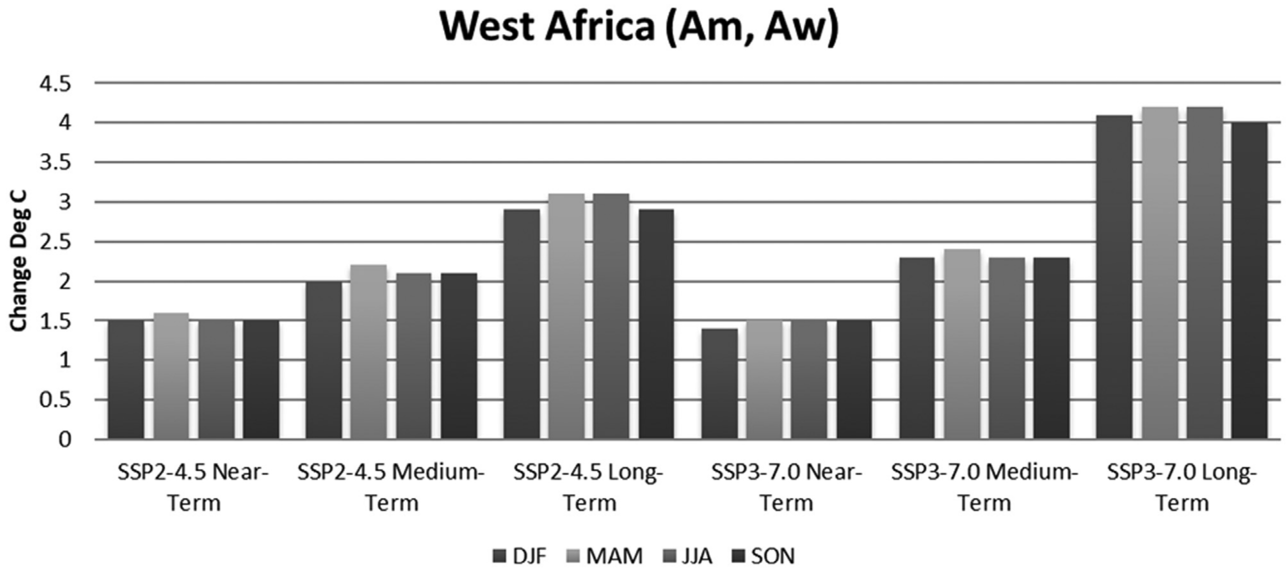

FIGURE A2.19 Same as A2.4 except for the West Africa ecoregion.

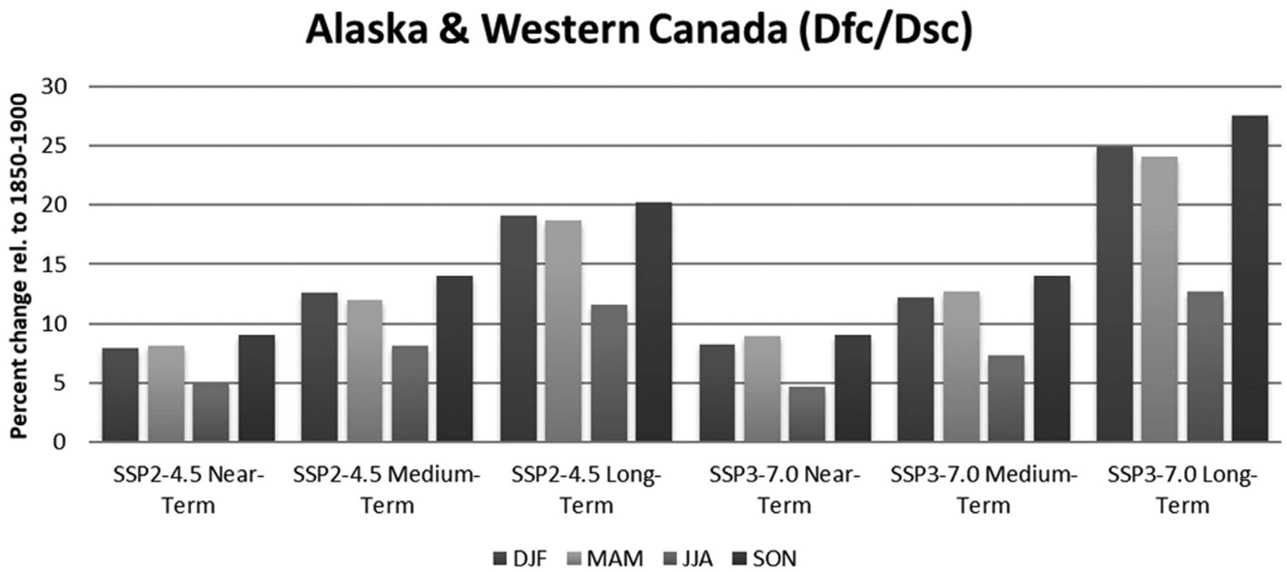

FIGURE A2.20 Percent change in total precipitation relative to a baseline from 1850 to 1900. Percent change is shown for each season during the near-term, medium term, and long-term periods and based on the SSP2-4.5 and SSP3-7.0 IPCC scenarios for the Alaska and Western Canada ecoregions.

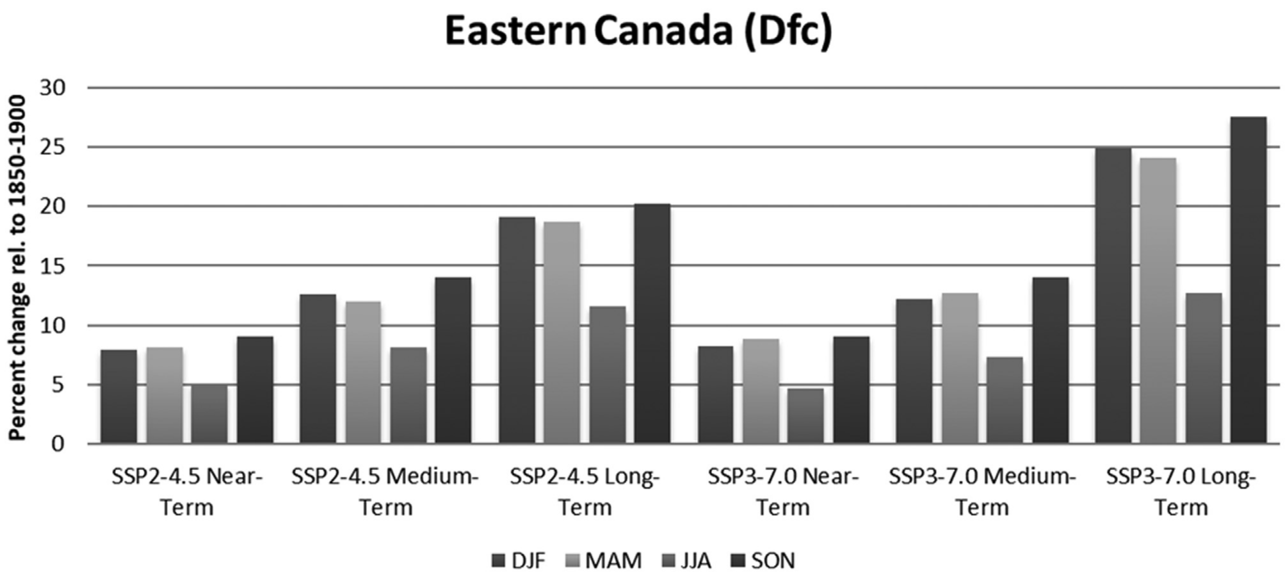

FIGURE A2.21 Same as A2.20 except for the Eastern Canada ecoregion.

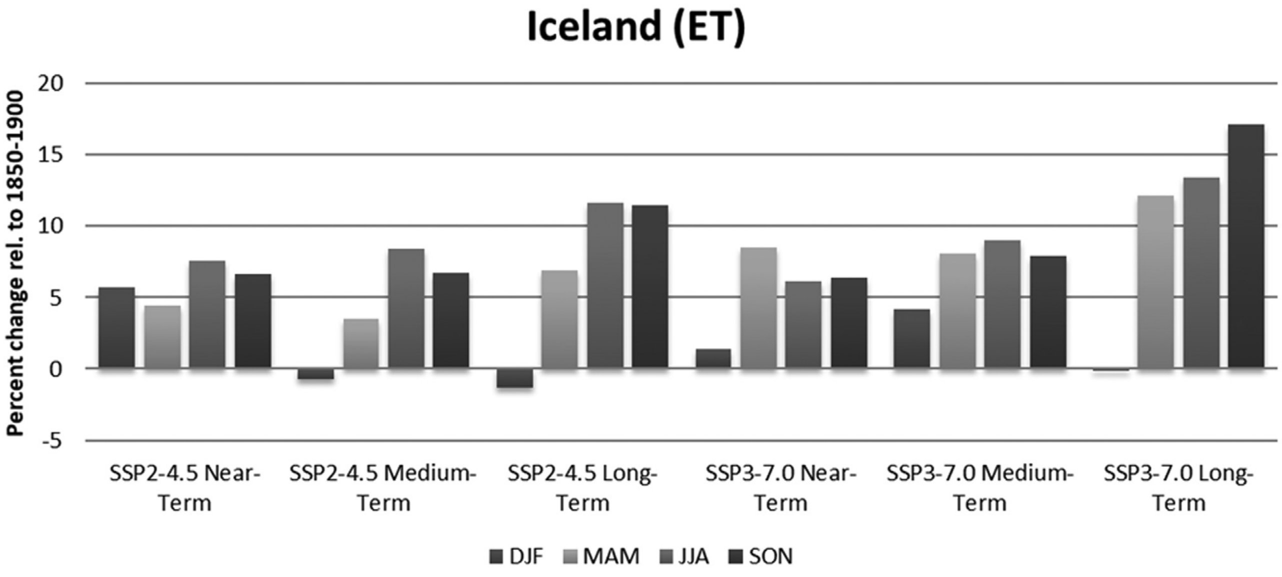

FIGURE A2.22 Same as A2.20 except for the Iceland ecoregion.

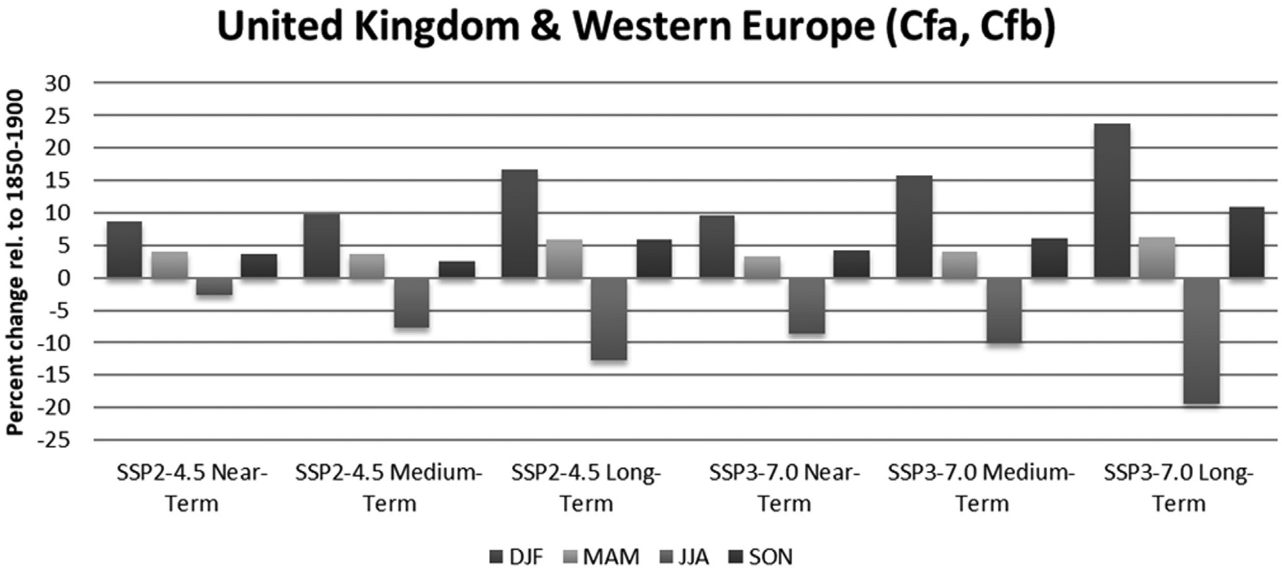

FIGURE A2.23 Same as A2.20 except for the United Kingdom and Western Europe ecoregions

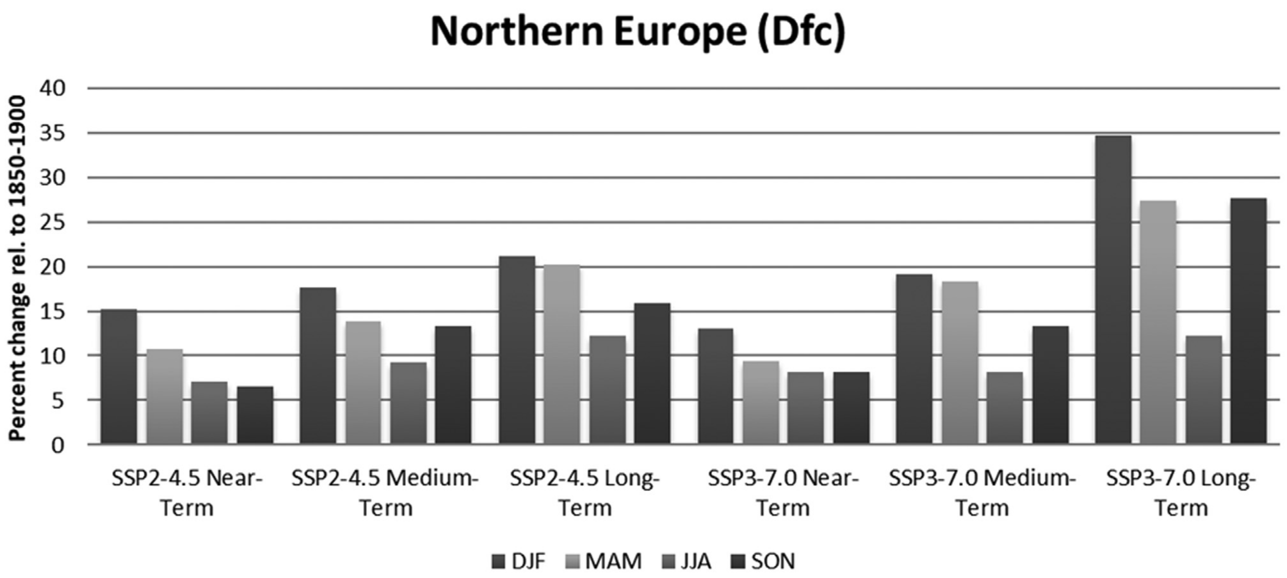

FIGURE A2.24 Same as A2.20 except for the Northern Europe ecoregion.

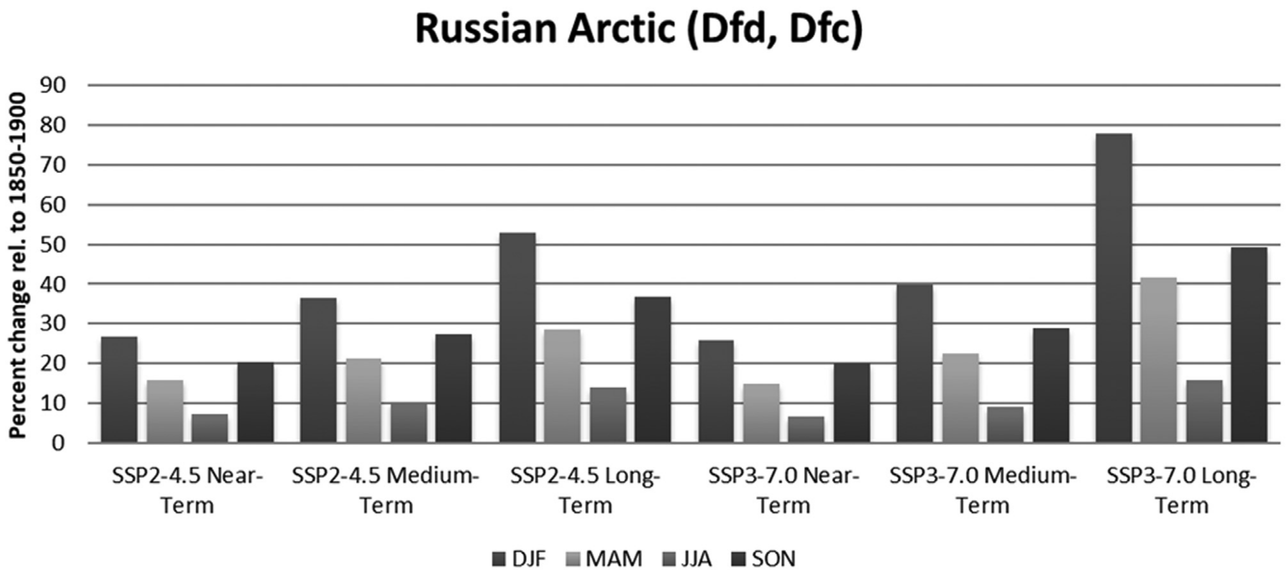

FIGURE A2.25 Same as A2.20 except for the Russian Arctic ecoregion.

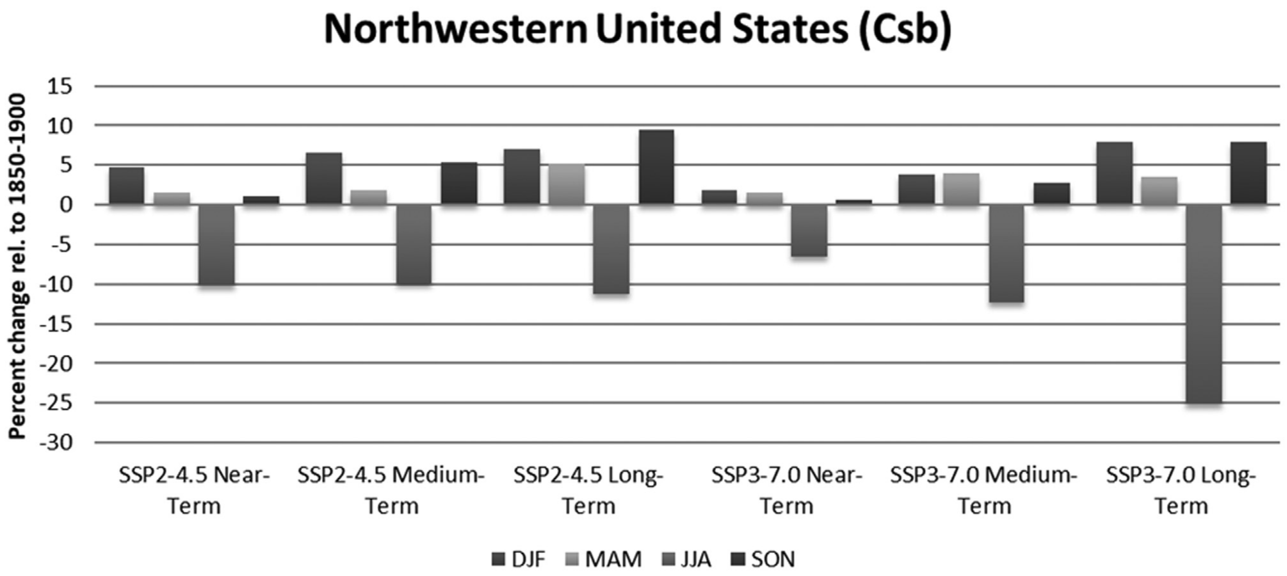

FIGURE A2.26 Same as A2.20 except for the Northwestern United States ecoregion.

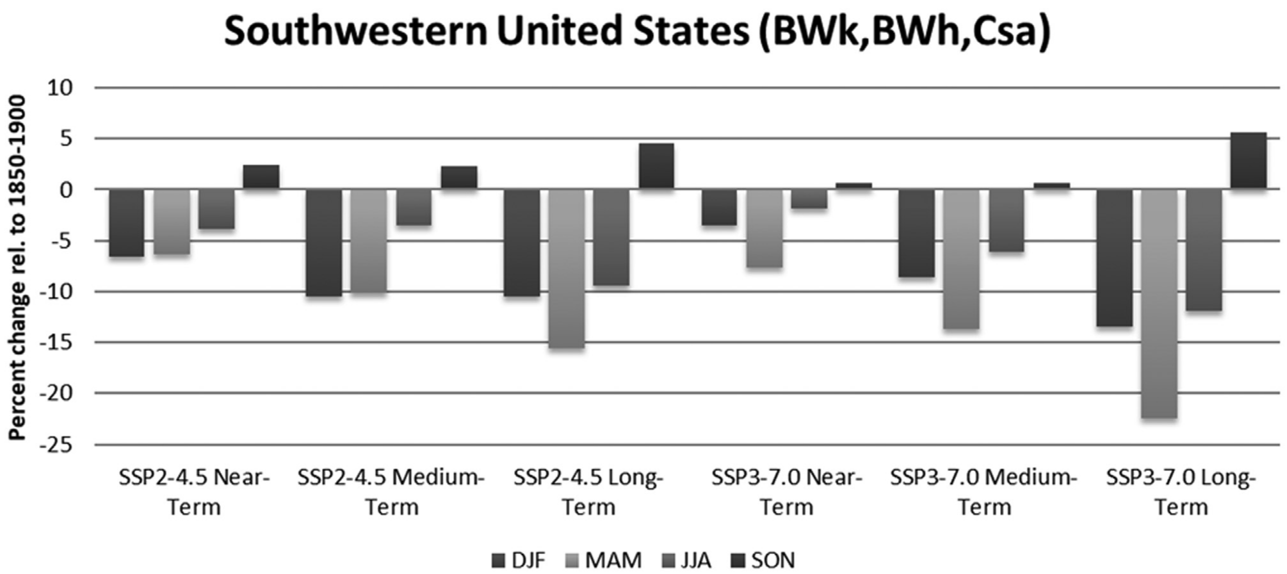

FIGURE A2.27 Same as A2.20 except for the Southwestern United States ecoregion.

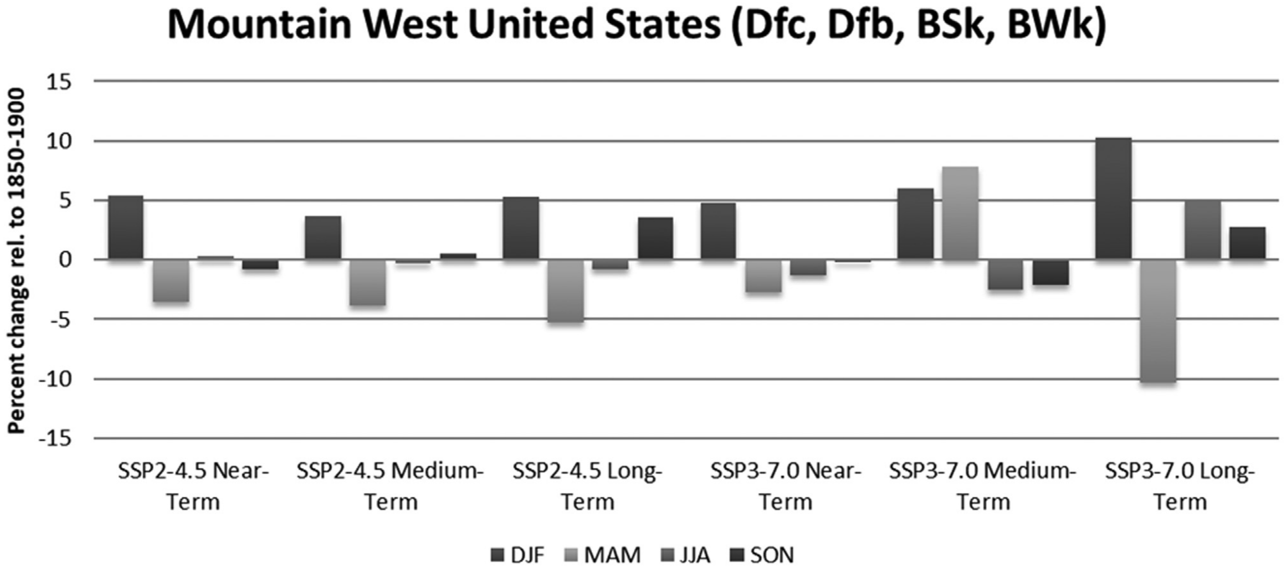

FIGURE A2.28 Same as A2.20 except for the Mountain West United States ecoregion.

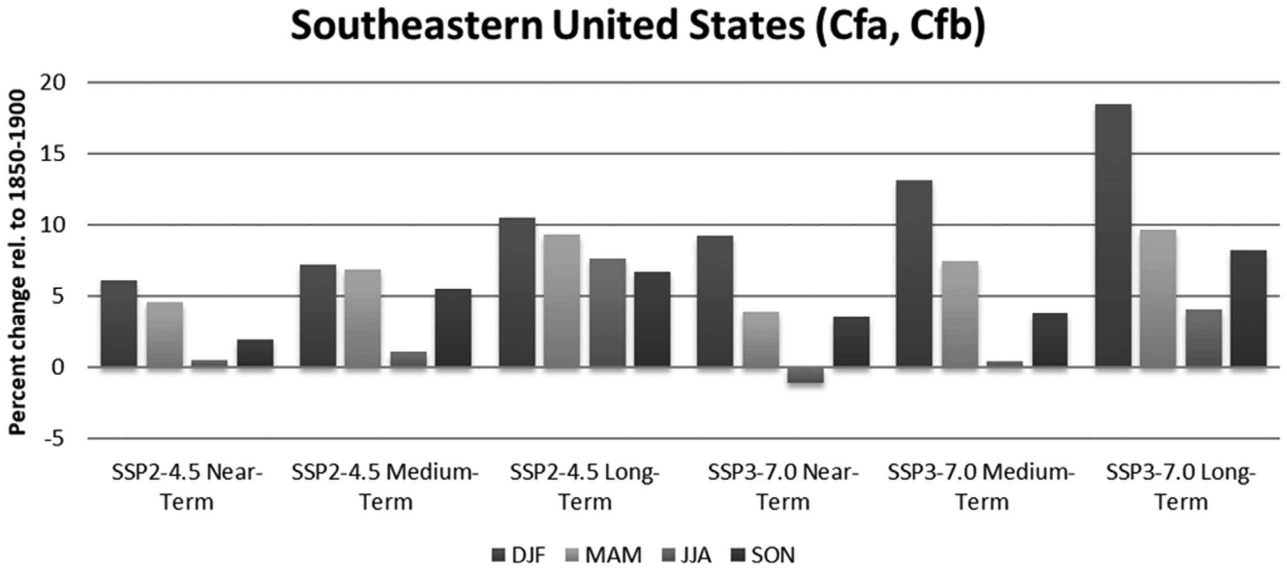

FIGURE A2.29 Same as A2.20 except for the Southeastern United States ecoregion.

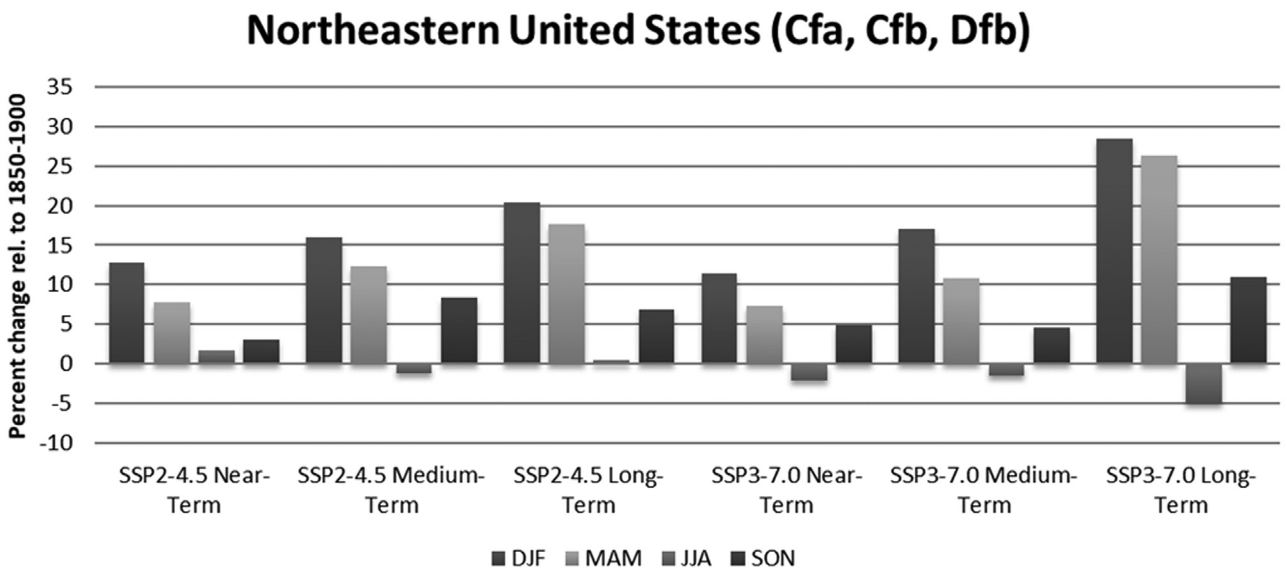

FIGURE A2.30 Same as A2.20 except for the Northeastern United States ecoregion.

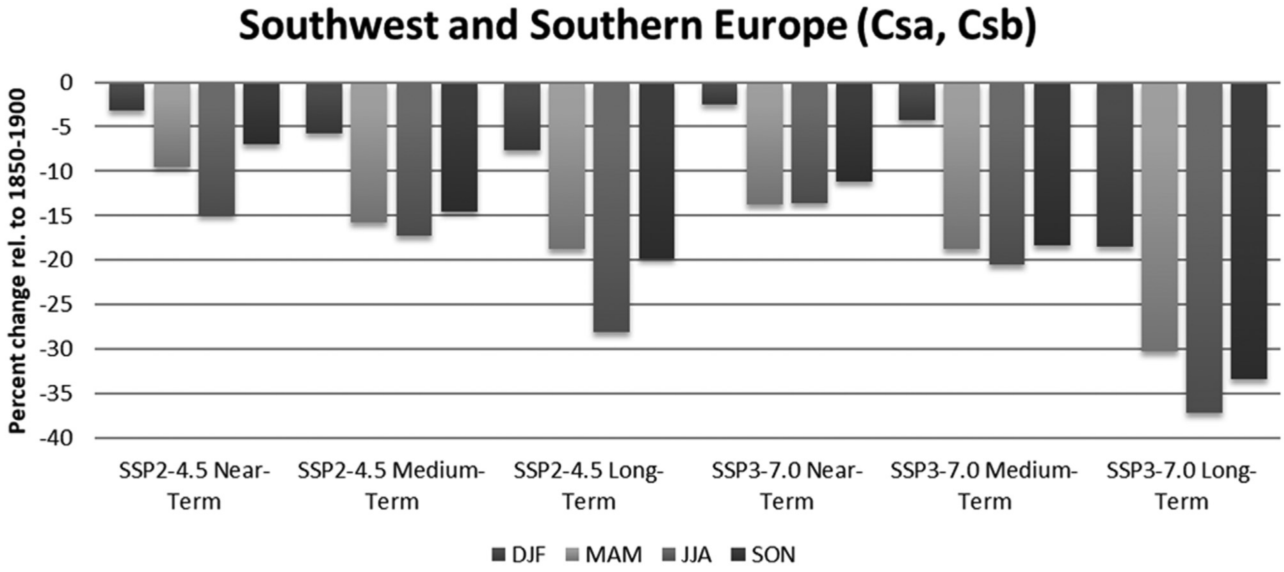

FIGURE A2.31 Same as A2.20 except for Southwest and Southern Europe ecoregions.

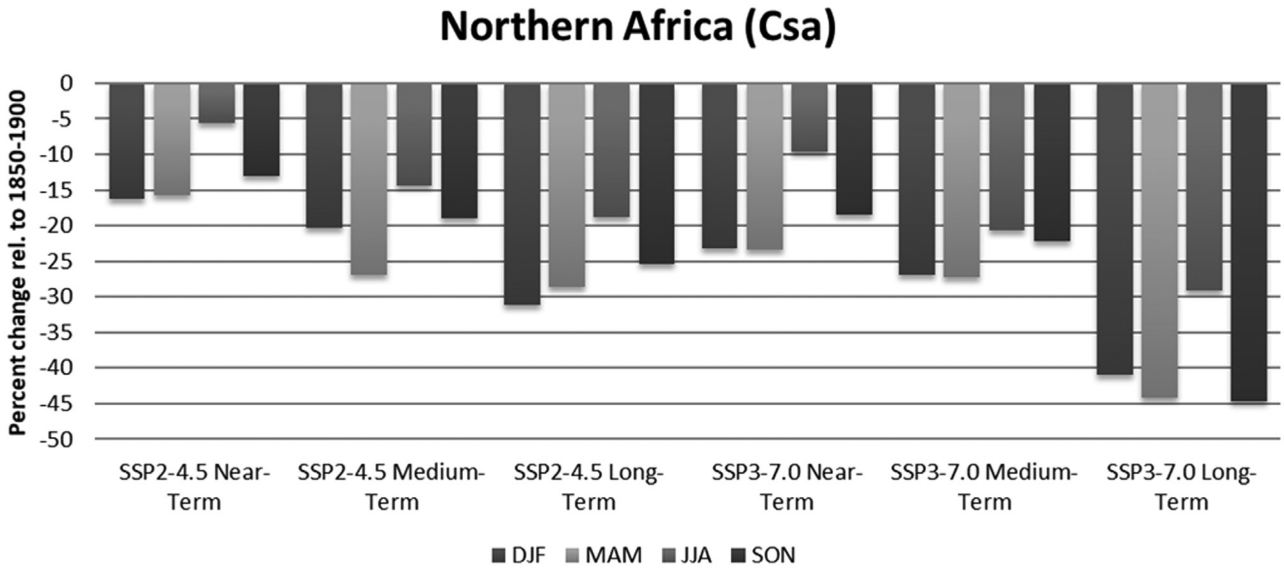

FIGURE A2.32 Same as A2.20 except for the Northern Africa ecoregion.

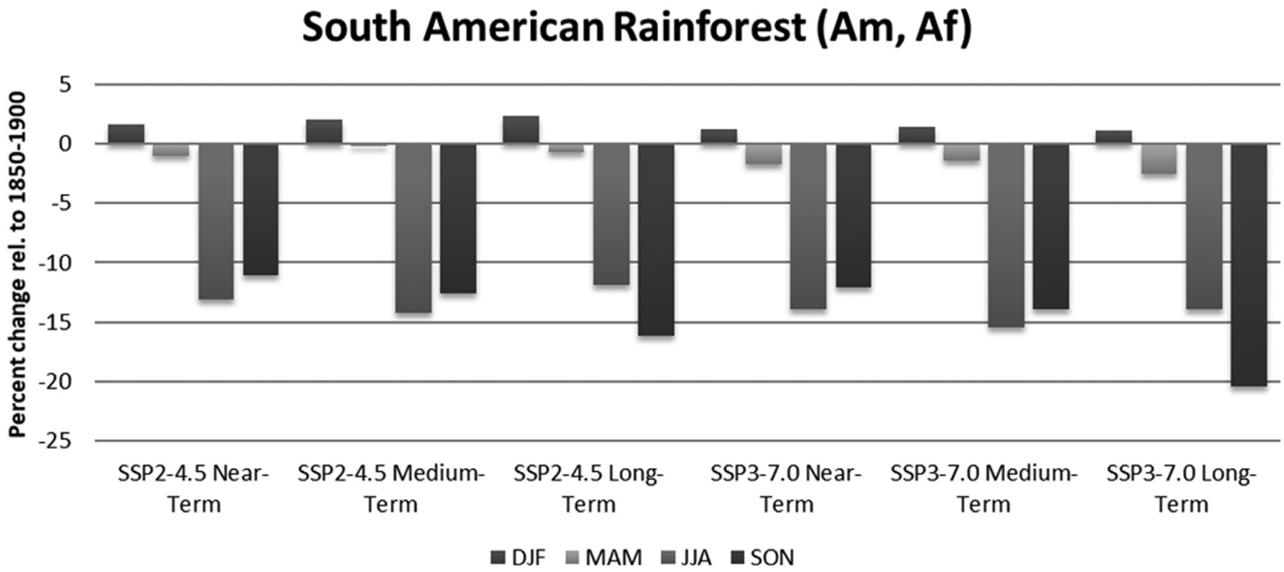

FIGURE A2.33 Same as A2.20 except for the South American Rainforest ecoregion.

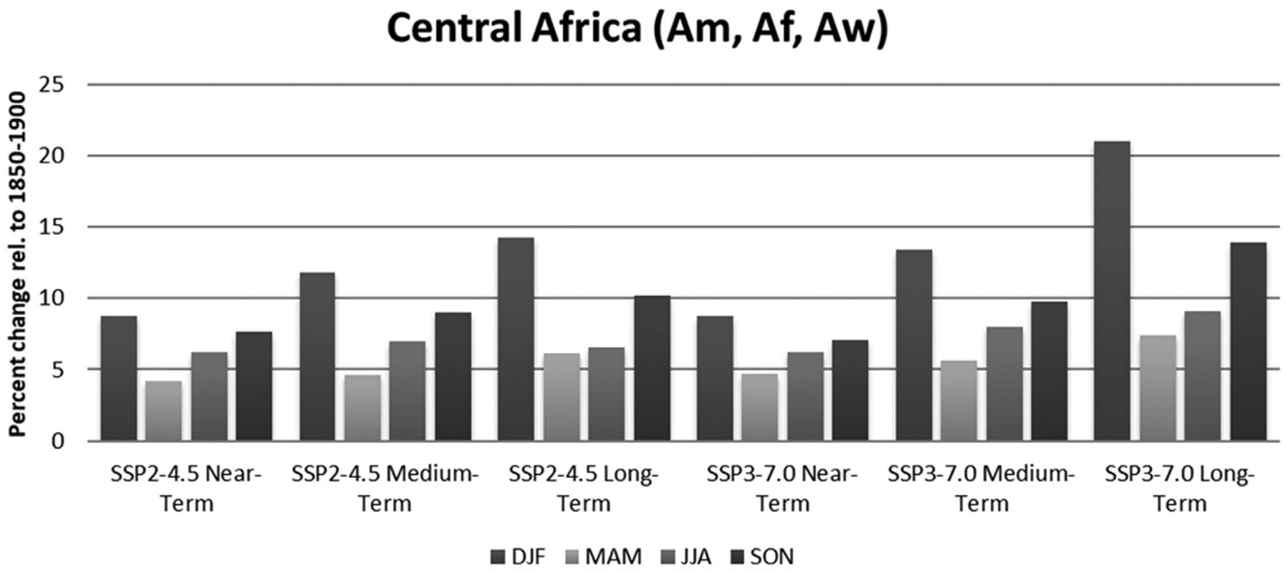

FIGURE A2.34 Same as A2.20 except for the Central Africa ecoregion.

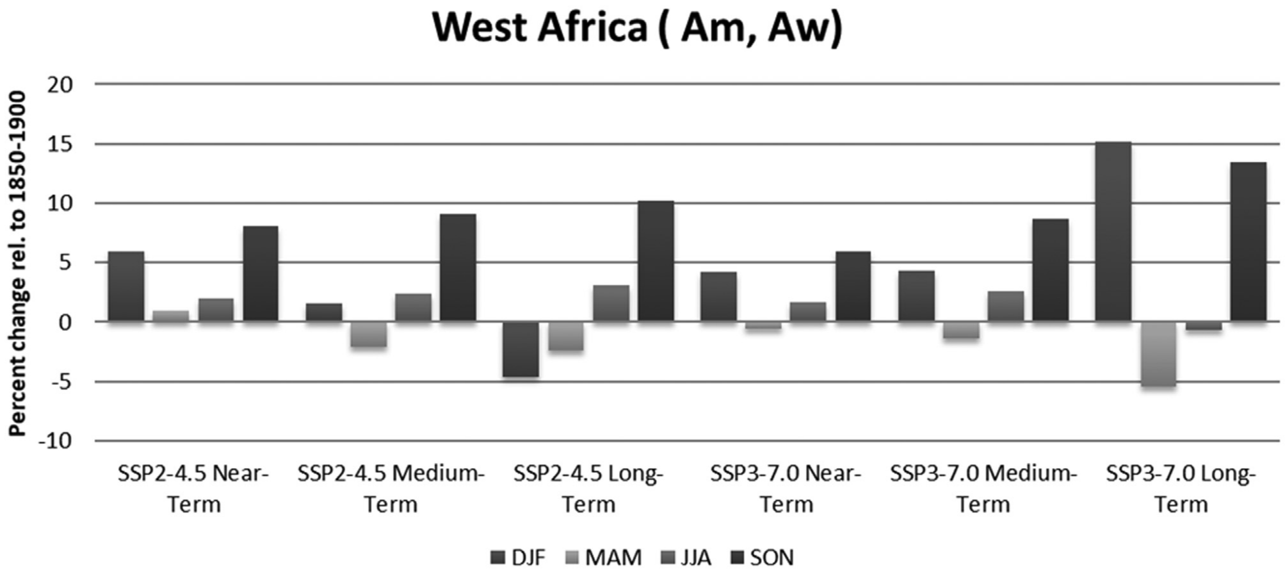

FIGURE A2.35 Same as A2.20 except for the West Africa ecoregion.

TABLE A2.1 Total precipitation trend in mm day^{-1} per decade for ecoregions with boreal forest.

	Alaska and Western Canada (Dfc,Dsc)	Eastern Canada (Dfc)	Iceland (ET)	United Kingdom and Western Europe	Northern Europe (Dfc)	Russian Arctic (Dfd, Dfc)
DJF	0	−0.1	0.3	0.5	0.8	0
MAM	0	0	0.2	0	0.3	0
JJA	0	0	−0.1	0	0.1	−0.1
SON	0	0	0.3	0.1	0	0

TABLE A2.2 Total precipitation trend in mm day^{-1} per decade for ecoregions with tropical forest.

	South America (Am, Af)	Central Africa (Am, Af, Aw)	West Africa (Am, Aw)
DJF	−0.4	0.1	0
MAM	0.4	−0.2	0
JJA	−0.3	−0.2	−0.4
SON	−0.5	−0.1	0.005

References

Abatzoglou, J. T., & Brown, T. J. (2012). A comparison of statistical downscaling methods suited for wildfire applications. *International Journal of Climatology*, *32*, 772−780.

Abram, N., Gattuso, J.-P., Prakash, A., Cheng, L., Chidichimo, M. P., Crate, S., . . . von Schuckmann, K. (2019). Framing and context of the report supplementary material. In H.-O. Pörtner, D. C. Roberts, V. Masson-Delmotte, P. Zhai, M. Tignor, E. Poloczanska, . . . N. M. Weyer (Eds.), *IPCC special report on the ocean and cryosphere in a changing climate*. Cambridge University Press.

Alder, J. R., & Hostetler, S. W. (2019). The dependence of hydroclimate projections in snow-dominated regions of the western United States on the choice of statistically downscaled climate data. *Water Resources Research*, *55*, 2279−2300. Available from https://doi.org/10.1029/2018WR023458.

Alder, J. R., & Hostetler, S. W. (2015). Web based visualization of large climate data sets. *Environmental Modelling & Software*, *68*, 175−180. Available from https://doi.org/10.1016/j.envsoft.2015.02.016.

Bachelet, D., Neilson, R. P., Lenihan, J. M., & Drapek, R. J. (2001). Climate change effects on vegetation distribution and carbon budget in the United States. *Ecosystems*, *4*, 164−185.

Barsugli, J. J., Guentchev, G., Horton, R. M., Wood, A., Mearns, L. O., Liang, X.-Z., . . . Ammann, C. (2013). The practitioner's dilemma: How to assess the credibility of downscaled climate projections. *Eos, Transactions American Geophysical Union*, *94*(46), 424−425. Available from https://doi.org/10.1002/2013EO460005.

Beer, J., & Wanner, H. (2012). Corrigendum to "Mid- to late Holocene climate change − an overview" [Quaternary Sci. Rev. 27 (2008) 1791−1828]. *Quaternary Science Reviews*, *51*, 93−99.

Bozkurt, D., Rojas, M., Boisier, J. P., Rondanelli, R., Garreaud, R., & Gallardo, L. (2019). Dynamical downscaling over the complex terrain of southwest South America: Present climate conditions and added value analysis. *Climate Dynamics*, *53*, 6745−6767. Available from https://doi.org/10.1007/s00382-019-04959-y4.

Brack, D. (2019). *Forests and climate change, the fourteenth session of the United Nations Forum on Forests* (56 pp.). https://www.un.org/esa/forests/wp-content/uploads/2019/03/UNFF14-BkgdStudy-SDG13-March2019.pdf

Briley, L. J., Ashley, W. S., Rood, R. B., & Krmenec, A. (2017). The role of meteorological processes in the description of uncertainty for climate change decision-making. *Theoretical and Applied Climatology*, *127*, 643−654. Available from https://doi.org/10.1007/s00704-015-1652-2.

Briley, L., Kelly, R., Blackmer, E. D., Troncoso, A. V., Rood, R. B., Andresen, J., & Lemos, M. C. (2020). Increasing the usability of climate models through the use of consumer-report-style resources for decision-making. *Bulletin of the American Meteorological Society*, *101*(10), E1709−E1717.

Brown, P., Li, W., Cordero, E., & Mauget, S. A. (2015). Comparing the model-simulated global warming signal to observations using empirical estimates of unforced noise. *Scientific Reports*, *5*, 9957. Available from https://doi.org/10.1038/srep09957.

Campisano, C. J. (2012). Milankovitch cycles, paleoclimatic change, and hominin evolution. *Nature Education Knowledge*, *4*(3), 5.

Carvalho, D., Rafael, S., Monteiro, A., Rodrigues, V., Lopes, M., & Rocha, A. (2022). How well have CMIP3, CMIP5 and CMIP6 future climate projections portrayed the recently observed warming. *Scientific Reports*, *12*, 11983.

Charney, J., Stone, P. H., & Quirk, W. J. (1975). Drought in the Sahara: a biogeophysical feedback mechanism. *Science (New York, N.Y.)*, *187*, 434−435. Available from https://doi.org/10.1126/science.187.4175.434.

Chen, C. A., Hsu, H. H., & Liang, H. C. (2021). Evaluation and comparison of CMIP6 and CMIP5 model performance in simulating the seasonal extreme precipitation in the Western North Pacific and East Asia. *Weather and Climate Extremes*, *31*, 100303.

Chen, L., Ma, Z., Li, Z., Wu, L., Flemke, J., & Li, Y. (2018). Dynamical downscaling of temperature and precipitation extremes in China under current and future climates. *Atmosphere-Ocean*, *56*(1), 55−70. Available from https://doi.org/10.1080/07055900.2017.1422691.

Cofino, A.S., San-Martın, D., & Gutiérrez, J.M. (2007). A web portal for regional projection of weather forecast using GRID middleware. In Y. Shi et al. (Eds.), *ICCS 2007, Part III. LNCS 4489* (pp. 82−89). Berlin Heidelberg: Springer-Verlag.

Connecticut Department of Energy and Environmental Protection. (2021). *How climate change impacts forests*. https://portal.ct.gov/DEEP/Forestry/Climate-Change/How-Climate-Change-Impacts-Forests

Contzen, J., Dickhaus, T., & Lohmann, G. (2022). Variability and extremes: Statistical validation of the Alfred Wegener Institute Earth System Model (AWI-ESM). *Geoscientific Model Development*, *15*, 1803−1820. Available from https://doi.org/10.5194/gmd-15-1803-2022.

De Sales, F., & Xue, Y. (2013). Dynamic downscaling of 22-year CFS winter seasonal hindcasts with the UCLA-ETA regional climate model over the United States. *Climate Dynamics*, *41*, 255−275. Available from https://doi.org/10.1007/s00382-012-1567-x.

Diffenbaugh, N. S. (2020). Verification of extreme event attribution: Using out-of-sample observations to assess changes in probabilities of unprecedented events. *Science Advances*, *6*, eaay2368.

Dixon, K. W., Lanzante, J. R., Nath, M. J., Hayhoe, K., Stoner, A., Radhakrishnan, A., & Gaitán, C. F. (2016). Evaluating the stationarity assumption in statistically downscaled climate projections: Is past performance an indicator of future results? *Climatic Change*, *135*, 395−408. Available from https://doi.org/10.1007/s10584-016-1598-0.

Eyring, V., Bony, S., Meehl, G. A., Senior, C. A., Stevens, B., Stouffer, R. J., & Taylor, K. E. (2016). Overview of the Coupled Model Intercomparison Project Phase 6 (CMIP6) experimental design and organization. *Geoscientific Model Development*, *9*(5), 1937−1958.

Fajardo, J., Corcoran, D., Roehrdanz, P. R., Hannah, L., & Marquet, P. A. (2020). GCM compareR: A web application to assess differences and assist in the selection of general circulation models for climate change research. *Methods in Ecology and Evolution*, *11*(5), 656−663. Available from https://doi.org/10.1111/2041-210X.13360.

Fasullo, J. T. (2020). Evaluating simulated climate patterns from the CMIP archives using satellite and reanalysis datasets using the Climate Model Assessment Tool (CMATv1). *Geoscientific Model Devlopment*, *13*, 3627−3642. Available from https://doi.org/10.5194/gmd-13-3627-2020.

Fick, S. E., & Hijmans, R. J. (2017). WorldClim 2: New 1 km spatial resolution climate surfaces for global land areas. *International Journal of Climatology*, *37*, 4302−4315. Available from https://doi.org/10.1002/joc.5086.

Fisher, J. B., Huntzinger, D. N., Schwalm, C. R., & Sitch, S. (2014). Modeling the terrestrial biosphere. *Annual Review of Environment and Resources*, *39*(1), 91−123.

Flato, G., Marotzke, J., Abiodun, B., ... Zhan, J. (2013). Evaluation of climate models. In *Climate change 2013: The physical science basis. Contribution of working group I to the 5th assessment report of the Intergovernmental Panel on Climate Change*.

Foster, G., & Rahmstorf, S. (2011). Global temperature evolution 1979−2010. *Environmental Research Letters*, *6*(4), 044022. Available from https://doi.org/10.1088/1748-9326/6/4/044022.

Franke, J., Brönnimann, S., Bhend, J., & Brugnara, Y. (2017). A monthly global paleo-reanalysis of the atmosphere from 1600 to 2005 for studying past climatic variations. *Scientific Data*, *4*(1), 1−19.

Gaffney, O., & Steffen, W. (2017). The anthropocene equation. *The Anthropocene Review*, *4*(1), 53−61.

Gershunov, A., Rajagopalan, B., Overpeck, J., Guirguis, K., Cayan, D., Hughes, M., ... Alexander, M.. (2013). Future climate: Projected extremes. In G. Garfin, A. Jardine, R. Merideth, M. Black, & S. LeRoy (Eds.), *Assessment of climate change in the Southwest United States: A report prepared for the national climate assessment* (pp. 126−147). A report by the Southwest Climate Alliance. Washington, DC.

Gilliam, F. S. (2016). Forest ecosystems of temperate climatic regions: From ancient use to climate change. *New Phytologist*, *212*(4), 871−887. Available from https://doi.org/10.1111/nph.14255.

Giorgi, F. (2010). Uncertainties in climate change projections, from the global to the regional scale. *EPJ Web of Conferences*, *9*, 115−129. Available from https://doi.org/10.1051/epjconf/201009009.

Giorgi, F., & Gutowski, W. J., Jr (2015). Regional dynamical downscaling and the CORDEX initiative. *Annual Review of Environment and Resources*, *40*, 467−490.

Girvetz, E. H., Zganjar, C., Raber, G. T., Maurer, E. P., & Kareiva, P. (2009). Applied climate-change analysis: The climate wizard tool. *PLoS One*, *4* (12), e8320. Available from https://doi.org/10.1371/journal.pone.0008320.

Grose, M. R., Bhend, J., Argueso, D., Ekström, M., Dowdy, A., Hoffmann, P., & Timbal, B. (2015). Comparison of various climate change projections of eastern Australian rainfall. *Australian Meteorological and Oceanographic Journal*, *65*(1), 67−84.

Gutiérrez, J.M., Jones, R.G., Narisma, G.T., Alves, L.M., Amjad, M., Gorodetskaya, I.V., ...Yoon, J.-H. (2021). Atlas. In V. Masson-Delmotte, P. Zhai, A. Pirani, S. L. Connors, C. Péan, S. Berger, ...P. Zhou (Eds.), *Climate change 2021: The physical science basis. Contribution of working group I to the 6th assessment report of the Intergovernmental Panel on Climate Change*. Cambridge University Press. Interactive Atlas available from http://interactive-atlas.ipcc.ch/.

Guttorp, P. (2011). The role of statisticians in international science policy. *Environmetrics (London, Ont.)*, *22*, 817−825.

Halofsky, J. E., Peterson, D. L., & Harvey, B. J. (2020). Changing wildfire, changing forests: The effects of climate change on fire regimes and vegetation in the Pacific Northwest. *Fire Ecology*, 4.

Harris, I., Osborn, T. J., Jones, P., & Lister, D. (2020). Version 4 of the CRU TS monthly high-resolution gridded multivariate climate dataset. *Scientific Data*, *7*(1). Available from https://doi.org/10.1038/s41597-020-0453-3.

Hathaway, D. H. (2015). The solar cycle. *Living Reviews in Solar Physics.*, *12*(4). Available from https://doi.org/10.1007/lrsp-2015-4.

Hawkins, E. (2013). Sources of uncertainty in CMIP5 projections. In *IPCC AR5, projections, temperature, uncertainty, variability, visualization*.

Hegerl, G. C., Brönnimann, S., Schurer, A., & Cowan, T. (2018). The early 20th century warming: anomalies, causes, and consequences. *Climate Change.*, *9*, e522. Available from https://doi.org/10.1002/wcc.522.

Hurrell, J.W., Kushnir, Y., Ottersen, G., & Visbeck, M. (2003). An overview of the North Atlantic oscillation. In J. W. Hurrell, Y. Kushnir, G. Ottersen, & M. Visbeck (Eds.), *The North Atlantic oscillation: Climatic significance and environmental impact* (pp. 1−35). Geophysical Monograph Series. Available from https://doi.org/10.1029/134gm01.

Hurrell, J. W., Holland, M. M., & Gent, P. R. (2013). The community Earth system model: A framework for collaborative research. *Bulletin of the American Meteorological Society.*, *94*, 1339−1360.

Intergovernmental Panel on Climate Change. (2001). Climate change 2001: The scientific basis. In J. T. Houghton, Y. Ding, D. J. Griggs, M. Noguer, P. J. van der Linden, X. Dai, . . . C. A. Johnson (Eds.), *Report of the Intergovernmental Panel on Climate Change*. Cambridge and New York: Cambridge University Press.

Intergovernmental Panel on Climate Change. (2007). Climate change 2007: The scientific basis. In S. S. D. Qin, M. Manning, Z. Chen, M. Marquis, K. B. Averyt, M. Tignor, & H. L. Miller (Eds.), *Report of the Intergovernmental Panel on Climate Change*.elseteusr5 Cambridge and New York: Cambridge University Press.

Intergovernmental Panel on Climate Change. (2013). *Climate change 2013: The physical science basis 4, 15*. http://www.climatechange2013.org/images/report/WG1AR5_SPM_FINAL.pdf [hereinafter WGI Summary for Policymakers].

Intergovernmental Panel on Climate Change. (2021). Climate change 2021: The physical science basis. In V. Masson-Delmotte, P. Zhai, A. Pirani, S. L. Connors, C. Péan, S. Berger, . . . B. Zhou (Eds.), *Contribution of working group I to the 6th assessment report of the Intergovernmental Panel on Climate Change*. Cambridge and New York: Cambridge University Press.

Iturbide, M., Fernandez, M., Gutiérrez, J., Bedia, J.M., Cimadevilla, J., Diez-Sierra, E., & Yelekci, O. (2021). *IPCC-WG1/Atlas: Repository supporting the implementation of FAIR principles in the IPCC-WGI Atlas*. Retrieved from https://github.com/IPCC-WG1/Atlas.

Jiang, Y., Kim, J. B., Still, C. J., Kerns, B. K., Kline, J. D., & Cunningham, P. G. (2018). Intercomparison of multiple statistically downscaled climate datasets for the Pacific Northwest, USA. *Scientific Data*, *5*(1), 1−18.

Jouzel, J., Hoffmann, G., Koster, R. D., & Masson, V. (2000). Water isotopes in precipitation: Data/model comparison for present-day and past climates. *Quaternary Science Review*, *19*, 363−379.

Keramidas, K., Diaz Vazquez, A., Weitzel, M., Vandyck, T, Tamba, M., Tchung-Ming, S., . . . Whn, X. (2020). *Global Energy and Climate Outlook 2019: Electrification for the low-carbon transition: The role of electrification in low-carbon pathways, with a global and regional focus on EU and China*. Available from https://doi.org/10.13140/RG.2.2.23781.35043.

Knutti, R., Masson, D., & Gettelman, A. (2013). Climate model genealogy: generation CMIP5 and how we got there. *Geophysical Research Letters*, *40*, 1194−1199.

Kottek, M., Grieser, J., Beck, C., Rudolf, B., & Rubel, F. (2006). World Map of the Köppen-Geiger climate classification updated. *Meteorologische Zeitschrift*, *15*(3), 259−263. Available from https://doi.org/10.1127/0941-2948/2006/0130.

Kusunoki, S., & Arakawa, O. (2015). Are CMIP5 models better than CMIP3 models in simulating precipitation over East Asia? *Journal of Climate*, *28*(14), 5601−5621. Available from https://doi.org/10.1175/JCLI-D-14-00585.1.

Lan, X., Hall, B. D., Dutton, G., Mühle, J., & Elkins, J. W. (2020). Atmospheric composition in "State of the Climate in 2018, Chapter 2: Global Climate.". *Special Online Supplement to the Bulletin of the American Meteorological Society*, *101*(8).

Liu, Y.-Q. (2011). A numerical study on hydrological impacts of forest restoration in the southern United States. *Ecohydrology*, *4*(2), 299−314.

Liu, Y.-Q. (2018). New development and application needs for Earth system modeling of fire−climate−ecosystem interactions. *Environmental Research Letters.*, *13*, 011001.

Liu, Y.-Q., Goodrick, S., & Stanturf, J.A. (2021). Climate downscaling for fire management. In W. Leal Filho et al. (Eds.), *Sustainability in natural resources management and land planning*. World Sustainability Series. https://doi.org/10.1007/978-3-030-76624-5_27.

Liu, Y.-Q., Liu, Y., Fu, J., Yang, C.-E., Dong, X., Tian, H., . . . Ke, Z. (2021). Projection of future wildfire emissions in the western United States under climate change: contributions from changes in wildfire, fuel loading, and fuel moisture. *International Journal of Wildland Fire*, *22*, 1003−1020.

Manzanas, R., Gutiérrez, J. M., Fernández, J., van Meijgaard, E., Calmanti, S., Magariño, M. E., . . . Herrer, S. (2018). Dynamical and statistical downscaling of seasonal temperature forecasts in Europe: Added value for user applications. *Climate Services*, *9*, 44−56.

Maraun, D., Shepherd, T. G., Widmann, M., Zappa, G., Walton, D., Gutiérrez, J. M., . . . Mearns, L. O. (2017). Towards process-informed bias correction of climate change simulations. *Nature Climate Change*, *7*, 764−773.

Masson, D., & Knutti, R. (2011). Climate model genealogy. *Geophysical Research Letters*, *38*, L08703. Available from https://doi.org/10.1029/2011GL046864.

Matthes, F. E. (1939). Report of the committee on glaciers. *Transactions of the American Geophysical Union*, *20*, 518−523.

McElwain, J. C., Beerling, D. J., & Woodward, F. I. (1999). Fossil plants and global warming at the Triassic-Jurassic boundary. *Science (New York, N.Y.)*, *285*(5432), 1386−1390.

Mearns, L. O., Arritt, R., Biner, S., Bukovsky, M. S., McGinnis, S., Sain, S., & Snyder, M. (2012). The North American regional climate change assessment program: Overview of phase I results. *Bulletin of the American Meteorological Society*, *93*(9), 1337−1362.

Meehl, G. A., Hu, A., Santer, B. D., & Xie, S. (2016). Contribution of the Interdecadal Pacific Oscillation to twentieth-century global surface temperature trends. *Nature Climate Change*, *6*(11), 1005−1008. Available from https://doi.org/10.1038/nclimate3107.

Meehl, G. A., Covey, C., Taylor, K. E., Delworth, T., Stouffer, R. J., Latif, M., . . . Mitchell, J. F. B. (2007). The WCRP CMIP3 multimodel dataset: a new era in climate change research. *Bulletin of the American Meteorological Society*, *88*(9), 1383−1394.

Meinshausen, M., Nicholls, Z. R. J., Lewis, J., Gidden, M. J., Vogel, E., Freund, M., . . . Wang, R. H. J. (2020). The shared socio-economic pathway (SSP) greenhouse gas concentrations and their extensions to 2500. *Geoscientific Model Devlopment*, *13*, 3571−3605. Available from https://doi.org/10.5194/gmd-13-3571-2020.

Miao, C., Duan, Q., Sun, Q., Huang, Y., Kong, D., Yang, T., . . . Gong, W. (2014). Assessment of CMIP5 climate models and projected temperature changes over Northern Eurasia. *Environmental Research Letters*, *9*(055007), 12. Available from https://doi.org/10.1088/1748-9326/9/5/055007.

Moberg, A., Sonechkin, D. M., Holmgren, K., Datsenko, N. M., & Karlén, W. (2005). Highly variable Northern Hemisphere temperatures reconstructed from low- and high-resolution proxy data. *Nature*, *433*, 613−617.

Moss, R. H., Edmonds, J. A., Hibbard, K. A., Manning, M. R., Rose, S. K., van Vuuren, D. P., . . . Wilbanks, T. J. (2010). The next generation of scenarios for climate change research and assessment. *Nature*, *463*, 747−756. Available from https://doi.org/10.1038/nature08823.

Nakicenovic, N., Alcamo, J., Grubler, A., Riahi, K., Roehrl, R. A., Rogner, H. H., & Victor, N. (2000). *Special report on emissions scenarios (SRES), a special report of Working Group III of the intergovernmental panel on climate change*. Cambridge University Press.

Natarajan, A., Hegde, R., Naidu, L. G. K., & Raizada, A. (2010). Soil and plant nutrient loss during the recent floods in North Karnataka: Implications and ameliorative measures. *Current Science*, *99*(10), 1333−1340.

Neukom, R., Steiger, N., Gómez-Navarro, J. J., Wang, J., & Werner, J. P. (2019). No evidence for globally coherent warm and cold periods over the pre-industrial Common Era. *Nature*, *571*, 550−554.

Nikulin, G., Asharaf, S., Eugenia., & Wysera, K. (2018). Dynamical and statistical downscaling of a global seasonal hindcast in eastern Africa. *Climate Services*, *9*, 72−85. Available from https://doi.org/10.1016/j.cliser.2017.11.003.

Norel, M., Kałczynski, M., Pinskwar, I., Krawiec, K., & Kundzewicz, Z. W. (2021). Climate variability indices: A guided tour. *Geosciences*, *11*, 128. Available from https://doi.org/10.3390/geosciences11030128.

Nussbaumer, S. U., Steinhilber, F., Trachsel, M., Breitenmoser, P., Beer, J., Blass, A., . . . Zumbühl, H. J. (2011). Alpine climate during the Holocene: A comparison between records of glaciers, lake sediments and solar activity. *Journal of Quaternary Science*, *26*(7), 703−713.

O'Neill, B. C., Kriegler, E., Riahi, K., Ebi, K. L., Hallegatte, S., Carter, T. R., . . . Vuuren, D. P. (2014). A new scenario framework for climate change research: the concept of shared socioeconomic pathways. *Climatic Change*, *122*, 387−400.

Pierce, D. W., & Cayan, D. R. (2014). Statistical downscaling using localized constructed analogs (LOCA). *Journal of Hydrometeorology*, *15*(6), 2558−2585.

Pourmokhtarian, A., Driscoll, C. T., Campbell, J. L., Hayhoe, K., & Stoner, A. M. K. (2016). The effects of climate downscaling technique and observational data set on modeled ecological responses. *Ecological Applications*, *26*(5), 1321−1337.

Rainforest. (n.d.). *Mission: Biomes*. Retrieved from https://earthobservatory.nasa.gov/biome/biorainforest.php.

Randel, W. J., Polvani, L., Wu, F., Kinnison, D. E., Zou, C.-Z., & Mears, C. (2017). Troposphere-stratosphere temperature trends derived from satellite data compared with ensemble simulations from WACCM. *Journal of Geophysical Research: Atmospheres*, *122*, 9651−9667.

Raynaud, D., Jouzel, J., Barnola, J. M., Chappellaz, J., Delmas, R. J., & Lorius, C. (1993). The ice record of greenhouse gases. *Science (New York, N.Y.)*, 926−934.

Robock, A. (2000). Volcanic eruptions and climate. *Reviews of Geophysics*, *38*(2), 191−219.

Roldin, P., Ehn, M., Kurtén, T., Olenius, T., Rissanen, M. P., Sarnela, N., & Boy, M. (2019). The role of highly oxygenated organic molecules in the Boreal aerosol-cloud-climate system. *Nature Communications*. Available from https://doi.org/10.1038/s41467-019-12338-8.

Royal Society & US National Academy of Science. (2020). Climate change evidence and causes: An overview from the Royal Society and the US National Academy of Sciences (2020 update). https://royalsociety.org/-/media/Royal_Society_Content/policy/projects/climate-evidence-causes/climate-change-evidence-causes.pdf.

Rupp, D. E., Abatzoglou, J. T., Hegewisch, K. C., & Mote, P. W. (2013). Evaluation of CMIP5 20th century climate simulations for the Pacific Northwest USA. *Journal of Geophysical Research: Atmospheres*, *118*(19), 10−884.

Sabzevari, M., Martínez-Muñoz, G., & Suárez, A. (2022). Pooling homogeneous ensembles to build heterogeneous ensembles. *International Journal of Machine Learning and Cybernetics*, *13*(1). Available from https://doi.org/10.1007/s13042-021-01442-1.

Salinger, J. (2005). Climate variability and change: Past, present and future − an overview. *Climatic Change*, 9−29.

Schoof, J. T. (2013). Statistical downscaling in climatology. *Geography Compass*, *7*, 249−265. Available from https://doi.org/10.1111/gec3.12036.

Sheffield, J., Barrett, A. P., Colle, B., Nelun Fernando, D., Fu, R., Geil, K. L., & Yin, L. (2013). North American climate in CMIP5 experiments. Part I: Evaluation of historical simulations of continental and regional climatology. *Journal of Climate*, 26. Available from https://doi.org/10.1175/JCLI-D-12-00592.1.

Sillmann, J., Kharin, V. V., Zhang, X., Zwiers, F. W., & Bronaugh, D. (2013). Climate extremes indices in the CMIP5 multimodel ensemble: Part 1. Model evaluation in the present climate. *Journal of Geophysical Research: Atmospheres*, *118*, 1−18. Available from https://doi.org/10.1002/jgrd.50203.

Singer, A. (2021). In-depth Q&A: The IPCC's sixth assessment report on climate science. *Carbon Brief*. August 9, 2021. https://www.carbonbrief.org/in-depth-qa-the-ipccs-sixth-assessment-report-on-climate-science.

Soja, A. J., Tchebakova, N. M., French, N. H., Flannigan, M. D., Shugart, H. H., Stocks, B. J., & Stackhouse, P. W. (2007). Climate-induced boreal forest change: Predictions versus current observations. *Global and Planetary Change*, *56*(3−4), 274−296.

Tanner, E. V. J., Rodriguez-Sanchez, F., & John, R. H. (2014). Long-term hurricane damage effects on tropical forest tree growth and mortality. *Ecology*, *95*(10), 2974−2983.

Taylor, K. E., Stouffer, R. J., & Meehl, G. A. (2012). An overview of CMIP5 and the experiment design. *Bulletin of the American Meteorological Society*, *93*(4), 485−498.

Thorarinsdottir, T. L., Gneiting, T., & Gissibl, N. (2013). Using proper divergence functions to evaluate climate models. *SIAM/ASA Journal on Uncertainty Quantification*, *1*, 522−534.

Thorarinsdottir, T. L., Sillmann, J., Haugen, M., Gissibl, N., & Sandstad, M. (2020). Evaluation of CMIP5 and CMIP6 simulations of historical surface air temperature extremes using proper evaluation methods. *Environmental Research Letters*, *15*, 124041. Available from https://doi.org/10.1088/1748-9326/abc778.

Thrasher, B., Wang, W., Michaelis, A., Melton, F., Lee, T., & Nemani, R. (2022). NASA global daily downscaled projections, CMIP6. *Scientific Data*, *9*, 262.

USGS. (2021). *What is the difference between global warming and climate change?* https://www.usgs.gov/faqs/what-difference-between-global-warming-and-climate-change-1?qt-news_science_products = 0#qt-news_science_products.

Van Vuuren, D. P., Edmonds, J., Thomson, A., Riahi, K., Kainuma, M., Matsui, T., . . . Hibbard, K. A. (2011). Representative concentration pathways: an overview. *Climate Change*, *109*, 5−31. Available from https://doi.org/10.1007/s10584-011-0148-z.

Vano, J. A., Kim, J. B., Rupp, D. E., & Mote, P. W. (2015). Selecting climate change scenarios using impact-relevant sensitivities. *Geophysical Research Letters*, *42*(13), 5516−5525.

Wang, T., Hamann, A., Spittlehouse, D., & Carroll, C. (2016). Locally downscaled and spatially customizable climate data for historical and future periods for North America. *PLoS One*, *11*(6), e0156720. Available from https://doi.org/10.1371/journal.pone.0156720.

Wang, W. J., He, H. S., Thompson, F. R., Fraser, J. S., & Dijak, W. D. (2017). Changes in forest biomass and tree species distribution under climate change in the northeastern United States. *Landscape Ecology*, *32*, 1399−1413.

Williams, A. P., Cook, E. R., Smerdon, J. E., Cook, B. I., Abatzoglou, J. T., Bolles, K., . . . Livneh, B. (2020). Large contribution from anthropogenic warming to an emerging North American megadrought. *Science (New York, N.Y.)*, *368*(6488), 314−318. Available from https://doi.org/10.1126/science.aaz9600.

Yang, Y., Franzke, C. L. E., & Fu, Z. (2020). Evaluation of the ability of regional climate models and a statistical model to represent the spatial characteristics of extreme precipitation. *International Journal of Climatology*, *40*, 6612−6628.

Zhang, X., Alexander, L., Hegerl, G. C., Jones, P., Tank, A. K., Peterson, T. C., . . . Zwiers, W. (2011). Indices for monitoring changes in extremes based on daily temperature and precipitation data, WIREs. *Climate Change*, *2*, 851−870.